بسم الله الرحمن الرحيم

Sudan University of Science and Technology

Faculty of Engineering

Aeronautical Engineering Department

Design optimization for a new vertical flight technique

Thesis submitted in partial fulfillment of the requirements for the Degree of Bachelor of science (B.SC honors)

By:

Zainab Mohamed Osman Ali

Supervised by:

Dr. Tarig Abu-rass

Eng. Abd'elaziz Abd'elmajed

October, 2016

الآيـة

قال الله تعالى :

(يَا مَعْشَرَ الْجِنِّ وَالإِنسِ إِنِ اسْتَطَعْتُمْ أَن تَنفُذُوا مِنْ أَقْطَارِ السَّمَاوَاتِ وَالأَرْضِ فَانفُذُوا لا تَنفُذُونَ إِلاَّ بِسُلْطَانٍ)

سورة الرحمن، آية (33)

Abstract

The economy of military aircrafts during mission is very bad, especially at takeoff followed by climb. Also, it is clear that, the value of any military aircraft evaluated by its maneuverability and capabilities. This project is a chance and step to improve all of the military aircrafts economy, maneuverability and capabilities that is by invent new technique to achieve a vertical flight depend on the wing lift itself and by the aid of additional device. SU-35S, the military supermaneuverable aircraft was used in this project.

After the field studies and data collection, this project start with a setup stage which include analysis and modeling for the SU-35S. This models includes: the aerodynamic model, the stability model, the structural model and prop-fan model. Using the models at the selected flight circumstances, MATLAB codes have been written to calculate the lift, check the stability, the structural strength and the axial momentum produced by the prop-fans. The second stage include the design optimization and consist for main two parts: the sliding part design optimization and the prop-fans rescale.

It was approved that, a considerable lift value can be produced by the fixed wing aircraft at zero forward speed using the designed vertical flight device which consist of series of small prop-fans and sliding part. The aircraft is not stable which is expected result for fighter. Due to the shortness of time, the structural analysis results is not completed. But it is expected that, there is no structural deformation because the applied load is less than the aircraft maximum load. Also, the produced momentum by the prop-fans is not enough to accelerate the aircraft in the forward direction. The consumed power by the prop-fans had been found much less than the consumed power by the other techniques to achieve vertical takeoff normal to the aircraft wing.

التجريد

إن اقتصادية الطائرات المقاتلة في كل المهمات سيئة جداً. خصوصاً عند الإقلاع يليها التسلق. أيضاً من الواضح أن قيمة الطائرة المقاتلة تحدد بمناويرتها و مقدراتها. هذا المشروع هو فرصة و خطوة لتحسين كل من اقتصادية الطائرة المقاتلة و مناويرتها و مقدراتها و ذلك باختراع طريقة جديدة لتحقيق طيران عمودي بالاعتماد على الرفع المنتج بواسطة الجناح نفسه و بمساعده من جهاز إضافي. سخوي 35 اس الطائرة المقاتلة ذات المناورية العالية استخدمت في هذا المشروع.

بعد جمع البيانات بدء هذا المشروع بمرحلة تمهيدية. تتكون هذه المرحلة من تحليل و نمذجة رياضية للطائرة سخوي 35 اس. تتضمن هذه النماذج الرياضية: النموذج الايروديناميكي، النموذج الخاص بالاستقراية، النموذج الخاص بهيكل الطائرة و نموذج المروحة. باستخدام النماذج الرياضية و عند ظروف الطيران المختارة، تمت كتابة برامج باستخدام البرنامج (MATLAB) وذلك لحساب الرفع المنتج، التحقق من استقرارية الطائرة و مقاومة الهيكل و الزخم المحوري المولد بواسطة المراوح. المرحلة الثانية تتضمن التصميم الأمثل و تتكون من جزئين أساسيين: التصميم الأمثل للجزء المنزلق من الجناح و تغير قياس و أبعاد المراوح.

تم اثبات أن قيمة معتبرة لقوى الرفع يمكن توليدها بواسطة الطائرة ذات الجناح الثابت عند سرعة أمامية تساوي الصفر باستخدام جهاز الرفع العمودي المصمم و الذي يتكون من مجموعة من المراوح الصغيرة و جزء منزلق. الطائرة ليست مستقرة و هي نتيجة متوقعة لمقاتلة. بسبب ضيق الزمن نتائج تحليل الهيكل لم يتم إكمالها. أيضاً الزخم المحوري المولد بواسطة المراوح ليس كافياً لتسريع الطائرة في الاتجاه الأمامي. وجد أن القدرة المستهلكة بواسطة المراوح أقل بكثير من القدرة المستهلكة بواسطة التقنيات الأخرى لتحقيق إقلاع عمودي على جناح الطائرة.

Acknowledgement

Firstly, I would like to acknowledge my supervisors Dr. Tarig Abu-rass and Eng. Abd'elaziz Abd'elmajed for their support for me during the research. I want to thank Eng. Ahmed Mokhtar and Ms. Raheeg Wahbi for advising. Also, it is pleasure to acknowledge all who help me in this project individual and groups.

الأهـــــداء

إلى والديَ العظيمين الذين أعطياني الكثير ...

إلى أساتذتي و إخوتي و من ساهم في تعليمي و نصحني ...

و إلى كل أصحاب الفضل ...

أهدي ثمرة هذا العمل عرفاناً بفضلهم علي

Table of Contents

List of figures

List of tables

Glossary

$\alpha_{L=0}$	Zero lift angle of attack
α	Airfoil geometrical angle of attack.
C_{l_0}	Airfoil lift coefficient without considering of the compressibility effects.
C_l	Airfoil lift coefficient with the considering of the compressibility effects.
C_L	Lift coefficient with the considering of the compressibility effects.
a	Wing lift curve slope
a_o	airfoil lift curve slope
a_t	The aircraft tail lift curve slope
C_D	Drag coefficient with the considering of the compressibility effects.
$C_{D,i}$	Induced drag coefficient with the considering of the compressibility effects.
$C_{D,w}$	Shock waves drag coefficient with the considering of the compressibility effects.
$C_{D,0}$	Zero lift drag coefficient with the considering of the compressibility effects.
AR	Aspect ratio
e	Oswald efficiency factor
e_0	span efficiency factor
δ	Tapper ratio
$C_{m_{c/4}}{}_0$	Airfoil moment coefficient around the quarter chord without considering of the compressibility effects.
$C_{m_{c/4}}$	Airfoil moment coefficient around the quarter chord with the considering of the compressibility effects.
α_{eff}	The effective angle of attack

α_i	The induced angle of attack
i_w	Wing setting angle
θ	The angle between the X-axis and a line connect the airfoil mid. chord point and a point on the airfoil camber line.
ac	Indicate the aerodynamic center of an airfoil
C	Chord line
ρ	The airflow density
V	Velocity of air
Γ	The circulation around an airfoil
Λ	Sweepback angle
Λ_2	Sweepback angle of spar No.2
Λ_{ac}	Sweepback angle of aerodynamic centers line
$\Lambda_{c/2}$	Sweepback angle at the half chord line
$\Lambda_{L.E.}$	Leading edge sweepback.
V_1	Airflow speed at station No.1= free stream velocity
V_2	Airflow speed at station No.2= speed at the entry of the prop-fans
V_3	Airflow speed at station No.3= speed at the outlet of the rotor
V_4	Airflow speed at station No.4= speed at the outlet of the stator
V_6	Airflow speed at station No.2= speed at the leading edge of the original wing.
w	Downwash (used in the modified lifting line theory)
h	The perpendicular distance between the vortex element and a point P in the space.
b	The wing span. Or the disc width for the prop-fans
ϑ	The angle between the aircraft longitudinal axis and wing station k.
A_n	Fourier serious coefficient.
n	Wing element in the modified lifting line theory.
k	Wing control point in the modified lifting line theory.
C_t	Wing tip chord

C_r or C_{re}	Wing root chord
$\bar{x}_{ac}$	The location of the aerodynamic center for airfoil as percentage of the chord.
k_1, k_3	constants
CG	Center of gravity
C_{m_α}	the change in the moment coefficient around the CG with respect to the angle of attack change.
$\bar{x}_{cg}$	The location of CG as percentage of the chord.
S	Wing area
S_{exp}	Wing or sliding part exposed area
l_f	The aircraft fuselage length
$\in$	The downwash at the tail due to the wing effect.
$\bar{C}$	Mean aerodynamic chord
q	Airflow kinetic energy
η_t	The aircraft tail efficiency.
V_h	The aircraft tail volume ratio.
β	Boom area for the structural model Blade inlet angle for the prop-fans model
θ	Wing twist angle for the structural model
b_r	The rotor disc width
r_{Pj}	The distance from any point at the panel *j* even the point control point k.
ϕ	Potential velocity
λ_i	Vortex strength of the panel i.
b	slot length
h	slot width
M	slots number

1 Introduction

1.1 Introduction

There is many maneuver allow for the A/C to translate from an altitude to another: climb, vertical takeoff (using: rotating wing as in helicopter, for fixed wing as in thrust vectoring and semi fixed (fixed/rotating) wing such the technologies used by NASA). The climb can perform at any altitude even reach the absolute ceiling while the vertical takeoff techniques are valid for takeoff just. [1],[2],[3],[4]

Firstly, for fixed wings, there is two main paths for vertical takeoff: upward normal to the wing and parallel to the wing. The first path is uncommon in spite of this maneuver done successfully at a certain conditions and certain techniques such as jet jump and fan in duct. The jet jump is thrust vectoring technique to rise the A/C up at zero X velocity its depend on engine thrust and some large fans it is uneconomical and heavier frames. Fan in duct depend on large fan locate in the wing and it used in horizontal flight path because it based in slip stream effect, this technology is unsuitable for fighters' layout in spite of that it is economical. [1],[2]

Secondly, for semi fixed wings, NASA develop three prototypes based on three similar concepts: Dos Samara, retracting wing and Trifecta technologies. Dos Samara has "outboard wing panels, which spin to generate thrust to lift the vehicle in vertical flight. In horizontal flight, the outboard wing panels lock. A pusher propeller is located on the tail to provide forward thrust in horizontal flight" figures (1) and (2). The Trifecta is a tri-copter vehicle which has a front propeller connected to a diesel engine which rotate 90 degrees to produce the lift at the nose in the vertical flight. Also two monoblade lift propellers are adding at the tip of the horizontal tail to produce the lift in the vertical flight at the rear, this blades rotating with direct electrical motors, figure (3). "The elevators deflect 90 degrees trailing edge down in hovering in order to reduce the download on the horizontal tail". The last concept, retracting rotor has a rotor completely retracted to the fuselage at horizontal flight while extended out in vertical flight. A pusher propeller also used to produce thrust in horizontal flight, figure (4). In the three concepts the main criteria are

that, independent vertical flight system work with motors (except in Trifecta concept where the front propeller is both part of the hovering and propulsive system) than the propulsive system which work with fuel. This criterion provides a two separated forces in the vertical and the horizontal directions rather than a resultant force separated into vertical and horizontal components so, it is wideness the semi-individual control for the forces for example the increasing of the vertical force mainly depend on the DC motors rpm and so on. But the three layouts are not suitable for fighters' layout and requirements. [1],[2],[3],[4],[5]

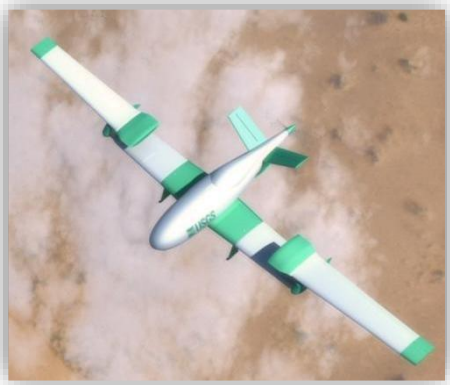

Figure 1. Dos Samara

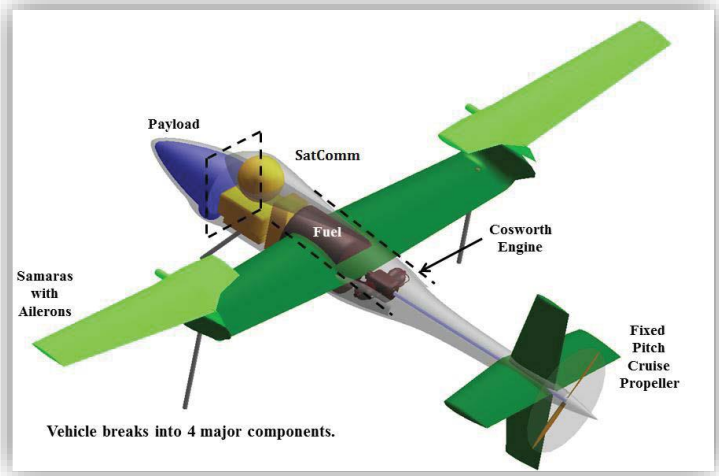

Figure 2. Dos Samara

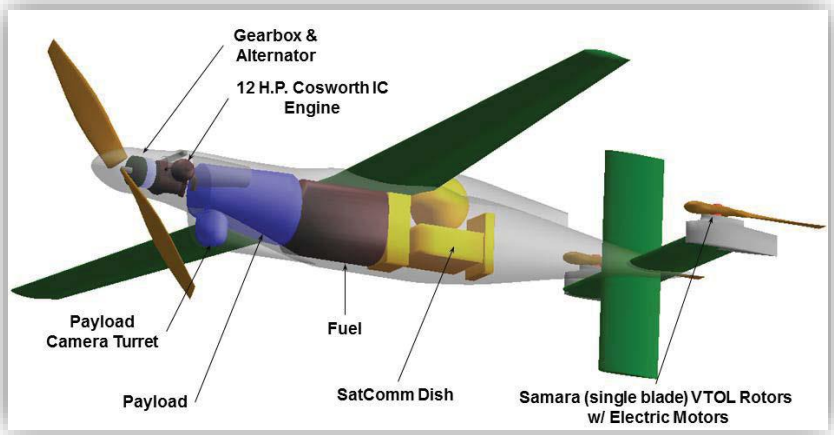

Figure 3. Trifecta

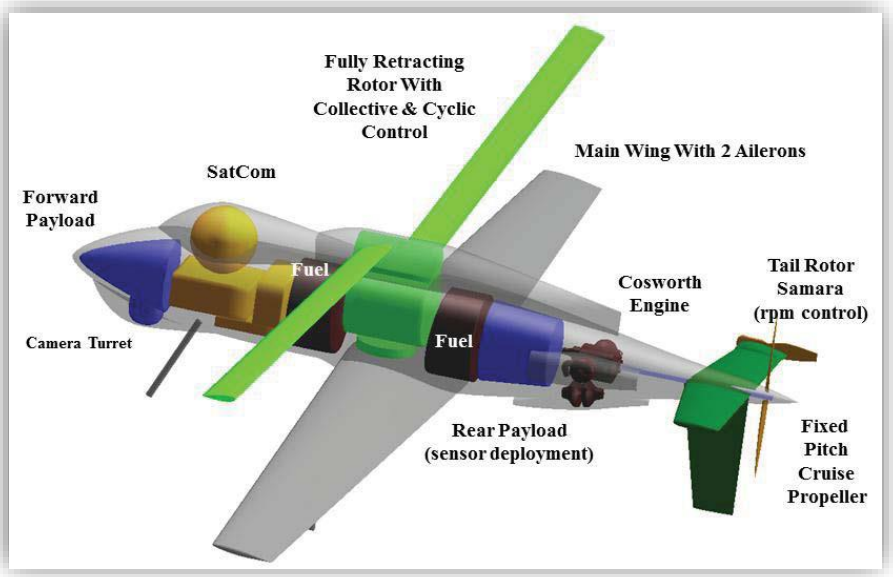

Figure 4. retracting rotor

This project is an establish to a combined between climb (at 0 deg.) which happen at any altitude even reach the limit ceiling and vertical takeoff normal to the fixed wings to produce a technique very similar in conditions to semi fixed NASA technologies (separated vertical and horizontal forces = semi-individual systems) which is more suitable for fighter layout. [2],[4],[6]

The A/C will be (case study: SU-35) capable to perform the vertical takeoff maneuver normal to the wing depending on the lift produced by the wing and at any altitude even reach the limit ceilings. [7]

1.2 Problem statement

Vertical takeoff maneuver is uncommon because of the high energy needed to perform it with jet jump besides the high fuel consumption (engine in high levels of producing thrust), additional heavy means added to suck air with large masses and the large fans used in fan in duct technique which incorporated into the wings is not suitable for super maneuverability fighters' layout.

To create a chance to reduce the fuel consumption and the time of clime needed by the A/C to translate through relatively short height and to keep suitable layout for fighters, a design of a device has been approach which make the A/C capable to perform the vertical flight maneuver normal to the wing depending on the lift produced by the wing from steady level flight at a wide range of altitudes by incorporate a new sliding part into the wing and fans as shown in figure (5) and estimate a vertical translating distance analytically. Nevertheless, this technique is a new level of technology.

Also, the effect of this incorporation on the A/C performance must be taken into account to note the benefits and penalties, the study of the effects on the A/C structure and stability has been considered.

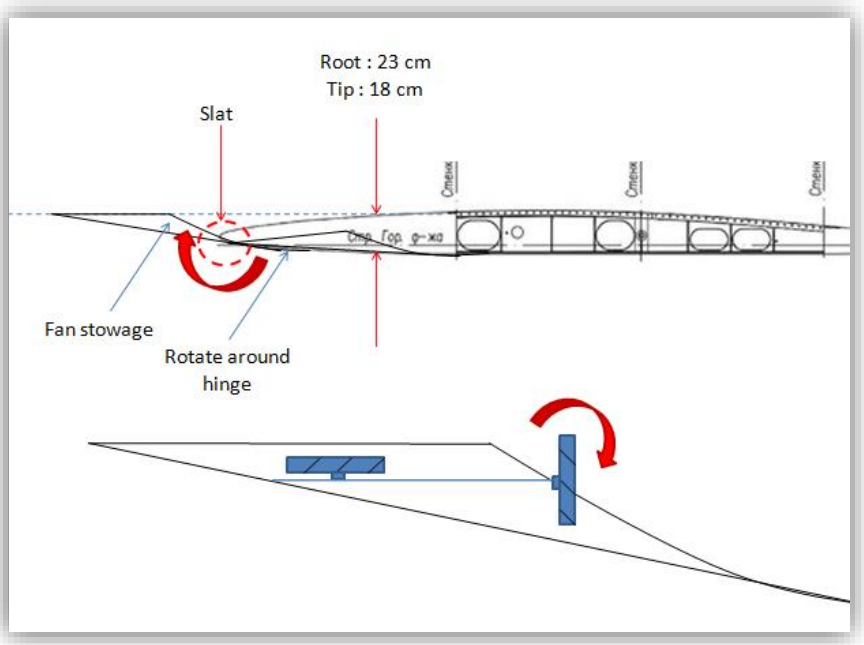

Figure 5. mechanism

1.3 Proposed solutions

To establish the technique a new sliding part from the wing has been designed and a series of special small diameters NASA prop-fans has been incorporated to accelerate the flow to higher Mach number. Make a suitable structural incorporation consider the effect on the structure and the stability. To make the analytical analysis, theoretical equations have been used.

1.4 Motivations

To improve the worse fighters' economy a little bit. And to appear and to exploit the capabilities of the fixed wing aircrafts.

1.5 Contribution

The vertical flight maneuvers have been relieved again using a new technique born of older known concepts and based on some same conditions of the previous two techniques (jet jump / fan ducts) but with lower fuel consumption as possible, more suitable for super maneuverability fighters' layout, approachable at wide range of altitudes not just at ground. Thus, the maneuverability of fixed wing A/Cs had been increased.

1.6 The aim and objectives

1.6.1 Aim

To establish a very efficient vertical flight technique from time, fuel consumption and maneuverability view. And to increase the fighters' capabilities.

1.6.2 Objectives

1. Aerodynamic modeling for SU-35S wing.
2. Structural modeling for SU-35S wing.
3. Stability modeling for SU-35S.
4. Estimation of the NASA STF fan model to predict the axial momentum.
5. Sliding part design optimization, its incorporation inside the wing and prop-fans rescaling and distribution.
6. Estimation of lift produced by the device action under the chosen flight conditions and the vertical upward acceleration.
7. Estimation of the consumed power by the device.

1.7 Methodology and methods

After the literature review and the critical literature review had been estimated to determine the most suitable methods to be used, the modeling had been starting with the aerodynamic model which had been estimated using the thin airfoil theory, the lifting line theory had been modified to estimate the lift distribution. Then, the wing structural model had been estimated using the idealization of the structure. A simple stability model had been built to be sure longitudinal stability during maneuver and a stable new wing. And for the prop-fan, an axial momentum model had been estimated to predict the axial momentum produced by the prop-fans series. A MATLAB codes had been written for the four models. A design optimization for the sliding part had been took place. This followed by prop-fans rescale and distribution along the semi-span.

The design optimization stage had been started with the representation of the objective functions for the single-objective case and the constraints. The optimization had been done using the MATLAB.

At the chosen flight conditions, and depending on the model estimated before, solutions for the lift produced under the device action and the drag also, the vertical displacement, the stability of the A/C and the structural strength had been estimated. The power consumed by the device had been calculated.

1.8 Research outlines

This research consists of seven chapters. The first chapter is introduction about the research topic and it illustrates the aim, objectives, the methodology and the methods of the research, the motivations and the contribution. The two next chapters are a background on the research topic. The first one is general background while the second is related. The fourth chapter illustrates the modeling procedure of the fighter SU-35S and the prop-fans. The fifth is about the design optimization of the sliding part and the prop-fan rescale procedure. The next chapter includes the research results. The last chapter is the research conclusion

2 Literature review

2.1 History and background on the fixed wing vertical takeoff

A different ideas and techniques had been brain stormed, tested, entered into service and some of them get out of service due to the limited benefits via the greater losses. For the fixed wing aircrafts and in 1930, an idea to use rotors in the tip of the fixed wing to achieve a vertical takeoff and landing when the rotor tilts upward and normal forward flight when the rotors tilts back to the horizontal position. George Lehberger was patented for the first modern tiltrotor design in May 1930. In 1942 (II-war) a German prototype was developed figure (6). This has been followed by a series of developing and future projects even this day. [8]

Figure 6. Focke -Achgelis Fa 269

Another idea shine during 1950s/1960s in USA, is the Fan-in-wing. The vertical takeoff and landing achieved through a large fans lies in large holes in the fixed wing. In the forward flight, the fans rotate by 90 degrees in a position seem likes conventional turboprop. [9]

The first representation of the fan-in- wing was coupled with the flying saucer (circular flying wing). The first project was Avro Canada Avrocar which established by USA in 1950. “The Avrocar intended to exploit the Coandă effect to provide lift and thrust from a single "turborotor" blowing exhaust out the rim of the disk-shaped aircraft to provide anticipated VTOL-like performance” [9],[10]

Figure 7. The Avro Canada Avrocar

In 1960s, many design was arising to achieve a vertical short takeoff and landing using the vectored thrust into the ground. The only successful design was the Harrier Jump Jet military series. F-35 Lightning II version B is the military aircraft which replace the Harrier. [9]

A fourth idea was to use individual engines for VTOL (lifting) and others for thrust. They are known as separated thrust and lift techniques. [11]

2.2 Background on the techniques that increase the fixed wing lift at low aircraft speed

2.2.1 Morphing wing

The morphing wing are the wings that can change their shapes under the command of control. They have been used to satisfy certain purposes such as increasing the wing lift through changing the wing geometrical parameters (wing area planform, the wing aspect ratio, the leading edge radius …etc.). [12]

A way using the morphing wing was used to improve the airfoil low speed performance (stall limit) is by increase the leading edge radius and the thickness chord ratio. The problem with this is the worse airfoil performance at the high speeds. [12]

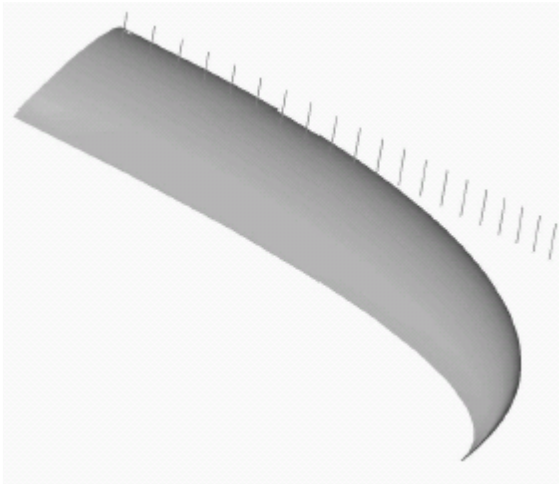

Figure 8. application to hyper-elliptical cambered span

1.1.1.1 Lift increasing using morphing various direction sliding parts

Many complex morphing shapes can be achieved using advanced morphing mechanism such as the complex shape: hyper-elliptical cambered span, see figure (). A complex sliding rib structure has been developed by Cornerstone Research Group, Inc. to "vary the planform area and aspect ratio of a wing. The structure consists of sliding wing boxes that can **move forward, backwards and outwards in the wing** thus increasing the net planform for the wing. The choice of for the structure is not clear but inchworm motors and piezoelectric actuators are considered as preferred choices. However, these actuators will need to be coupled to other mechanisms to increase their overall strain to achieve significant aerodynamic benefits of wing morphing" see the figure (9). [12]

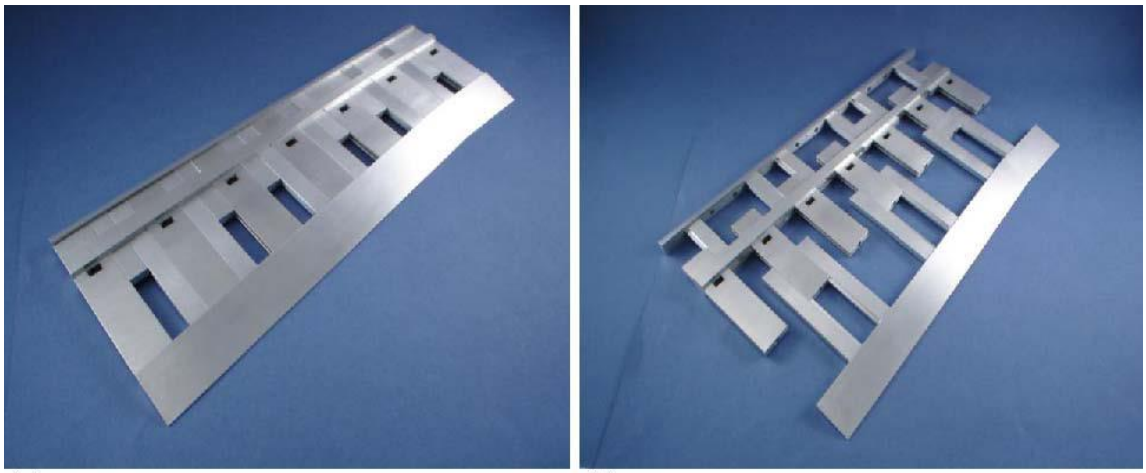

Figure 9. (a) Closed Configuration of Corner Stone Wing (b) Open Configuration

2.2.2 Coanda effect

2.2.2.1 Introduction

One of the earlier techniques had been used to increase the wing lift was the coanda effect. The coanda effect" is the tendency of a fluid jet to stay attached to a convex surface. The principle was named after Romanian aerodynamics pioneer Henri Coandă, who was the first to recognize the practical application of the phenomenon in aircraft development". [10]

"Several aircraft, notably the Boeing YC-14 (the first modern type to exploit the effect), NASA's Quiet Short-Haul Research Aircraft, and NAL's Asuka research aircraft have been built to take advantage of this effect, by mounting turbofans on the top of the wings to provide high-speed air even at low flying speeds, but to date only one aircraft has gone into production using this system to a major degree, the Antonov An-72 'Coaler' " see figure (10). [10]

Figure 10. Antonov An-72 'Coaler'

2.2.2.2 spiral slipstream effect

Generally, the slipstream is

> "a region behind a moving object in which a wake of fluid (typically air or water) is moving at velocities comparable to the moving object, relative to the ambient fluid through which the object is moving. The term slipstream also applies to the similar region adjacent to an object with a fluid moving around it. "Slipstreaming" or "drafting" works because of the relative motion of the fluid in the slipstream". [13]

Whenever the object shape is more aerodynamically, the slipstream effect become weaker. Another important point is that, the slipstream effects the aircraft stability and there are ameans introduced into the design to counteract this. [13]

The slipstream is used to increase the lift at low speed as one of the main purposes. "The Shin Meiwa US-1A flying boat utilizes a similar system, only it directs the propwash from its four turboprop engines over the top of the wing to generate low-speed lift. More uniquely, it incorporates a fifth turboshaft engine inside of the wing center-section solely

to provide air for powerful blown flaps". The purpose of this was to improve the STOL capabilities. [10]

2.2.2.3 Circulation control wing CCW

"The CCW works by increasing the velocity of the airflow over the leading edge and trailing edge of a specially designed aircraft wing using a series of blowing slots that eject jets of high-pressure air. The wing has a rounded trailing edge to tangentially eject the air through the Coandă effect thus causing lift. The increase in velocity of the airflow over the wing also adds to the lift force through conventional airfoil lift production" see figure (11). [14]

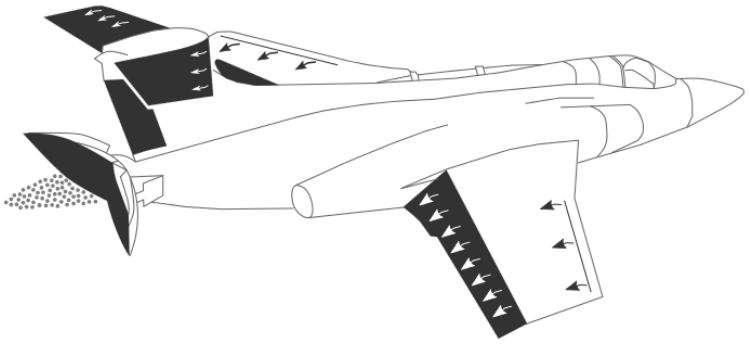

Figure 11. blown slots

The CCW is mainly used when there is a need to a high lift at low speed. The special thing about the CCW is that there is no increment in the drag as the lift increases. In has another secondary usage such as the increasing of the maneuverability of the aircraft at the low speeds by increase the efficiency of the control surfaces using the circulation control. The CCW must be used in multi-engines aircrafts. Also, the CCW actually consume the engines power and thus counteracts the wing's purpose. Some options are available to solve this such as the using of cooled engine exhaust or light air generators. [14]

2.2.2.4 Flap blown

Flap blown techniques improved the lift about two to three times. [15]

- **Internal blown flap**

This technique is increase the lift through delaying the stall and thus increase the maximum lift coefficient. “A small amount of the compressed air produced by the jet engine is "bled" off at the compressor stage and piped to channels running along the rear of the wing. There, it is forced through slots in the wing flaps of the aircraft when the flaps reach certain angles. Injecting high energy air into the boundary layer produces an increase in the stalling angle of attack and maximum lift coefficient by delaying boundary layer separation from the airfoil. Boundary layer control by mass injecting (blowing) prevents boundary layer separation by supplying additional energy to the particles of fluid which are being retarded in the boundary layer. Therefore, injecting a high velocity air mass into the air stream essentially tangent to the wall surface of the airfoil reverses the boundary layer friction deceleration thus the boundary layer separation is delayed”. Hunting H.126 use the internal blown flap (jet flap) to improve the lift confident to 9. See Figure (12). [15]

Figure 12. hunting H.126

- **External blowing flap**

"The externally blown flap arranges the engine to blow across the flaps at the rear of the wing. Some of the jet exhaust is deflected downward directly by the flap, while additional air travels through the slots in the flap and follows the outer edge due to the Coandă effect". Boeing YC-14 use this type to produce lift coefficient about 7, see figure (13). [15]

Figure 13. Boeing YC-14

- **Upper surface blown**

It "arranges the engines over the wing and relies completely on the Coandă effect to redirect the airflow. Although not as effective as direct blowing, these "powered lift" systems are nevertheless quite powerful and much simpler to build and maintain". [15]

- **Counter flow system**

"In this case the air blow slit is located at the pressure side near the leading edge stagnation point location and the control air-flow is directed tangentially to the surface but with a forward direction. During the operation of such a flow control system two different effects are present. One effect, boundary layer enhancement, is caused by the increased turbulence levels away from the wall region thus transporting higher-energy outer flow into the wall region. In addition to that another effect, the virtual shaping effect, is utilized to aerodynamically thicken the airfoil at high angles of attack. Both these effects help to delay or eliminate flow separation". [15]

2.3 SU-35 data

2.3.1 The specification of SU-35S

- **Dimensions:**
  - **Length:** 21.9 m (72.9 ft)
  - **Wingspan:** 15.3 m (50.2 ft, with wingtip pods)
  - **Height:** 5.90 m (19.4 ft)
  - **Wing area:** 90 m² (667 ft²)
  - **Exposed wing area:** 62m^2

- **Weight:**
  - **Empty weight :** 18,400 kg (40,570 lb)
  - **Loaded weight (normal (2 x RVV-AE + 2 x R-73E)):** 25,300 kg (56,660 lb) at 50% internal fuel
  - **Max. takeoff weight :** 34,500 kg (76,060 lb)

- **Coefficients:**
  - **Parasite drag coefficient:** 0.02

- **Engines:**
  - 2 × Saturn 117S (AL-41F1S) turbofan with thrust vectoring nozzle.
  - **Thrust:**
    - **Combat mode:**
      - **Max. dry thrust:** 8,800 kgf (86.3 kN, 19,400 lbf) each.
      - **Thrust with full afterburner :** 14,000 kgf
    - **Special mode:**
      - **Thrust (Max. afterburner thrust):** 14,500 kgf (142 kN, 31,900 lbf) each.

- **Thrust vectoring nozzle:**
  - 3D thrust vector nozzle.
  - The engine can deflect its nozzle to a maximum of ±15° in the all directions at a rate of 30°/sec.
  - Temp. at the inlet: reach 2000 deg. C.
  - Pressure: 5 to 7 atmospheres.
- **Dimensions:**
  - **Fan Diameter:** 932 millimeters.
  - **Low pressure compressor inlet diameter:** 932 millimeter
  - **Overall length:** 4945 mm, 4990 mm
  - The engine is fully ducted.
- **Number of spools:** 2
- **Number bearings:** "**6** in main transmission line ".
- **Compressor:**
  - **Low pressure compressor** consists of 4 stages with one stage of inlet guided vanes have a pressure ratio of 3.5.
  - **High pressure compressor** consists of 9 stages with 3 stages of variable stator vanes which has a pressure ratio of 6.6.
  - **Bearings:** 2 of the total 6, front support roller bearing and rear support ball bearing.
  - **Combustion chamber:**
    - **Type:** annular.
    - **Number of igniters:** 3
    - **Number of fuel nozzles:** 28 duplex.
- **Dry mass:** 1490 kg (1520 kg).
- **Service (ultimate) Life:** 4,000 hours. ("The engine lifetime is determined on the operational condition with the possibility of units' replacement at the operation site. The TVC nozzle's lifetime corresponds to the engine lifetime ")
- **Time Between Overhaul:** 1,000 hours.

❖ **fuel:**

- **Fuel capacity (max.):** 11,500 kg (25,400 lb.) internally.
- The fighter has range in excess of 3,500 kilometers without refueling.

❖ **Performance:**

- **Maximum airspeed:**
  - **At altitude H = 11000 m:** Mach 2.25 (2,390 km/h, 1,490 mph)
  - **At sea level H = 200 m:** Mach 1.15 (1,400 km/h , 870 mph)
- **Range** (with max. fuel load):
  - **At altitude (Hcr , Mcr) :** 3,600 km (1,940 nmi)
  - **At sea level (H = 0 , M = 0.7) :** 1,580 km (850 nmi)
- **Ferry range:** 4,500 km (2,430 nmi) with 2 × PTB - 2000 external fuel tanks (increase to 6500km with refueling at air)
- **Service ceiling:** 18,000 m (59,100 ft)
- **Acceleration time at H=1,000 m and fuel bingo 50% of the standard capacity:**
  - **From 600 km/h to 1,100 km/h:** 13.8 sec.
  - **From 1,100 km/h to 1,300 km/h:** 8 sec.
- **Max. rate of climb at H = 1000 m:** >280 m/s (>55,000 ft/min)
- **Wing loading:** 408 kg/m² (500.8 kg/m² with full internal fuel) (84.9 lb/ft² 50% fuel)
- **Max. combat load:** 8000 kg.
- **Thrust/weight:** 1.126 at 50% fuel (0.92 with full internal fuel)
- **Take-off run in "full afterburning" mode with standard take-off weight :** 400-450m
- **Landing roll on concrete runway in braking mode with brake parachute and wheel brakes use, with standard landing weight :** 650m

❖ **G-load:**

- **Maximum g-load :** +9 g
- **Most forward CG location:** 1.98 m
- **Most rearward CG location:** 2.12 m

1.1.1.2 Some of the aircraft main features

❖ **The airframe:**

- Generally:
  - The reinforced airframe of a titanium alloys , increasing its durability to some 30 years or 6,000 service hours, and raising the maximum take-off weight to 34.5 tones.
  - strong superficial. [17]
- Wing:
  - Swept wing blends into the fuselage at the leading edge extensions and is essentially a cropped delta (the delta wing with tips cropped for missile rails or ECM pods) . [18]
- Tail unit:
  - tailed delta wing configuration, retaining conventional horizontal tail-planes, though it is not a true delta.
  - height reduction of the vertical stabilizers. [18]
- fuselage:
  - smaller aft-cockpit hump.
  - shorter rearward-projecting "sting". [18]
- Weapon:
  - "12 hard points with 2-station racks available
  - High combat load
  - High-efficiency "air-to-air" and "air-to-surface" weapons including long-range ones

- Built-in 30-mm gun “ [19]

Figure 14: SU-35S weapons

❖ Power plant

- Generally:
  - “Two powerful bypass turbojet engines. All-axis thrust vector control Power plant fly-by-wire control (FADEC type) “. [19]
  - Each features “with the multi-axis thrust vector control, auxiliary turbine engine, fuel system, fire-extinguishing system, and auxiliary gearbox.” [19]

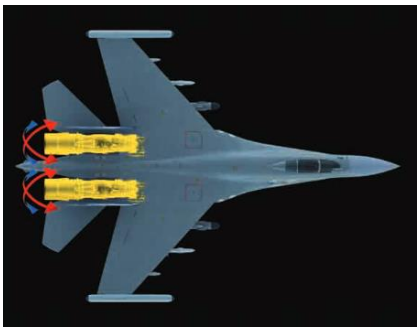

Figure 15. SU-35S power plant

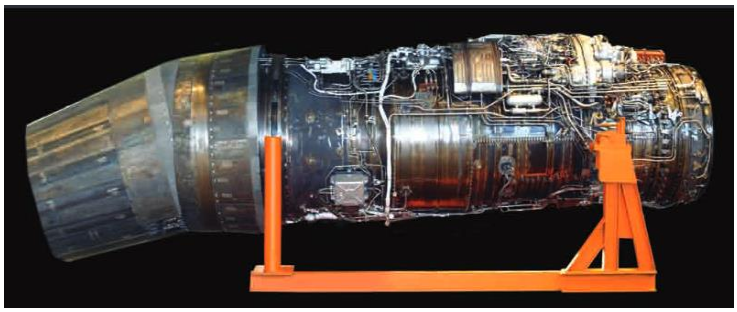

Figure 16. AL41F1S turbofan engine (side view)

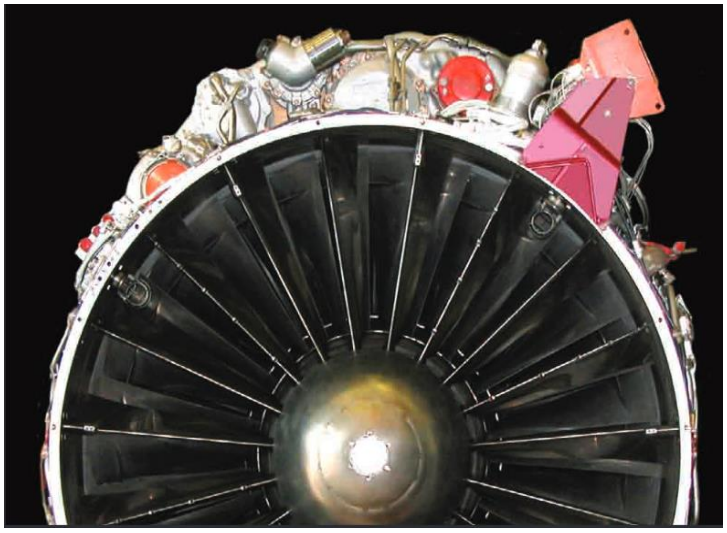

Figure 17. AL41F1S turbofan engine (front view)

- Thrust vectoring control:
  - the two engines feature multi axis thrust-vectoring control . [19] [18]
  - the system enhanced aircraft maneuverability. [18]
  - Each thrust vectoring (TVC) nozzle has its rotational axis canted at an angle. [18]
  - The thrust vectoring nozzles operate in one plane for pitch, but the canting allows the aircraft to produce both roll and yaw by vectoring each engine nozzle differently. [18]
  - the engine is capable of mounting 3D thrust vectoring nozzles for extra maneuverability. [18]

- The engine gives the Su-35 limited super cruise capability, or sustained supersonic speed without the use of afterburners . [18]

- Radar-absorbent material is applied to the engine inlets and the front stages of the engine compressor to halve the Su-35's frontal radar cross-section (RCS); the canopy was also modified to deflect radar waves. [18]

❖ **Systems:**

- Integrated control system (generally mention):
  - "Stick control
  - Hands-off control
  - Stabilization and sensitivity
  - Automatic trimming
  - TVC nozzle control
  - Supermaneuvrability mode support
  - Aircraft taxiing control system
  - Wheel braking control
  - Definition of aerodynamic characteristics
  - Stall warning/stick pusher
  - Quadruple redundancy ". [19]

Figure 18. SU-35S systems

- brakes system: differential deflection of the vertical stabilizers.
- Fuel system:
    - Tanks:
        - Internal fuel capacity of 11.5 tons, and could be raised to 14.5 tons with the addition of drop tanks . [18] this capacity provides for flight range of 3,600 km. [19]
        - " 2 external fuel tanks of 2,000 l capacity " [19]
    - Inflight refueling system: in-flight refueling can also be used to extend missions. [19] [18]
    - " Tanker function (with external fueling unit) " [19]

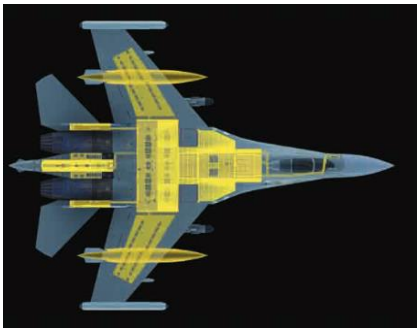

Figure 19. SU-35S fuel system

❖ **Enhanced maintainability:**

- "Increased life time and service life of airframe
- Increased engine life time
- Onboard oxygen generator
- Auxiliary power plant
- Checkability and maintainability " [19]

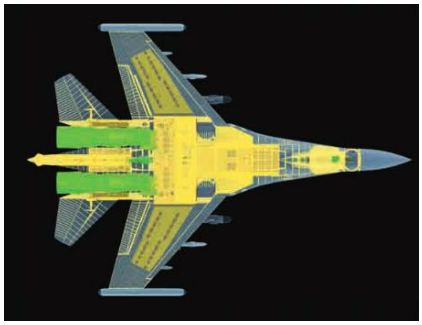

Figure 20. Enhanced maintainability

2.4 Background on the efficient high speed propellers and fans

2.4.1 High speed propellers

"During the 1990s, the development of high speed regional turboprops became the obvious step to counter the attack of regional jets on their traditional market. Since 2000, the orders for new and larger turboprops have been increasing again and it is anticipated that their maximum speed will eventually increase to Mach 0.7. This is also the design speed of the Airbus A400M military freighter which is powered by four of the West's most powerful Europrop TP400-D6 engines each producing 7 830 kW. Their propellers feature eight crescent-shaped composite blades" see Figure (21).

" High speed propellers were studied extensively resulting in the so-called propfan. The combination of a gas turbine engine and a propfan is now categorized as an open rotor engine".[20]

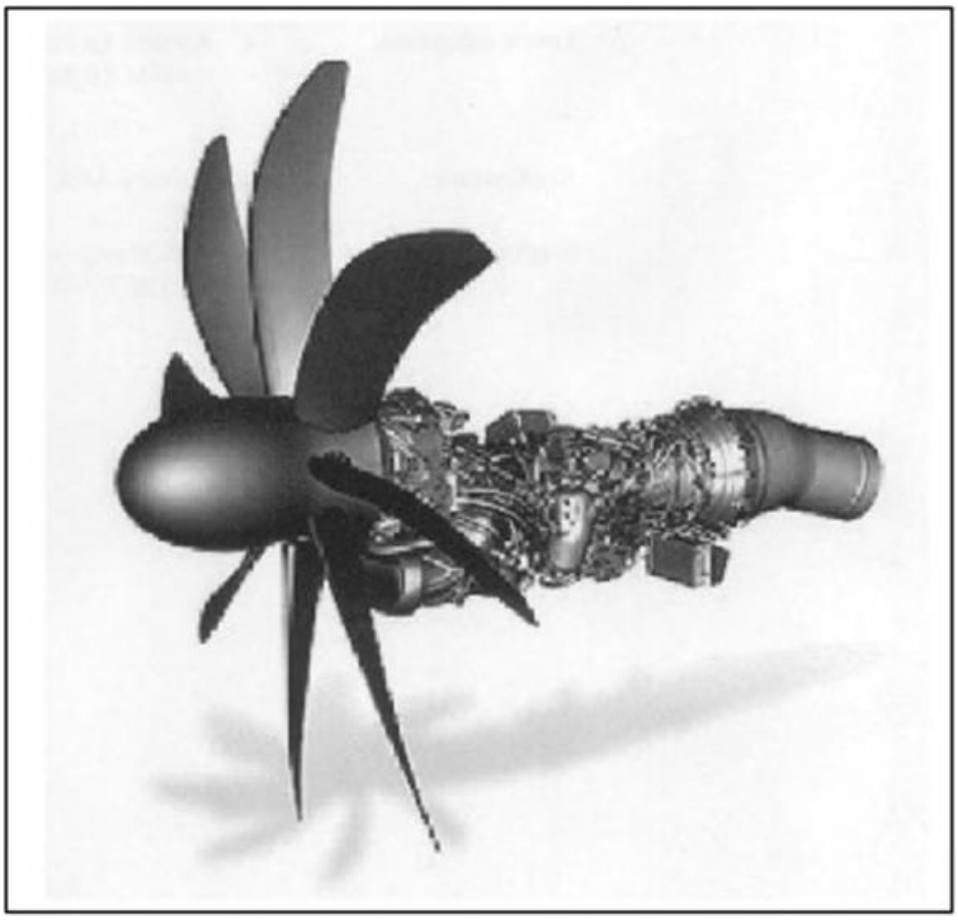

Figure 21. The Euro prop International TP 400 three-shaft turboprop engine with high-speed propeller.

2.4.2 Rise and Fall of the Prop-fans

"During the 1970s, NASA made an ambitious effort to stimulate the development of an advanced turboprop aircraft cruising at Mach 0.80 and altitudes up to 30 000 ft. that could reduce fuel consumption by 30% compared to jetliners. This required the development of advanced high-speed propellers known as propfans. Proposed in 1975 by propeller manufacturer Hamilton Standard, propfans were introduced with multiple crescent-shaped highly loaded blades designed to maintain at least 80% propulsive efficiency. The company was awarded an advanced blade development contract and in 1981 began to design the composite blade set of a large single stage demonstration propfan dubbed SR-7A which was tested in 1986. The complete engine with an eight-bladed unit flew on a modified Gulfstream II in 1987". [20]

“Propfan is a portmanteau word coined to describe a propulsion concept which combines some of the characteristics of a turboprop with those of a turbofan. Although early propfans had a much higher disk loadings than a conventional propeller, both were driven by a turboshaft engine via a gearbox. The essential difference with turbofans is the much higher propfan BPR between 25 and 40, variable-pitch blades and the absence of a rotor duct. The term propfan was originally applied to a multiple-bladed single rotor; however, since contra-rotation makes no fundamental difference, the term propfan still applies. Contra-rotation of the blades eliminates much of the swirl in the rotor slipstream, making the propulsive efficiency about 7% higher compared to the single-stage layout”. [20]

“In the 1980s, all the major airliner manufacturers considered adopting propfan technology for clean sheet designs. This required tractor engine arrangements which could be mounted to the wing leading edge or pusher arrangements mounted to the rear fuselage” see figure (22). [20]

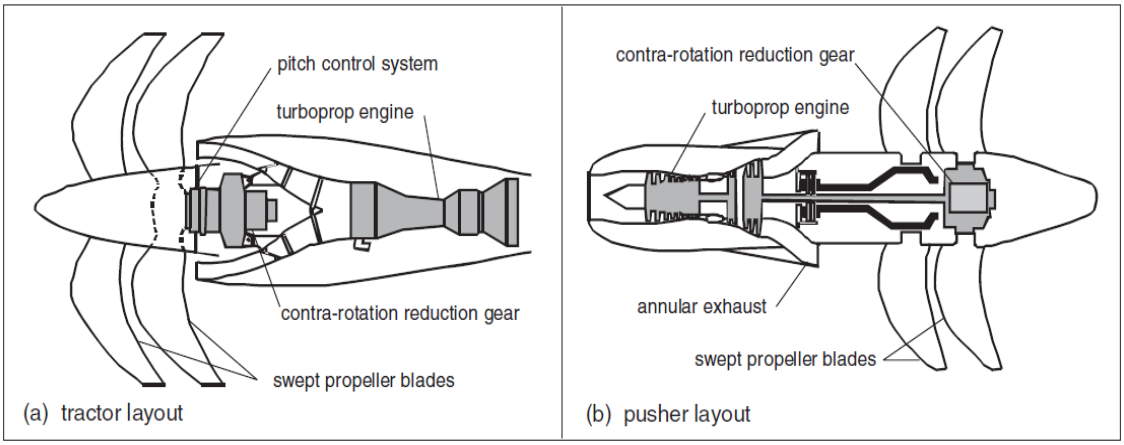

Figure 22. General arrangements of prop-fans with contra-rotating geared open rotors. The output is expressed as shaft horsepower (SHP) because there is a turboshaft engine and gearbox involved

“Moving away from the geared propfan trend with the revolutionary unducted fan (UDF) concept, GE concentrated on the tail-mounted pusher configuration to limit cabin noise. Their UDF arrangement dispenses with the gearbox and features a gas generator to power a pair of CR statorless free turbines carrying the rotor blades”, as illustrated in figure (23). [20]

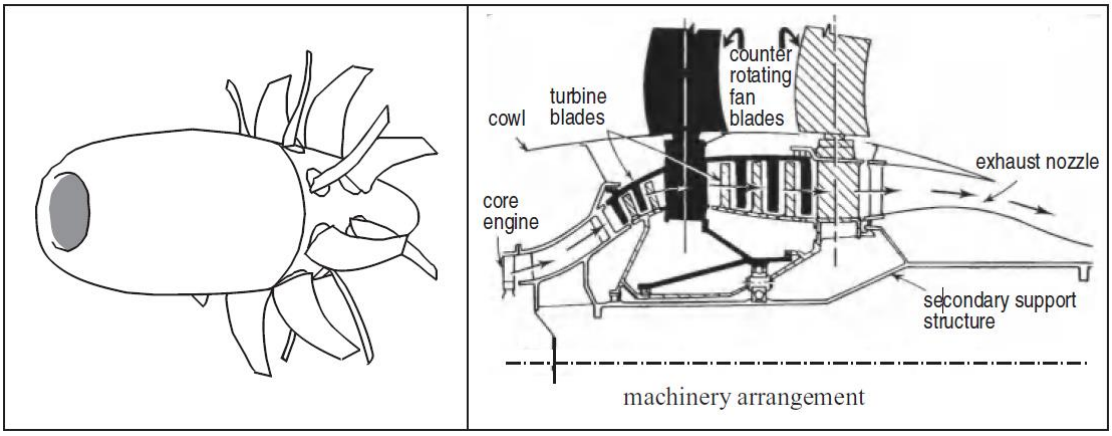

Figure 23. General Electric GE 36 unducted fan (UDF) of the 1980s

"American airframers were the most active investigators of the propfan. Boeing and McDonnell Douglas teamed with GE and P & W/Allison to evaluate the technology, culminating in the demonstrator engines GE 36 and PW 578-D mounted on 727-100 and MD-80 aircraft. In Europe, Rolls-Royce worked along the lines of a geared open rotor in pusher configuration but did not produce a full-scale demonstrator. The relatively low price of fuel at the time meant that potential concerns such as noise and reliability problems prevented the promising propfan technology from being adopted. The designs studied during the 1980s were at least three decennia ahead of their time, except for the Progress D-27 CR propfan which powers the machinery Antonov AN-70. This military freighter had its public debut in 1997 and is the only application of propfans in operational aircraft up to 2010". [20]

2.4.3 Rebirth of the Open Rotor?

After the turn of the twentieth century, with soaring fuel prices and emphasis on reducing environmental emissions, the aeronautical industry is showing a renewed interest in the virtues of propfans.

High-speed propellers "developed for speeds up to Mach 0.70 are becoming operational. Their diameter and detailed design are optimized for installation in a specific airplane. Different from turboprops, propfans are complete systems developed and produced by gas turbine engine manufacturers featuring variable pitch rotors with pressure ratios between 1.05 and 1.40, dependent on BPR. Application of contra-rotating open

rotors lead to uninstalled cruise SFC reductions between 25 and 30% with similar noise levels compared to high BPR turbofans. Due to the varying blade pitch with speed, the gain in propulsive efficiency is even greater at low speeds;". "Hence, similar to turboprops, open rotor systems improve low speed performances which makes them especially fit for application in short-haul airplanes. However, complex airframe integration issues and acquisition costs will be high since open rotors are mechanically more complex than turboprops as well as turbofans. Major technical concerns exist regarding safety (blade failure), cabin noise, maintenance costs, reliability and fan efficiency at cruise speeds above Mach 0.75". [20]

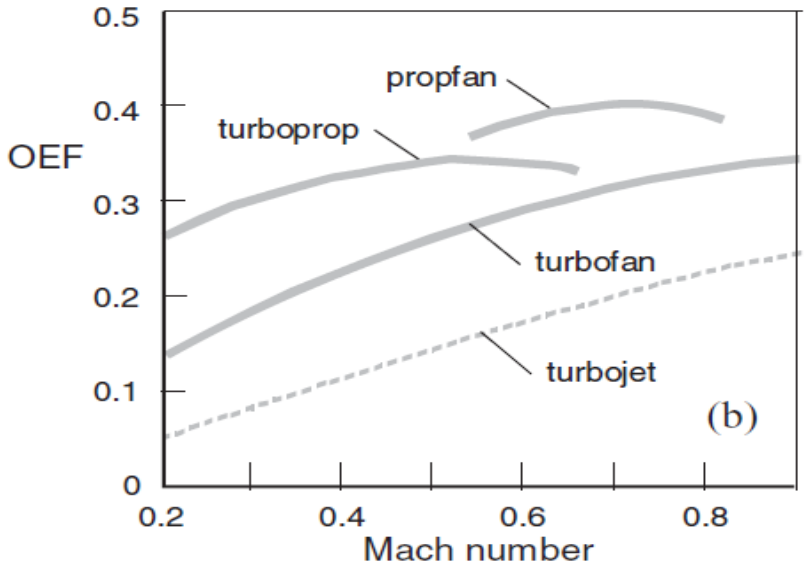

Figure 24. Fuel efficiency trends of gas turbine aero engines in cruising flight. (b) Variation of overall efficiency with speed.

2.4.4 Supersonic through flow fan (STF fan)

"Ferri was the first one to indicate the potential advantages of high fan pressure ratio (in single stage) and elimination of the subsonic portion of the supersonic inlet with the use of an STF fan. Franciscus showed that the STF fan equipped engine would significantly reduce specific fuel consumption compared with a conventional turbofan engine for a supersonic cruise mission. For a supersonic transport operating at Mach number of 2.7, Tavares suggests that an STF fan efficiency of only 68 percentages is necessary to have performance advantage over a turbojet engine. These estimates of

performance improvement from the cycle studies were based on assumed characteristics of the STF fan obtained from transonic fan data". [21]

"All these cycle studies have an inherent uncertainty because of the lack of experimental data for the STF fan. A prototype STF fan rotor was designed, built, and tested by Breuge lmans. However, before the design speed could be attained a blade failure was encountered and the limited data obtained was insufficient to determine if supersonic through-flow was achieved". [21]

"Considering the large potential advantages of using a STF fan in advanced propulsive systems, NASA Lewis has embarked on a program to experimentally prove the concept of an STF fan system". [21]

2.5 History and background about the optimization

"**Optimization** is an important tool in making decisions and in analyzing physical systems. In mathematical terms, an **optimization problem** is the problem of finding the best solution from among the set of all feasible solutions". [22]

2.5.1 Historical Review of Engineering Optimization

"Optimization involves the pursuit of the "best" – or a significant "better". Better what? A better value of some defined "measure of merit" or "objective function". For aircraft conceptual design, the measure of merit is typically weight and/or cost for some specified capability, or capabilities such as range or payload at a specified weight or cost. This pursuit of better/best is limited by specified conditions involving real-world operational aspects or must-meet capabilities, which in mathematical terms are the "constraints" of the optimization. Fundamentally, we can define optimization as the determination of a minimum or maximum of one or more objective functions such that no constraints are violated. While equality constraints weigh heavily in other applications of optimization, in aircraft design optimization the constraints are almost always of the inequality sort – it is acceptable to be better than the required value, just don't be worse!". [23]

"Optimization is nothing new – it is inherent in the laws of physics. A massive collection of particles, floating freely in space, will form a sphere that is the optimum shape for minimizing surface area for an enclosed volume. A ball rolling down a hill will automatically, under the direction of nothing more than the laws of gravity and motion, find the fastest way down from a given starting point. Pebbles will, over time, pack themselves into the smallest possible volume". [23]

"Human efforts at optimization go back as far as humans have existed. Even a primitive man tries to find a better way to kill prey, gather foods, carry water, defend loved ones, and provide shelter from the elements. In fact, optimization by a-priori thought rather than instinct is a key factor that makes us human (although some animals look pretty thoughtful at times – like a dog trying to get to an out-of-reach bone!)". [23]

"Prior to the last few hundred years, optimization was largely by trial-and-error, with good results passed down as heuristic folklore. The great cathedrals of Europe were designed with every intent to minimize material (for cost) and column size and number (for aesthetics), but the only available tools were the study of prior successes and failures and the construction and test of portions of the design under consideration". [23]

"In the world of shipbuilding, quite close to the world of aircraft design, the disaster of the Swedish warship Vasa is instructive concerning the problems of attempting to optimize with insufficient analytical tools to assess the design constraints. Vasa was ordered during a time of war (1625) as a single-deck warship with a keel length of 108 ft and a width and ballast load suitable for such a length, based on prior experience. The customer - the king who was away fighting in Germany - sent an order to make the ship "more optimal" for its military purpose, namely by adding guns which required the ship to be longer (135 ft.) and to have an unplanned-for second gundeck and bigger sails". [23]

"Since there were no technical means to calculate the stability or ballast requirements except by past experience, nobody could prove that it wouldn't work (i.e., the stability constraint could not be calculated to determine an upper limit on the design variables "number of guns" and "number of gundecks"). So, they built it that way rather than incur the delay needed to start over with a broader hull and more ballast space. When

the hull was floated and the guns installed, they performed the usual stability test in which 30 men would run from side to side to see if the rolling motion would grow excessively. The Boatswain later said “If they had run across the ship one more time she would have capsized." Unfortunately, the king had sent clear instructions: "Vasa shall be ready by next (25 July), and if not, those responsible would be subject to His Majesty's disgrace." They finished it, launched it, and watched it roll over and sink in 100 ft of water”. [23]

“Optimization by mathematical analysis became possible in the 1600’s when Isaac Newton and Gottfried Leibniz independently developed calculus. About the same time, Pierre de Fermat defined a general approach to compute local minimums and maximums of functions by solving for the derivative and setting it to zero – the basis of most analytical optimization today. Fermat, along with Blaise Pascal, founded the theory of probability that is critical to Monte Carlo techniques and the recently developed evolutionary/genetic optimization algorithms. Interestingly enough, Fermat and Pascal became involved in probability theory when a gambler asked Pascal for advice as to how to best divide game winnings - and even today game theory provides a powerful optimization tool”. [23]

“In the 1700’s, Leonhard Euler developed methods to find the extreme values of functions, along with many other contributions to mathematics and physics including definition of a basic equation of hydrodynamics still used in computational aerodynamics. Joseph Lagrange, together with Euler, developed the calculus of variations. This remains highly useful in optimizing real-world problems such as those that are time-dependent. Lagrange also developed generalized equations of motion and developed the concept of partial differential equations, two of the foundations of engineering dynamic analysis”. [23]

“In the early 1800’s, Adrien-Marie Legendre and Carl Friedrich Gauss developed the method of least-squares curve fit that is often used in optimization, especially the modern Response Surface method. Later Pierre Laplace developed a formal proof of the leastsquares method, on which the estimation of curve fit errors is based. In the mid-1800’s, William Hamilton developed theorems concerning differential equations, dynamic analysis, and imaginary numbers which have great application for the solution of optimum design problems”. [23]

“Andrei Markov in the early 1900’s developed the theory of stochastic processes and pioneered the study of what became known as Markov Chains. These are sequences of random variables in which the future value of the variable is determined by the present value but is independent of the way in which the present value was derived from its predecessors. In other words, a Markov Chain has no history and no after-effects, which is typically true of iterative optimization processes”. [23]

“Vilfredo Pareto, an economist in the early 1900’s, developed the principle of multiobjective optimization for use in allocation of economic resources. His concepts became known as "Pareto optimality", defined as a situation in which you cannot make someone better off without making someone else worse off. A graphical representation of Pareto optimality is widely used to depict two-objective optimality. An aircraft design example might be a requirements trade study in which you attempt to maximize both range and payload weight, and plot a curve showing the optimum tradeoff between the two”. [23]

“In 1947 George Dantzig developed the Simplex Method to optimize problems involving scheduling of training, supply and deployment of personnel for the U.S. Air Force. In the military terminology of the day such planning was known as “programming”, and since the equations were linearized, this became known as "Linear Programming" (not to be confused with computer programming, which didn’t exist at that time). A key aspect of linear programming is its ability to deal with constraint functions independent of the objective function. Linear programming has become widespread in its usage, especially for business decision making”. [23]

“The Kuhn-Tucker Theorem (Albert Tucker and Harold Kuhn) of 1950 is considered to have launched the modern field of nonlinear programming (although it was apparently defined twice previously, by William Karush in 1939 and by Fritz John in 1948). Kuhn-Tucker gives necessary and sufficient conditions for the existence of an optimal solution to a nonlinear objective in the face of constraints. Fundamentally it says that at the optimum, the only direction you can move to improve the objective function is one that will violate one or more constraints. Kuhn-Tucker is widely used in the proofs of analytical optimization methods. As described above, the classic aircraft design carpet plot is actually an excellent illustration of Kuhn-Tucker” see figure (25). [23]

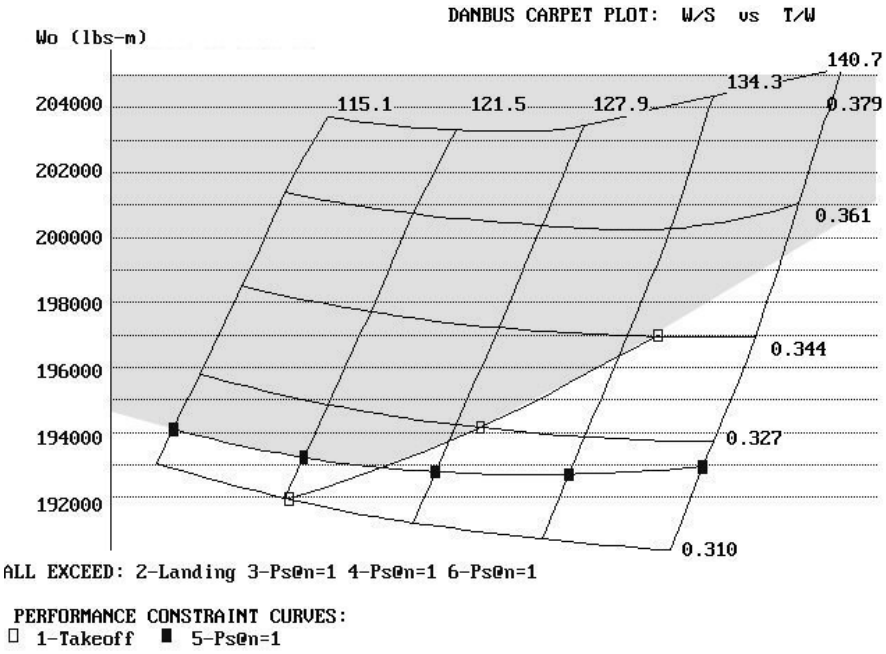

Figure 25. Classical Optimization via Carpet Plot

"Since the 1970s, there has been a tremendous expansion of optimization strategies and algorithms supporting advanced designers. The introduction of automated optimization has enabled designers to go into much greater in depth and fidelity of analysis than before. Synthesis programs effectively connecting the inputs and outputs of the functional group disciplines by means of an automatic control logic have been developed at aircraft manufacturers, research establishments and academia. Sophisticated computer assisted design (CAD) systems for defining three-dimensional body geometries and computer graphics tools for rapidly preparing parametric surveys are available at a modest cost. System engineering methods have brought about a paradigm shift in project development towards integrated product development (IPD) and – at least for traditional designs – this approach is highly refined and widely accepted. For an unusual aircraft concept, however, existing synthesis programs will have to be thoroughly modified as the risk of the results being unreliable is high since methods cannot be calibrated with statistical data. Moreover, advances in the field of practical optimization do not depend exclusively on the availability of fast computers or efficient optimization algorithms but on the overall company-wide development of computational frameworks geared toward flexibility, automation, and exploitation of high-fidelity analysis systems".[23],[20]

2.5.2 Optimization elements and terminology

1. Objective function

"is a scalar function of the design variables that is to be minimized or maximized during the optimization". [23]

2. Design parameters

The design parameters are the design's variable, unknown and controllable properties and quantities which we want to find their values in a way that maximize or minimize the objective function and vitrify the constrains. The design parameters such as the wing span. It is important to specify how the design parameters defining the values of the properties and the quantities to categorize them during the computational process as shown below: [23]

- **Pre-assigned parameters:** they are the properties and the quantities which stated by the designer to be constant during the optimization. They derived from such as the design requirement or the previous experience. [20]

- **Independent variables are parameters:** they called also selection variables and they are the parameters which ranged between maximum and minimum values. They subdivided into:
    - Integers: known also as discrete, when the selection variables are integers such as the number of ribs.
    - contiuous: when the selection variables "can be defined by any real number in a specific interval" such as the wing area.
    - Boolean: "such as whether to build a monoplane or a biplane". [20],[22],[24]
- **Dependent variables:** – "also known as behavior variables – are parameters generated by the design (optimization) process. Forming the outcome of design analysis, their values are controlled by the selection variables. Typical dependent design variables are geometric parameters derived from geometric selection variables, weight and inertia moments of airframe components, aerodynamic

parameters such as lift and drag coefficients and stability derivatives, and numbers characterizing the impact on the environment of aircraft operation". [20]

3. **Constraints**

"Constraints are functions of the design variables representing limitations imposed upon the design". The constrain "must be satisfied in order for the design to be feasible". They are divided into: [24],[20]

- **Equality constraint:** where two variables are set to be equality. "Many sizing conditions are translated into equations acting as equality constraints. For example, the condition that in straight and level flight T = D can be interpreted as: 'In a specified flight condition and cruise rating, engines are sized to deliver the thrust required to balance drag.". [20]
- **Inequality constraint:** is a condition which is almost function in the independent variables to be sure a feasible design is estimated by the optimization process. For example, "the condition that the wing must have enough volume to contain all the fuel required for a specified long range mission. Depending mainly on wing planform shape and mean thickness ratio, this constraint leads to a lower limit for the wing area".[20]
- **Side constraint:** is to range the selection variables between upper and lower limits.

4. **Design space**

2.5.3 Types of optimization problems

- **Continuous optimization versus discrete optimization problems**

The continuous optimization is defined as a process where the objective to be optimized is expressed as a function of real variables. while the discrete optimization is encountered with the integer variables.[25]

- **None, single or multi-objectives optimization problems**

The non-objective problem is that, when "the goal is to find values for the variables that satisfy the constraints of a model with no particular objective to optimize". The

single objective problems are encounter with single objective to represent the overall quality of the design. The multi-objectives problems are "when optimal decisions need to be taken in the presence of trade-offs between two or more conflicting objectives. For example, developing a new component might involve minimizing weight while maximizing strength or choosing a portfolio might involve maximizing the expected return while minimizing the risk.".[20],[25]

- **Unconstrained Optimization versus Constrained Optimization**

"Another important distinction is between problems in which there are no constraints on the variables and problems in which there are constraints on the variables. Unconstrained optimization problems arise directly in many practical applications; they also arise in the reformulation of constrained optimization problems in which the constraints are replaced by a penalty term in the objective function. Constrained optimization problems arise from applications in which there are explicit constraints on the variables. The constraints on the variables can vary widely from simple bounds to systems of equalities and inequalities that model complex relationships among the variables. Constrained optimization problems can be furthered classified according to the nature of the constraints (e.g., linear, nonlinear, convex) and the smoothness of the functions (e.g., differentiable or nondifferentiable)". [25]

- **Deterministic Optimization versus Stochastic Optimization**

"In deterministic optimization, it is assumed that the data for the given problem are known accurately. However, for many actual problems, the data cannot be known accurately for a variety of reasons. The first reason is due to simple measurement error. The second and more fundamental reason is that some data represent information about the future (e. g., product demand or price for a future time period) and simply cannot be known with certainty. In optimization under uncertainty,

or stochastic optimization, the uncertainty is incorporated into the model. Robust optimization techniques can be used when the parameters are known only within certain bounds; the goal is to find a solution that is feasible for all data and optimal in some sense. Stochastic programming models take advantage of the fact that probability distributions governing the data are known or can be estimated; the goal is to find some policy that is feasible for all (or almost all) the possible data instances and optimizes the expected performance of the model". [25]

2.5.4 Optimization process

2.5.5 The general steps of the process

1. Constructing a Model (problem formulation)

"modeling is the process of identifying and expressing in mathematical terms the objective, the variables, and the constraints of the problem". [22]

2. Express the problem in the standard form

"Once the design variables, constraints, objectives, and the relationships between them have been chosen, the problem can be expressed in the following form:

find $\mathbf{x}$ that minimizes $J(\mathbf{x})$ subject to $\mathbf{g}(\mathbf{x}) \leq \mathbf{0}$, $\mathbf{h}(\mathbf{x}) = \mathbf{0}$ and $\mathbf{x}_{lb} \leq \mathbf{x} \leq \mathbf{x}_{ub}$

where J is an objective, $\mathbf{x}$ is a vector of design variables, $\mathbf{g}$ is a vector of inequality constraints, $\mathbf{h}$ is a vector of equality constraints, and $\mathbf{x}_{lb}$ and $\mathbf{x}_{ub}$ are vectors of lower and upper bounds on the design variables. Maximization problems can be converted to minimization problems by multiplying the objective by -1. Constraints can be reversed in a similar manner. Equality constraints can be replaced by two inequality constraints".[24]

3. Determining the Problem Type

The third step in the optimization process is "determining in which category of optimization your model belongs" [22]

4. The choice of optimization strategy

5. Selecting Software

The fifth step in the optimization process is "selecting software appropriate for the type of optimization problem that you are solving. Optimization software comes in two related but very different kinds of packages:

- **Solver software** is concerned with finding a solution to a specific instance of an optimization model. The solver takes an instance of a model as input, applies one or more solution methods, and returns the results.
- **Modeling software** is designed to help people formulate optimization models and analyze their solutions. A modeling system takes as input a description of an optimization problem in a symbolic form and allows the solution output to be viewed in similar terms; conversion to the forms required by the algorithm(s) is done internally. Modeling systems vary in the extent to which they support importing data, invoking solvers, processing results, and integrating with larger applications. Modeling systems are typically built around a modeling language for representing the problem in symbolic form. The modeling language may be specific to the system or adapted from an existing programming or scripting language." [22]

"Most modeling systems support a variety of solvers, while the more popular solvers can be used with many different modeling systems. Because packages of the two kinds are often bundled for convenience of marketing or operation, the distinction between them is sometimes obscured, but it is important to keep in mind when attempting to sort through the many alternatives available". [22]

2.5.6 Design optimization

"Design optimization refers to computational methods used to search for designs that are as efficient and effective as possible. The mathematical statement of design optimization problems takes the form of an objective function that calculates a value that represents the critical measure of design performance or merit. The optimum design is the design that is found to have a minimum merit function while satisfying all constraints.

Constraints are formulated as statements of equality or inequality that must be satisfied to keep the design feasible. Additionally, search boundaries are usually specified". [26]

2.5.7 Multi-Disciplinary Design Optimization

"MDO can be defined as "a methodology for the design of systems in which strong interaction between disciplines motivates designers to simultaneously manipulate variables in several disciplines." Independent optimizations of individual disciplines considering local goals does not guarantee an optimum overall design, which requires the consideration of the synergy between each contributing analysis method. Modern engineering optimization has reached a level of complexity that nearly always requires a strategy to handle many coupled disciplines. Inter-disciplinary coupling occurs when the output of one analysis package is required as input for another independent analysis package. This creates a more complex computational problem than single-discipline optimization. Aerospace conceptual design presents a classic example of a coupled system.".[26]

Figure (27)" shows the interaction between disciplines for a hypothetical aircraft conceptual design process. System design variables are shared by all disciplines and denoted by Z. Local variables, X, are specific to individual disciplines and Y denotes the information pathway from one discipline to another. The aerodynamics solver supplies the drag properties that the performance analysis needs in order to run. In turn, the performance analysis supplies the Mach number that the aerodynamics discipline needs to compute the aircraft drag. Similar couplings are indicated between the other disciplines as well". [26]

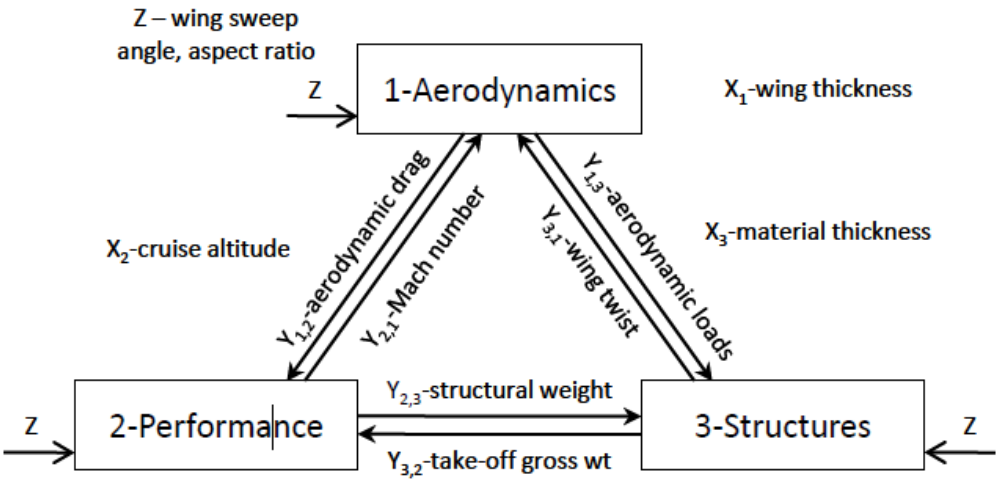

Figure 26. Coupled System Example

"The multidisciplinary nature of most design problems complicates model choice and implementation. Often several iterations are necessary between the disciplines in order to find the values of the objectives and constraints".[24]

3 Critical literature review

3.1 Introduction

In this part of the project, relevant cases and backgrounds have been discussed. At the first, a comparison between the vertical flight types has been made to show the more efficient type. Then, aircrafts closer to this project in the concept of work have been illustrated and discussed. The third part illustrates the type of the fan which has been used and rescaled in this project. The final part discusses three design optimization case to choose the suitable methods to work with in this project.

3.2 Vertical flight paths for the fixed wing fighters

To discuss the benefits and penalties provided by the vertical flight path itself. In this project the vertical flight paths were classified into: normal to the wing (NW)and parallel to the wing (PW). And the harrier jump was taken as a case study for the first path while the F-35 was taken as case study for the second one.

F-35 depends on the engine thrust to achieve the vertical takeoff. At the takeoff mission the engine must be in the maximum power condition which allow the fighter to accelerate quickly vertically.

In harrier jump case, at the vertical takeoff mission the engine is in the maximum power position.

Evaluation

At the vertical flight PW, the fighter travels a long distance (ALT) in a fraction of seconds before the pilot can stop the vertical flight due to that, the thrust force is parallel to the flight path and the engines in the maximum power position while the drag force is not the same higher. As a result, a net upward force is generated and fighter start to accelerate vertically and very quickly. So, it is not suitable for short upward travels. While in the vertical flight NW, it is more difficult to produce a force normal to the wing than the first case even when the engine in the maximum power position. Although the fighter will experience a higher vertical drag and as a result a lower acceleration and thus velocity in

the path direction will be produced and sure a slower upward travels which gives the pilot more time to perform a control.

The F-35 has a much lower time of climb than the harrier jump due to the same reason mentioned above.

Both flight paths have bad economic due to the high fuel consumption at the takeoff mission generally.

3.3 Independent propulsive-vertical takeoff and landing systems aircrafts

Some of vertical takeoff and landing (VTOL) systems are independent or semi-independent on the propulsive system which provide the forward speed mainly.

A project was established in the eightieths to introduce VTOL aircrafts have four times higher endurance than the traditional VTOL aircrafts (helicopters). In three techniques of seventeen (3/17) aircrafts prototypes, they reduce the fuel consumption by replacing the VTOL system which work with fuel by electrical system plus longitudinal fuel-dependent propulsive system. The three techniques were: Dos Samara, Trifecta and retracting rotor. [4]

"The first vehicle brought forward into the prototyping phase was the Trifecta. This vehicle is a tri-copter configuration with the diesel engine connected to the front propeller. This enables the diesel to be directly connected to the forward flight propulsor." [4]

"The front propeller and Cosworth engine together rotate 90 degrees to provide lift at the vehicle nose. Monoblade lift propellers were added to the tips of the horizontal tail to provide lift at the rear of the vehicle. In hover, pitch is controlled by varying the propeller pitch on the front and rear props. Direct electric motor rpm control may provide sufficient response rate for these smaller, lower moment of inertia rear prop-rotors; however, this has not yet been verified. Roll is controlled by variable pitch on the rear props. Yaw is controlled by gimbaling the rear lift props. The elevators deflect 90 degrees trailing edge down in hover in order to reduce the download on the horizontal tail."[4]

Dos Samara, “This design utilizes outboard wing panels, which spin to generate thrust to lift the vehicle in vertical flight. In horizontal flight, the outboard wing panels lock. A pusher propeller is located on the tail to provide forward thrust in horizontal flight. Electric motors power the outboard wing panels in vertical flight. The batteries are used as counter weights to balance the outboard wing panels. Figure 5 depicts an engineering visualization of the concept”. [4]

Retractable wing was had a “great potential but at a low technology readiness level (TRL)”. This concept has not had any sizing or performance analysis performed on it because a better estimate of the overall system weight needs to be developed first. Assuming the weight of the retracting rotor is reasonable, the concept would have the best performance of all the vehicle configurations assessed. The large diameter low disc-loading rotor would be the quietest, and have the lowest power required in hover. With the ability of the rotor to completely retract into the fuselage, the configuration is also the lowest drag solution – which would make it the best performing concept in forward flight as well. [4]

Evaluation

An importance point about the above project is that, the combination between the fixed wing which provide the lift during the cruise mission and the rotating part which carry the A/C during the vertical flight (takeoff or landing).

The use of independent (VTOL) and longitudinal fuel propulsive system is very efficient method to reduce the fuel consumption of the vertical takeoff mission (which has the maximum power consumed. Thus, maximum fuel consumption) as mentioned at the results. And it had been used to achieve the low fuel consumption which was a reason to establish the vertical flight maneuver in this project.

For retractable wing (VTOL) technique the extension of rotor blades from the fuselage will take a time to reach the full extension position (time penalty). Also, there is a weight penalty due to the rotor large rotor and extension-retraction mechanism inside the fuselage. Besides, the fixed wing structure must have high stiffness to resist the rotor down wake (relatively heavier structure penalty). Neither, it is not suitable for super-maneuverability fighters’ layout.

Dos Samara and Trifecta technologies have the ability of interaction between directional (vertical) velocity and the longitudinal velocity (Vz≠0 and Vx≠0 at the same time) at the transition seconds between vertical takeoff– cruise– vertical landing missions. At the first seconds of vertical takeoff-cruise transition, the directional velocity is greater than the longitudinal velocity as result to: RPM of rotors works in the directional axis >>> the RPM of rotors works in the longitudinal axis. This will result in general directional motion (not sensible longitudinal motion) and vice versa at the last seconds. At the cruise-landing transition, in the first seconds: ($Vx >>> Vz$) so, the resultant movement is longitudinally while the vice versa at the last seconds.

The transition from cruise mission to the vertical landing mission in both Dos-Samara and Trifecta simulate (similar to) the transition from cruise mission into the vertical flight maneuver established in this project. While the transition vertical takeoff into the cruise mission simulate the transition from vertical flight maneuver into the cruise mission again.

The endurance results mentioned above by the project prove that, the Dos-Samara which is entirely independent fuel propulsive /VTOL electrical system is more economical than the Trifecta (semi-independent). So, entirely independent electrical vertical flight system/fuel propulsive system had been used.

3.4 The selected prop-fan, NASA STF fan

To prove the concept of the STF fan experimentally (maintain a supersonic flow through compression system with only weak shock waves flow losses) NASA Lewis research Centre embarked a program contain the design of STF fan using four advanced computational codes due to the lack in the experimental data base to depend on it in the design. The other part of the program is the test of fan using a modified multi-stage compressor facility to be suitable for the new fan design. [27]

the research follows the methodology shown below:

- Detail design and the estimation of off-design performance with the use of advanced computational codes

- Selecting of potentially good blade shapes using the computational codes.
- Selecting of overall fan design conditions
- Testing the STF fan by a modified multistage compressor facility ("the facility modification essentially consists of adding a translating nozzle inlet and translating diffuser. [27]

As result to the absence in the experimental data base for the STF fan they depend over the computational in-house codes to achieve the design requirements. mainly they have two codes, the first is related to the compressor blade geometry. The second one is the viscous code which indicate what happen inside the boundary layer (such as velocity gradient). [27]

The project can be divided into three phases, the first one is about the computational codes build up, the second phase is about the detail design and analysis of the fan (computationally proving for the concept), the last phase is experimentally proving for the concept by connecting the fan into the system if the compression system receive a supersonic flow from the fan then the concept is proved. The detail design phase had been started with the computational phase where they decide their requirements and they state initial values for blade geometrical variables and other variables as shown below in tables (1) and (2). [27]

Table 1. overall STF fan (design conditions)

Pressure ratio	2.45
Weight flow, lb./sec	31 .5
Inlet axial Mach number	2.0
Tip speed, ft/sec	1 500
rotation speed, rpm	17 189
Diameter, in.	20
Hub-tip ratio	0.7

Table 2. rotor and stator design parameters

	Rotor	Stator
Rotation speed	17 188.7 rpm	-
Total pressure ratio	2.1	-
Tip radius, constant. in.	10	10
Hub radius, constant, in.	7	7
Blade number	44	52
Aero-chord, in.	4.45 (tip) to 3.56 (hub)	3.65 (tip) to 3.28 (hub)
Aspect ratio, span to mean chord ratio	0.97	0.86
Solidity, blade chord to spacing ratio	3.11 (tip) to 3.56 (hub)	3.02 (tip) to 3.88 (hub)
Maximum thickness/chord, percent	4 to 7	5
Leading edge thickness/chord. percent	0.15 to 0.19	0.14 to 0.15
trailing edge thickness/chord, percent	0.27 to 0.037	0.27
Leading edge radius, in	0.005	

As any traditional fan, STF fan stage consist of rotor and stator. The stator is designed to eliminate the swirl of the rotor.

Rotor design

The establishing of the rotor velocity diageram was the step that follow the specifiction setting; because it "specify the mass f low and energy addition given the wheel speed and f low path geometry" table (3), figure (28). [27]

Table 3. rotor blade

	Tip	Hub
Relative tip Mach number	2.7	2.36
Flow turning by	32 deg.	22.6 deg.

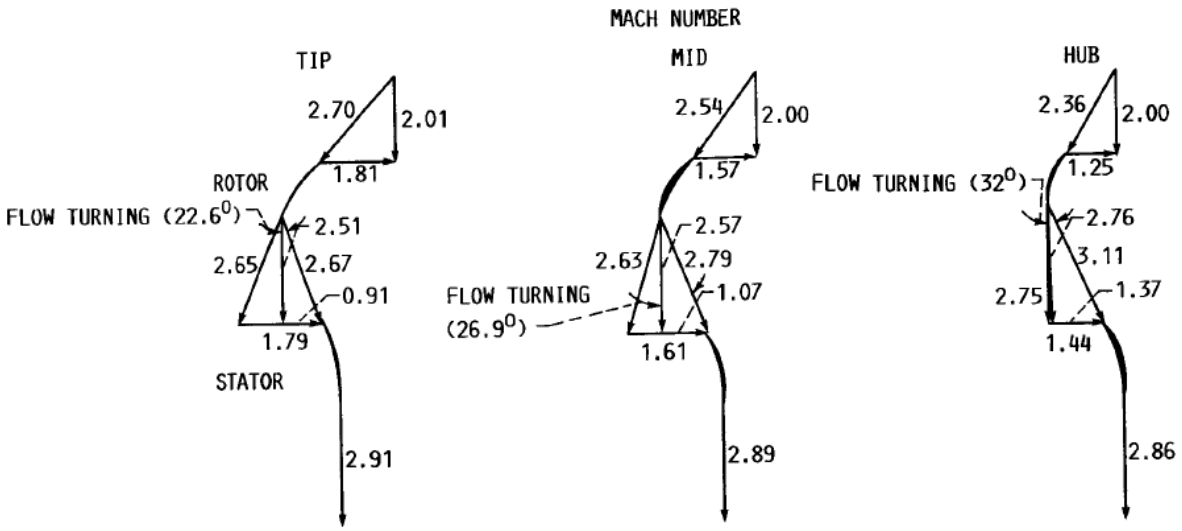

Figure 27. STF fan vector diagram

The solidity, the chord and the thickness ratio of the tip and the hub was chosen in a compromising way to be sure the upper and the lower surface static pressure at the trailing edge was matched (equally) "then the f low can leave the blade almost tangent to the blade angle and no large e adjustments (such as shock waves) to the flow are necessary at the trailing edge or downstream of the blade row." also to be sure a good blade performance and mechanical stresses within the acceptable limit at the hub also to be sure the relatively thick hub didn't cause any strong shock waves at the leading edge which result in a poor aerodynamic performance. Table (4) describe the tip and the hub. [27]

Table 4. rotor blade design

	Blade solidity	Max. Thick. Chord	Blade chord (in)
Hub	3.56	0.07	3.56
Tip	3.11	0.04	4.45

"The blade angle distribution was varied to fine tune the flow distribution over the blade". "a fairly sudden rise in blade angle near the leading edge which was used to decrease the leading edge wedge angle in order to reduce the strength of the leading edge shock wave. This rise was followed by a rapidly decreasing blade angle until mid-chord. The rear half of the blade had a linear blade angle distribution which produced a large static pressure gradient on the suction surface and practically no loading over the last 25 percent of the blade. The effect of the static pressure gradient on the suction surface is evident on the contour plot of Mach number by a significant increase in the viscous dominated region downstream of the location where a weak shock impacts the surface at about 50 percent of the chord" figures (29) (30) (31) shows the angle distribution. [27]

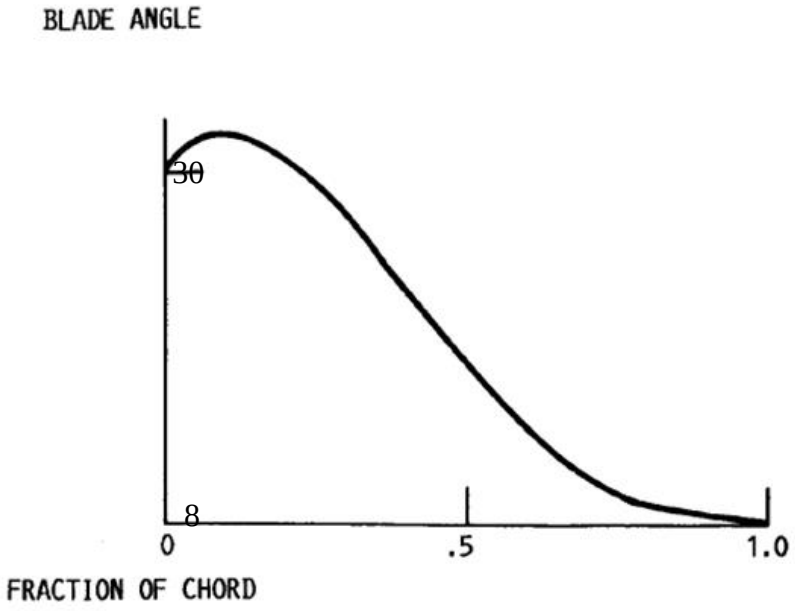

Figure 28. the near hub section blade angle distribution (solidity of 3.42)

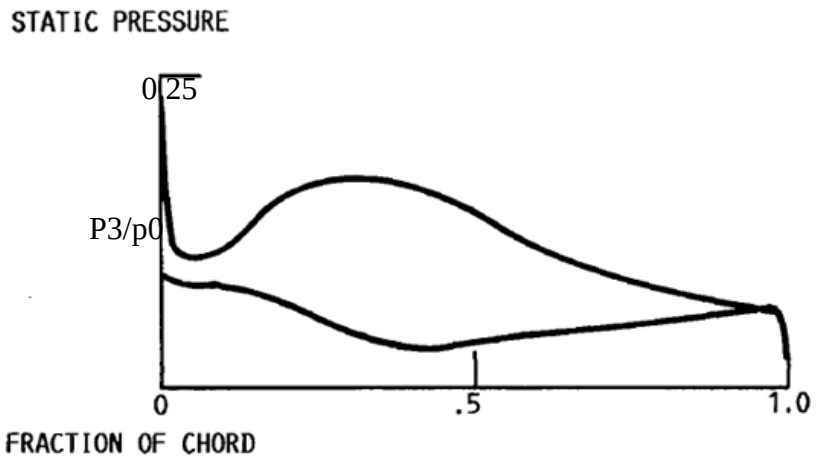

Figure 29. the near hub section static pressure distribution for the chosen blade angle distribution (solidity of 3.42)

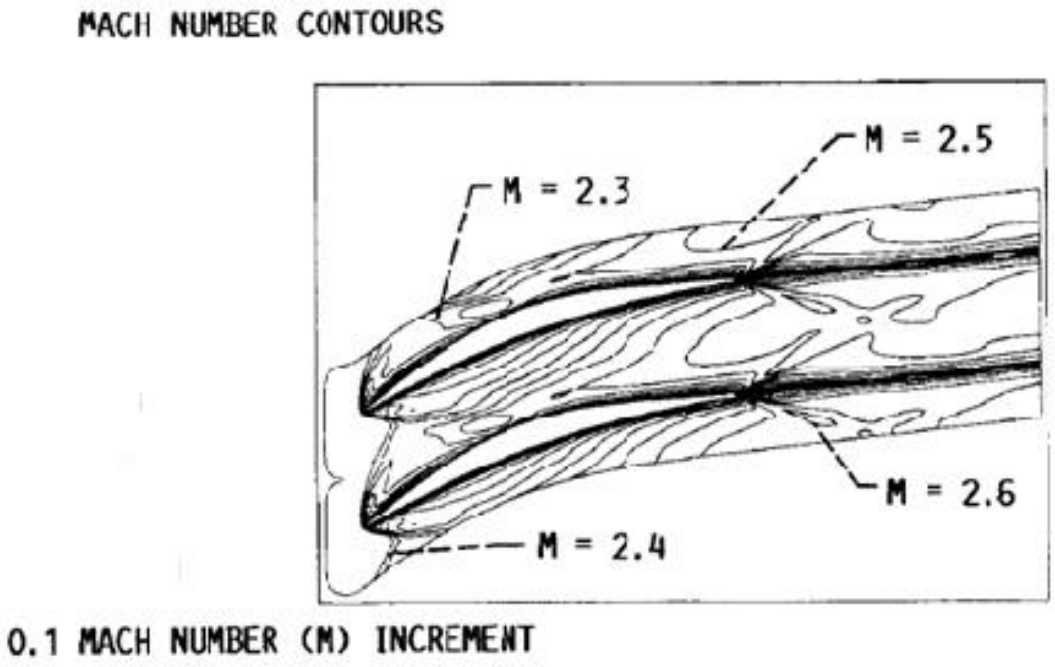

Figure 30. near hub section velocity contours for the chosen blade angle distribution (solidity of 3.42)

From the above figures we see that, the chosen blade angle distribution "yields much smoother static pressure distribution. The blade is loaded all the way to the trailing edge. Also, the static pressure on both the suction and pressure surfaces is equal at the trailing edge so that no strong adjustment of the flow downstream of the blade (like a shock wave) is required". [27]

Figure (32) shows “the velocity vector plot at the trailing edge shows t h a t the flow exits smoothly from the blade. The reduction in the static pressure gradients in the improved blade design results in Mach number contours which indicate a very thin viscous flow region. Also, the leading edge weak shock wave is completely contained in the covered flow passage and does not impact on the suction surface of the adjacent blade”. [27]

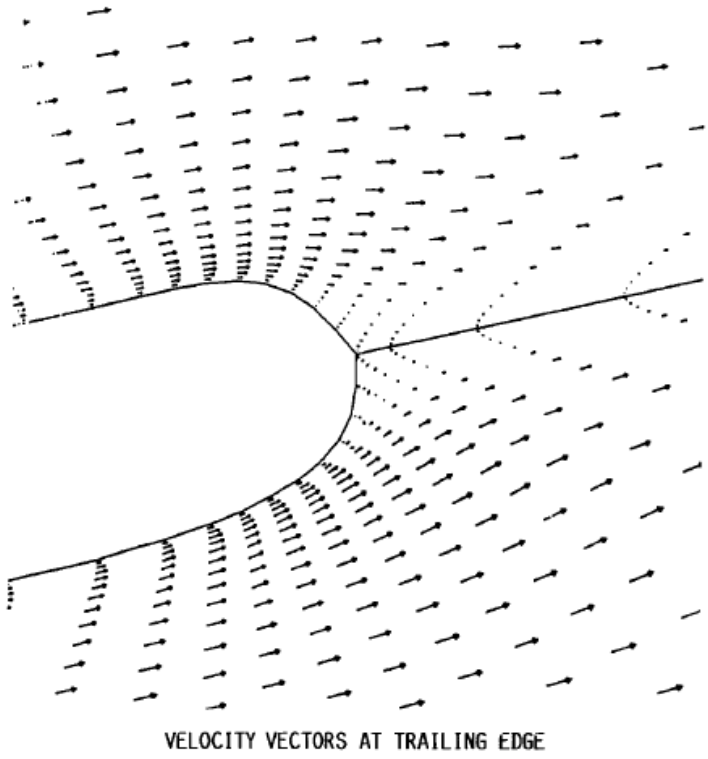

Figure 31. near hub section (solidity 3.42) trailing edge velocity vectors

A double circular arc (DCA) and an improved polynomial curve fitted thickness distribution are illustrated by figure (33). “The almost constant static pressure variation in the trailing edge region of the blade for the DCA thickness distribution produces essentially no loading over the last 20 percent of the blade. Also, the Mach number contour plot indicates a weak shock wave may be occurring at the trailing edge of the thicker DCA blade”. “The static pressure distribution for the improved polynomial thickness distribution shows moderate blade loadings and a thinner more streamlined blade (especially evident over the rear portion of the blade) as seen by the Mach number contour plot”. [27]

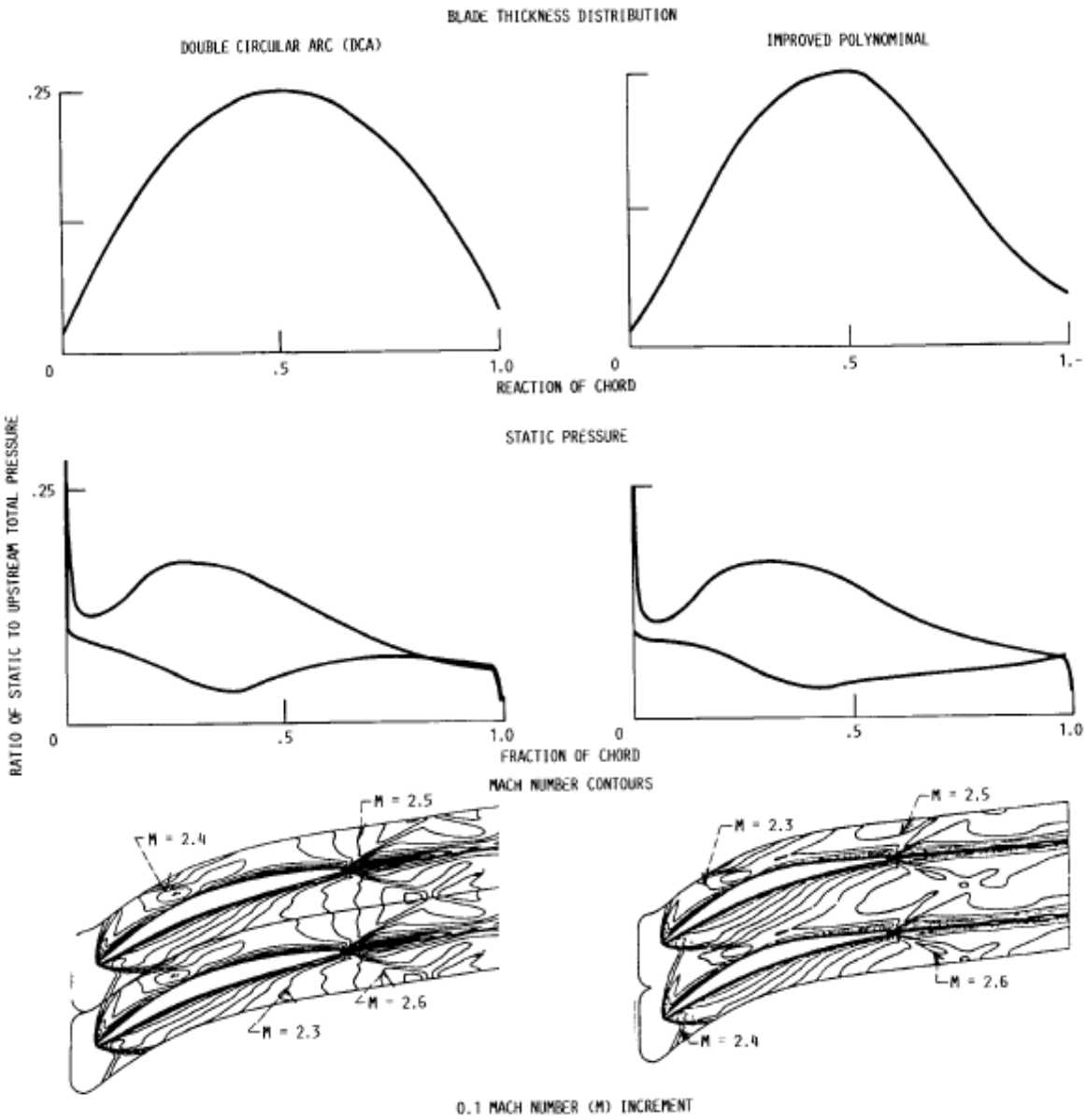

Figure 32. near hub section (solidity of 3.42) blade thickness distribution and its static pressure distribution and velocity contours

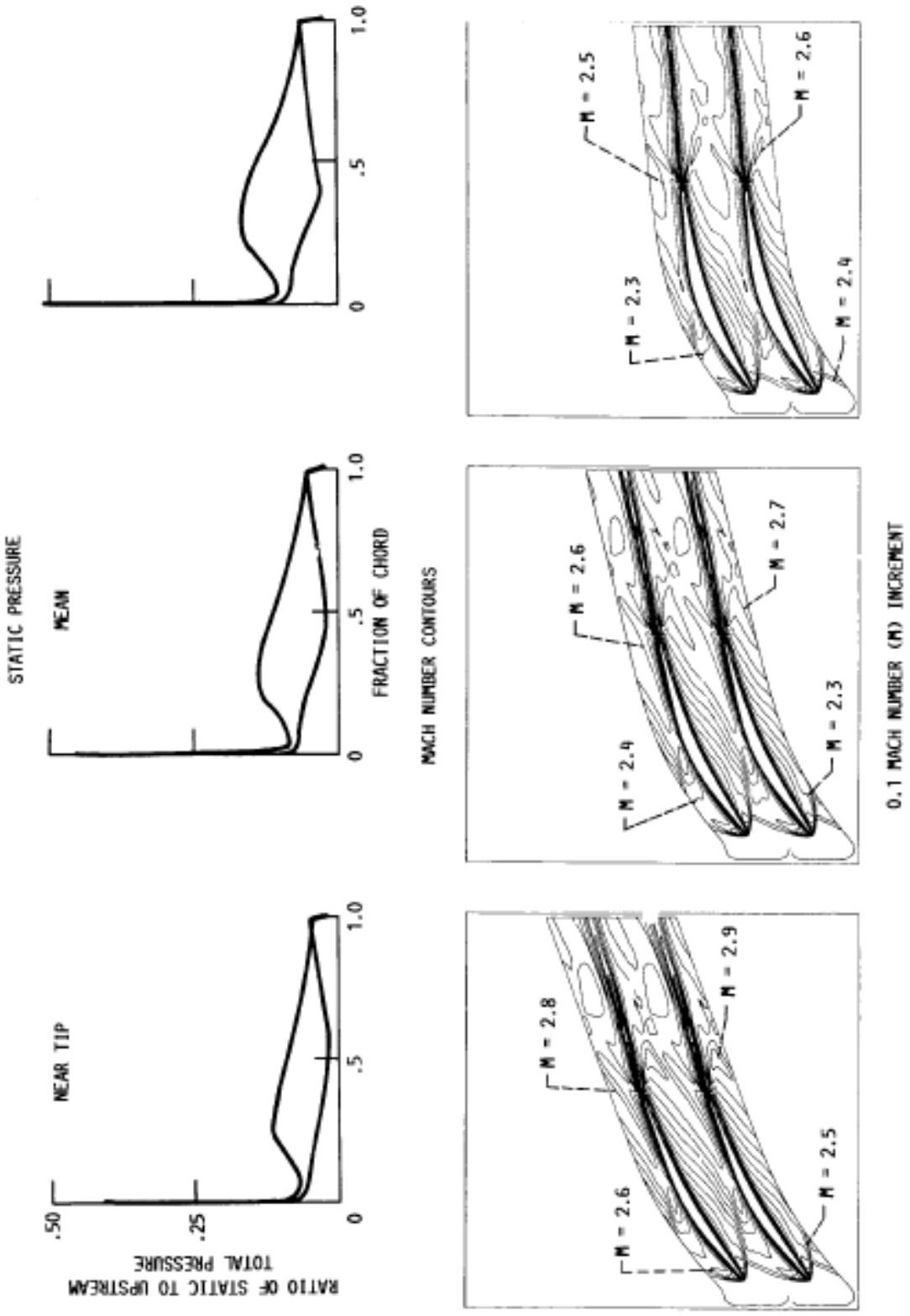

Figure 33. flow performance for the final rotor blade design at the near tip, mean and near hub sections (solidity 3.17, 3.27and 3.42)

Stator design

As minsioned before the stator is designed in a way that eliminate the swirl of the rotor with the same philosophy that used in rotor design. Figure (35) illustrate the static pressure distribution and the Mach number counters. [27]

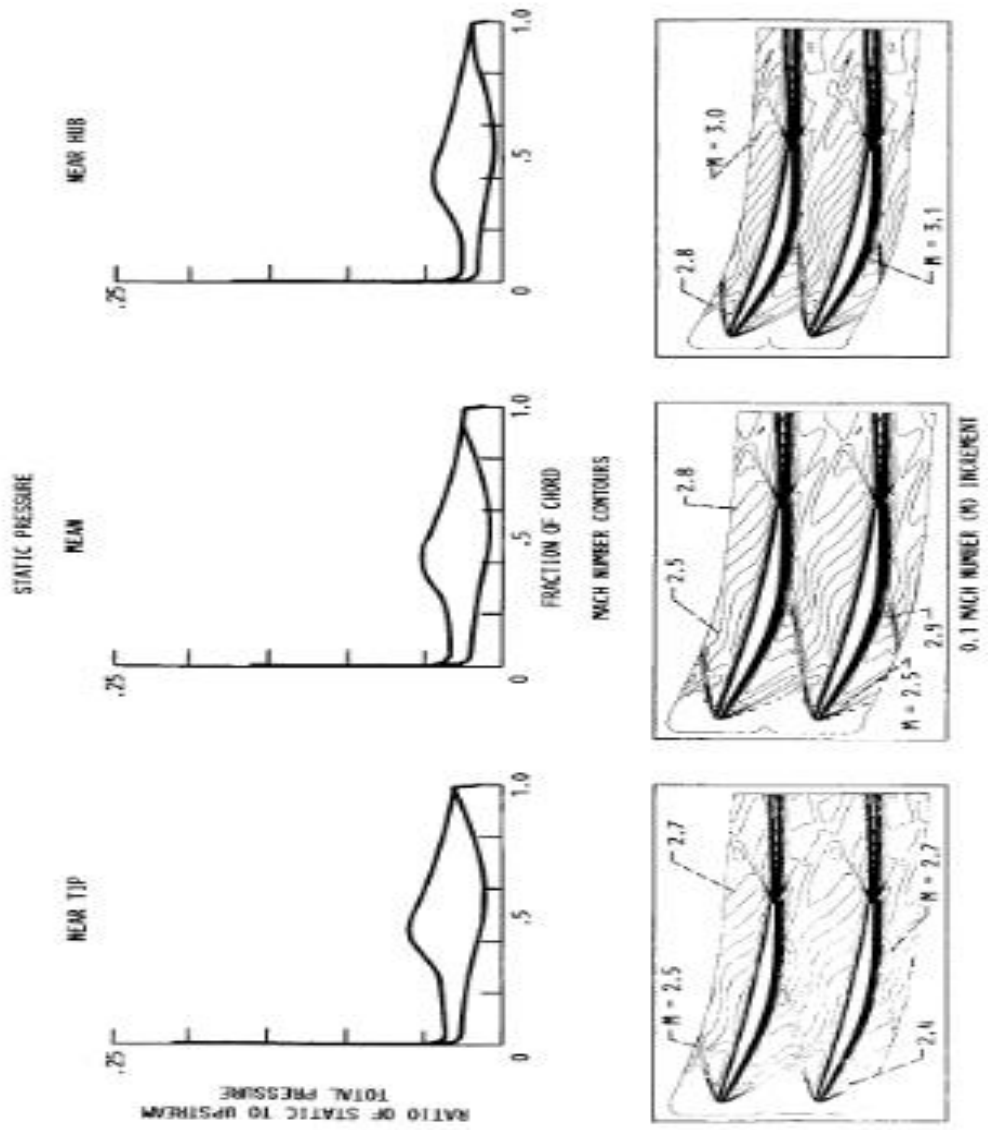

Figure 34. flow performance for the final stator blade design at the near tip, mean and near hub sections (solidity 3.12, 3.40and 3.60)

Off desgin condition diagram

The off-design condition diagram illistrated by figure (36) shows the relation between the the pressure ratio, the mass flow rate and the Mach No. at blade insidance changes between -5 even +5. The design point is chosen to be at the zero incidance line. [27]

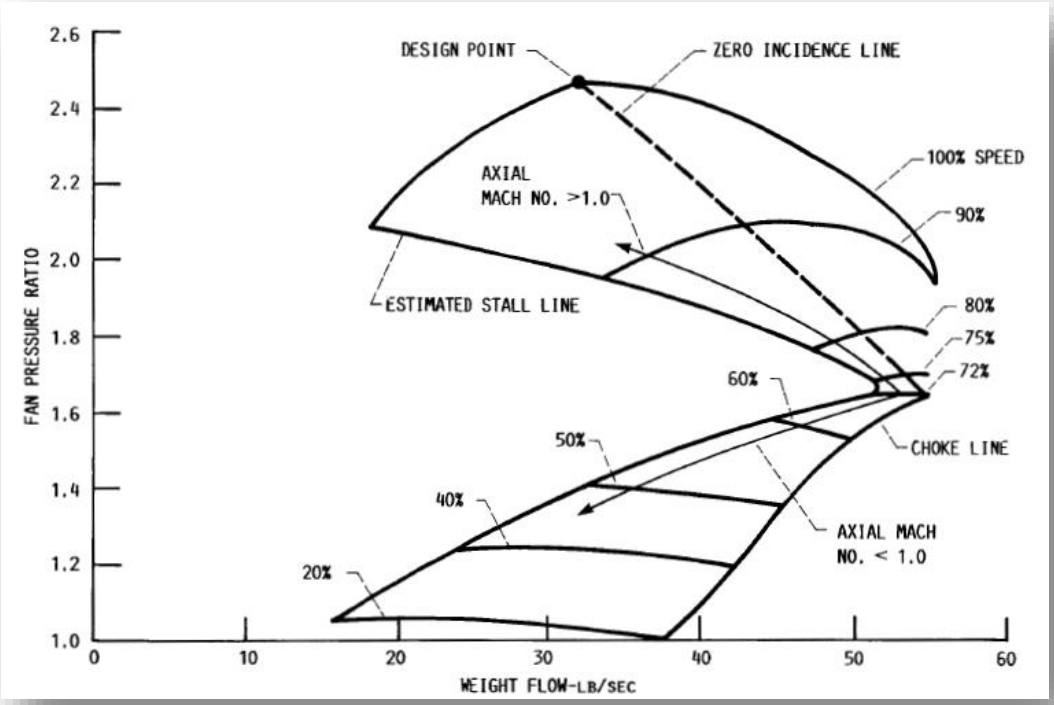

Figure 35. predicted STF fan performance map

The results were that, they proved the concept of the supersonic through flow fan computationally then experimentally, the STF fan blade which they had been designed has the characteristics mentioned in the tables (3) and (4) and figures (35) and (36). And they success in keeping two weak shock waves at the leading and trailing edges and satisfying the requirements they had been decided.

3.5 Design optimization methods

The first methodology had been established at Linkoping university, where "a novel design framework is being developed to support the initial conceptual design phase of new

aircraft. By linking together various modules via a user-friendly spreadsheet interface, the framework allows multidisciplinary analysis and optimization to be carried out" see figure (37). This framework sacrifice with the accuracy via does not considering of the uncertainty effect to meet the required computing time. The framework was tested through *two different case studies.* "The first one is a hypothetic wing-box design that is studied with respect to aerodynamic efficiency and loads, and to structural analysis. In this study two approaches were compared. In one case the wing-box design was optimized with a fixed number of structural elements, where only dimensions and position were allowed to change. Then the same wing-box was analyzed allowing also the number of structural elements to vary. Thus only the parts that are required are left and a more efficient design can be obtained. In the second case study a mission simulation is performed on a UAV-type aircraft. Required data for the simulation are gathered from the CAD model and from aerodynamic analysis carried out with PANAIR, a high order panel code. The obtained data are then used as inputs parameters for flight simulation in order to determined hydraulic systems characteristic".

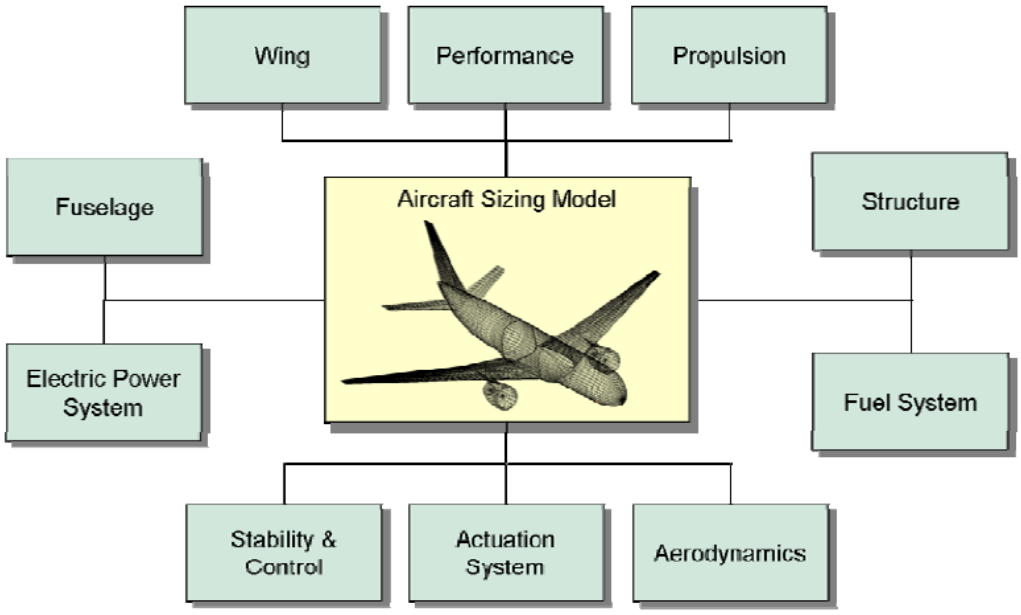

Figure 36. The complete aircraft design framework

The second case is a simple case, an airfoil design. The problem goal is to design an efficient wing which serve also as voluminous fuel tank. the efficient wing design requires lower wing thickness while the voluminous fuel tank need a higher wing thickness. The problem shows a discrepancy between two objectives. The problem can be categorized as one discipline multi-objectives optimization problem. The optimization of this problem will based on Pareto surfaces or Pareto fronts concept. [28]

"From the flow conditions and the overall estimated weight of the aeroplane", the required lift coefficient was computed. For each candidate design, an iterative flow analysis was taking place until the angle of attack that yields that target lift coefficient was found. The efficient airfoil shape represented as that one produce minimum drag coefficient and so, for each candidate airfoil design, the drag coefficient at the angle of attack was calculated using full potential codes with viscous corrections and stated as low-level efficiency objective. The airfoil shape was parameterized using Ferguson splines. Using 2D viscous flow simulation code (2D panel code with viscous boundary layer, implemented in MATLAB® and Python), the airfoil shape was outlined. "The maximum thickness used as a surrogate for the fuel tank volume". "A 'brute force' technique is therefore to spray the design space defined by the variables of the parametric aerofoil with a uniform, dense coverage of designs" (a Latin hypercube sample planning algorithm). "The two objectives can be calculated for all of these designs, and the boundary of the cloud of points thus obtained will be the Pareto front" see figure (37). [28]

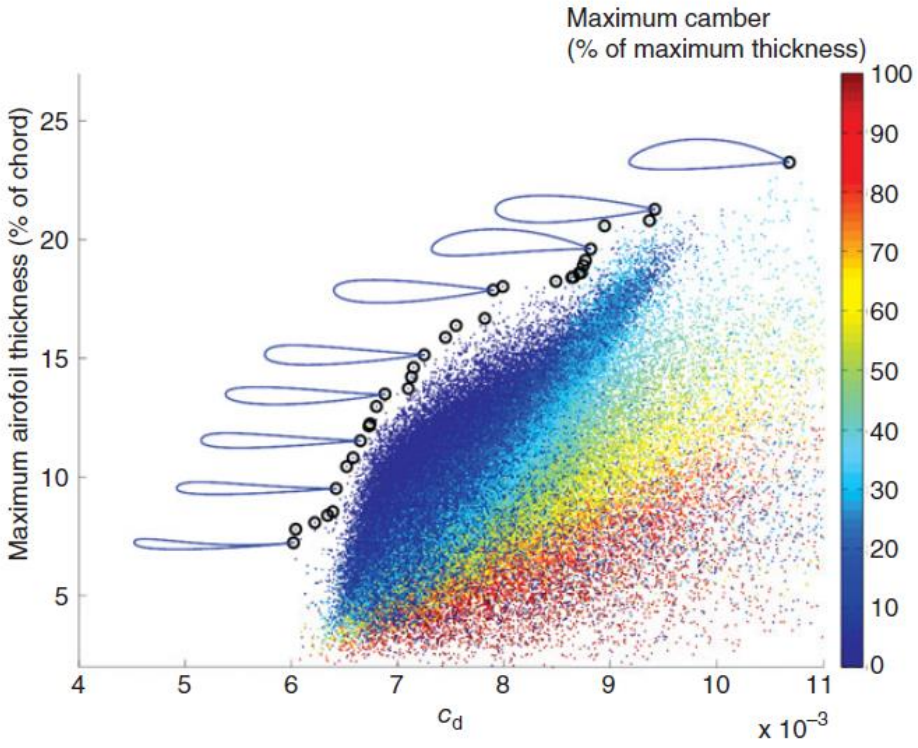

Figure 37. The two objectives, cd and maximum thickness, corresponding to just over 130 000 airfoils generated using a parametric model and a space-filling experiment planning algorithm. The non-dominated points are highlighted with black circles and the aero foils they represent are also shown alongside some of them.

"The Pareto front of this cloud of points (coloured according to the camber of the aerofoils) is the top-left boundary" which the most that satisfy the design goals, maximize the thickness and maximize the wing efficiency which represented in a form of minimizing the produced drag. "The Pareto optimal, or non-dominated subset of this large set of designs is highlighted by black circles. This set is selected such that any other selection that would lead to an improvement against one objective, would lead to a deterioration against another". Also, some airfoils corresponding to the black circles was plotted. [28]

Evaluation

Since all the black circles are optimal designs, there is a need to another “objective or some design constraint to pick the final design”. This method is simple reliable if the available information and the analysis are trusted.

4 Modeling

4.1 Introduction

The models are equations that approximate and describe the response of the wing combination to the air loads. They are works together as **Frame** to define the wing combination. ***The wing combination divided into 7 stations***: the first at the sliding part leading edge and the second after the sliding part trailing edge, the third at the rotor inlet while the fourth after its outlet, station 4 after the stator outlet. Stations 6 and 7 at the original wing leading and trailing edges respectively.

4.2 System of axes

The aircraft main axes are: X_{CG}, Y_{CG} and Z_{CG}. They pass through the aircraft center of gravity. Secondary axes had been used for simplicity of work such as: X, Y and $Z, X', Y'$and Z', $X'', Y''$and Z'' …etc. they are translated or rotated by angle from the main axes. Once the maneuver will be established from level flight, it will be achieved in short time and the fuel consumption will decrease as the aircraft deaccelerates and the fan build up to carry the aircraft; it is fair to take the aircraft mass to be constant during the maneuver besides, the only reason lead to the aircraft center of gravity shift is the extending of the sliding part which carry the fans mass which shift the CG forward into certain point, we took this point as a constant origin for the aircraft for simplicity where the axes X_{CG}, Y_{CG} and Z_{CG} located. Its location depends on the mass of the sliding part, the fans and their mass distribution. Thus, t had been estimated after the design of the sliding part and the modification of the fans and then the secondary axes were translated to that origin.

System 1:

It has the samples X, Y and Z. The X-axis coincides with the rib number 1. While the origin point locates at the rib leading edge:

X: parallel to the axis X_{CG} with a shift distance of -2.28

Y: parallel to the axis Y_{CG}.

Z: parallel to the axis Z_{CG}.

System 2:

X': corresponding to the axes X_{CG}.

Y': parallel to the axis Y_{CG}.

Z': parallel to the axis Z_{CG}.

System 3:

It has the samples X'', Y'' and Z''. The origin point locates at the intersection of the rib No.1 and the spar No.2. While the Y''-axis coincides with the spar No.2:

X'': rotated than the axis X_{CG} by 29 degrees with a shift distance of -2.28

Y'': rotated than the axis Y_{CG} by 29.

Z'': parallel to the axis Z_{CG}.

System 4:

It has the samples X^m, Y^m and Z^m. It is a movable system serves to scale the wing sections from the rib No.1 section. The origin point locates at the leading edge of the section while the positive X^m-axis coincides with the section chord line.

Z^m: parallel to the axis Z_{CG}.

System 5:

It has the samples X''', Y''' and Z'''. This system used to model the prop-fans. All axes are parallel to the aircraft axes with shift distance. The origin point coincides with the fan huh center while the Z'''-axis is parallel to the radius direction for the chosen control volume.

4.3 SU-35S wing aerodynamic model

4.3.1 Introduction

The wing aerodynamic model was needed to provide the values of:

- The wing lift including the increment in the lift due to the prop-fans action.
- The wing lift distribution.
- The wing total drag.
- The wing aerodynamic moment produced by the total wing lift.

4.3.2 The total lift

The prop-fans distributed along the wing span such that the wing upper surface is supplied by a constant mass flow rate taking into account there is no swirl.

It is possible to supply the lower surface of the wing by a percentage of the prop fans flow through a slots. The distribution of the prop-fans and the slots is smooth such that a homogenous flow cover the wing.

For the traditional wings, at the moment of the impact of the flow with the wing L.E, the mass flow rate is equally for the upper and the lower surface of the wing (since the area of the flow, the speed and the density are the same, not distributed yet) but here, there are two cases:

1. If the slots are closed: the flow pass into the upper and the lower surface of the wing combination with the forward speed, but due to the action of the prop fans the air which pass into the upper surface will accelerated. Thus, the freestream velocity for the upper V_{6_u} surface is higher than for the lower surface V_{6_l}:

   $V_{6\_u} = V_{6\_l} + \Delta V$ … (1)

   Then the lift can be divided into two parts:

   - L_1: due to the equally $V_6 = V_{6\_l} = V_1 = V_\infty$: this part is produced by the wing shape and it estimated by the traditional lift equation:

     $L_1 = \frac{1}{2}\rho {V_\infty}^2 S C_L$ … (2)

- L_2: due to ΔV: this part has estimated using the source panel method by substituting:

  $V_\infty = V_{6\_u} - V_{6_l} = \Delta V_6$ … (3) for the upper surface panels

  $V_\infty = 0$ … (4) for the lower surface panels

2. If an amount of the flow upper surface pass to the lower surface of the wing through the slots (controlled); a different mass flow rates will supply the upper and the lower surface. This difference produces pressure difference between the upper and the lower surface and thus produce additional lift value effect in the previous lift produced in point 1.

The first case has been discussed.

Note: Each lift branch has been estimated individually (the interaction is not considered for simplicity which effect the accuracy of the solution).

4.3.3 (L_1) estimation

Since SU-35S is a fighter, it has a thin airfoil. The classical thin airfoil theory for a cambered airfoil had been used to model the wing for incompressible inviscid flow and then a correction for the compressibility effects, 3D-wing effects and the viscosity effects took place. To simulate the aerodynamic forces and moments distribution along the semi-span, the process had been repeated on finite number of sections (airfoils).

Generally, the classical thin airfoil theory is for inviscid incompressible ir-rotational flow. But, below the stall angle of attack and at low airflow speeds over the airfoil, the actual experimental data for the lift and moment agrees very well with that values predicted by the inviscid classical thin airfoils theory, see table (5) which compares the experimental and theoretical data for NACA 23012 airfoil. In other word the classical thin airfoil theory cannot predict the flow separation.

Since the small angle of attack are one of the maneuver constraint and the flow over the real wing below the 0.7 Mach, the using of the inviscid classical thin airfoils theory had been acceptable.

Table 5. thin airfoil theory (calculated and experimental data)

	Calculated by the classical thin airfoil theory	Experiment
$\alpha_{L=0}$	-1.09°	-1.1°
$C_{l\ 0}\ at\ \alpha = 4^{\circ}$	0.559	0.55
$C_{m_{c/4}\ 0}$	-0.0127	-0.01

The flow over the wing is ir-rational because the wing receives axial flow from the rotor-stator combination and because the angle of attack is small, the separation over the wing is inconsiderable. Thus, the thin airfoil theory and Prandtl-Glauert compressibility correction are available to use.

4.3.4 Modeling process

The whole airfoil is approximated by the camber line and the effect of the airfoil shape on the flow is represented by a vortex sheet placed on the chord line in the plan (X-Z) and extended to a unit length along the Y-axis. See figure (38) below.

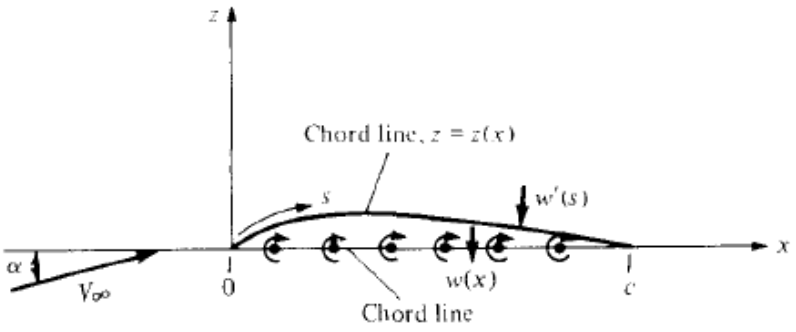

Figure 38. thin airfoil theory

This model is based on making the camber line a streamline in the flow.

A constraint on the using of the classical thin airfoil theory is that the angle of attack must be small (in radian) and this constraint considered in the optimization.

SU-35S has no aerodynamic twist. Thus the zero-lift angle of attack still constant. The zero-lift angle of attack has been estimated for near root section using the classical thin airfoil theory for cambered airfoils:

$$\alpha_{L=0} = -\frac{1}{\pi}\int_0^{\pi}\frac{dz}{dx}\,(cos\theta_0 - 1)\,d\theta_0 \ldots (5)$$

To estimate $\frac{dz}{dx}$ for the thin airfoil smooth camber line at the near the root section, a second order equation is solved for its coefficients A, B and C to estimate z(x) at first:

$$Ax^2 + Bx + C = z(x) \ldots (6)$$

Using the excel table (7) below:

Table 6. section N1 data

X	Z-upper surface	Z-lower surface	Camber line
0	0	0	0
0.002206	0.006618	-0.00551	0.000551
0.011029	0.014706	-0.01103	0.001838
0.036765	0.029412	-0.02206	0.003676
0.110294	0.047794	-0.03493	0.006434
0.147059	0.055147	-0.04044	0.007353
0.367647	0.088235	-0.05699	0.015625
0.551471	0.110294	-0.06985	0.020221
1.102941	0.147059	-0.09559	0.025735
1.470588	0.165441	-0.10846	0.028493
1.838235	0.176471	-0.11765	0.029412
2.205882	0.180147	-0.11765	0.03125
2.941176	0.165441	-0.11029	0.027574
3.67647	0.128676	-0.09191	0.018382
4.227941	0.084559	-0.05882	0.012868
4.595588	0.055147	-0.03676	0.009191
4.963235	0.025735	-0.01471	0.005515
5.279411	0	0	0

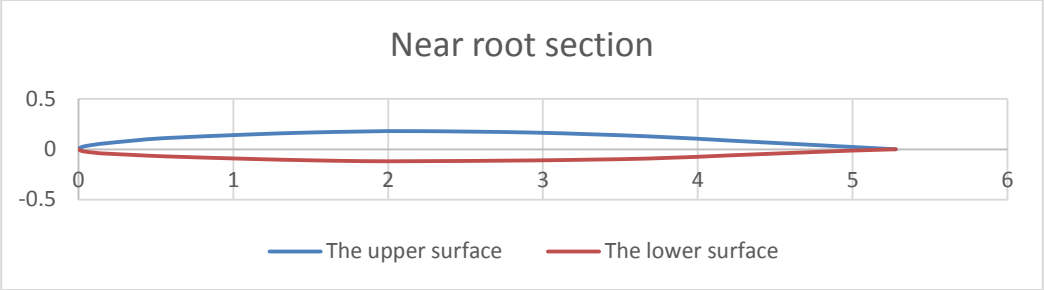

Figure 39. near root section

Note: X- has been measured from the near root section leading edge in meters.

At $x = 0$: $z = 0$

$\Rightarrow C = 0$

At $x = 0.002206$: $z = 0.000551$

$\Rightarrow A(0.002206)^2 + B(0.002206) = 0.000551$ … (7)

At $x = 0.036765$: $z = 0.003676$

$\Rightarrow A(0.036765)^2 + B(0.036765) = 0.003676$ … (8)

Solving equations (7) and (8) together:

$A = -2.591$

$B = 0.195$

$\Rightarrow z(x) = -2.591\ x^2 + 0.195\ x$ … (9)

Using this equation to calculate the Z coordinate of the camber line for the X values, the resulting camber line is corresponding to the real camber line except between [0:0.002206 m] and for accuracy purposes, the value of B has been adjusted to 0.250 through this sector. See figure (40) and (41).

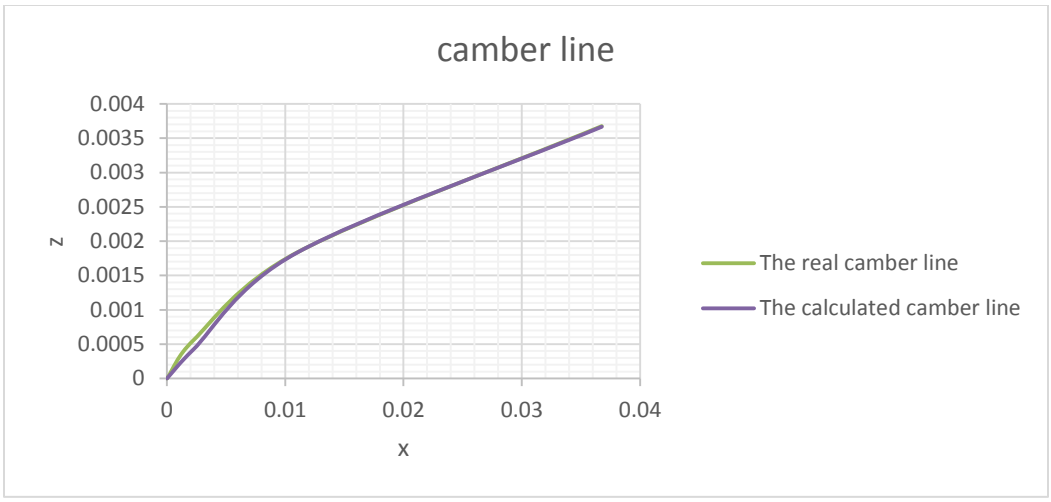

Figure 40. camber line 1

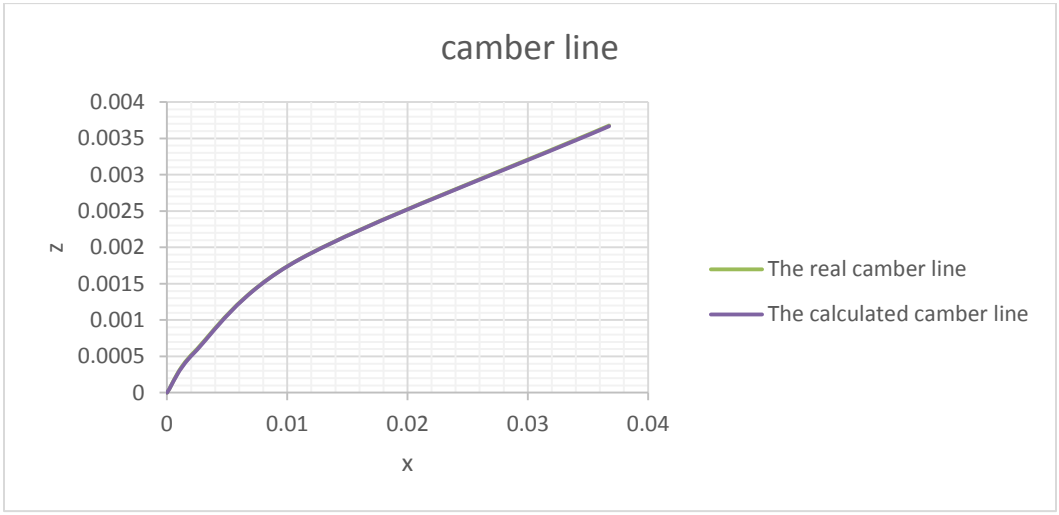

Figure 41. camber line 2

Thus:

$$Z(X) = -2.591X^2 + \ 0.250X \Rightarrow \frac{dz}{dx} = -\ 5.902\ x + 0.250, \ldots\ (10) \qquad for: 0 \leq X \leq 0.002206$$

$$Z(X) = -2.591\ X^2 + \ 0.195X \Rightarrow \frac{dz}{dx} = -\ 5.902\ x + 0.195, \ldots\ (11) \quad for: 0.002206 < X \leq 0.036765$$

The procedure has been repeated along the chord line, and a 6 equations had been estimated to describe the camber line:

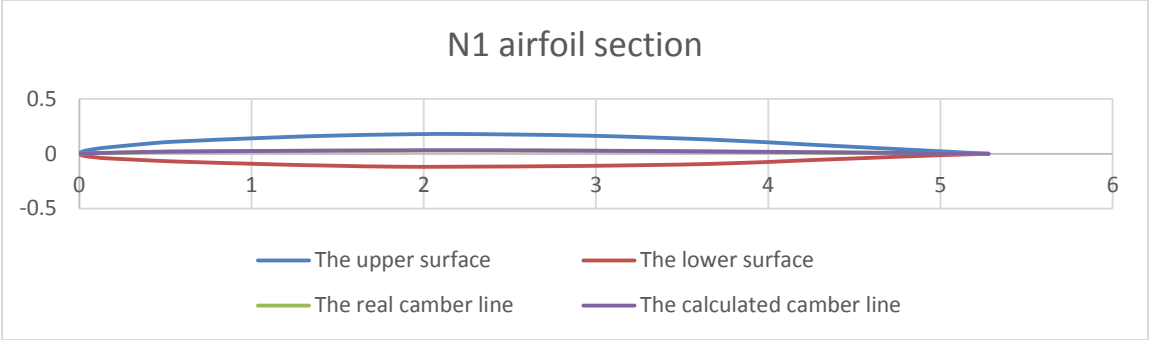

Figure 42. wing airfoil section

Table 7. wing airfoil section equations

X limits	The equation	The derivation
$0 \leq X \leq 0.002206$	$-2.591X^2 + \ 0.250X$	$-5.902\ x + 0.250$
$0.002206 < X \leq 0.036765$	$-2.591\ X^2 + \ 0.195X$	$-5.902\ x + 0.195$
$0.036765 < X \leq 0.551471$	$-0.003X^2 + 0.036X + 0.003$	$-0.006x + 0.036$
$0.551471 < X \leq 2.205882$	$-0.003X^2 + 0.015X + 0.013$	$-0.006x + 0.015$
$2.205882 < X \leq 4.227941$	$-0.003X^2 + 0.011X + 0.022$	$-0.006x + 0.011$
$4.227941 < X \leq 5.279411$	$-0.007X^2 + 0.055X - 0.095$	$-0.014x + 0.055$

$\theta_0 = \ cos^{-1}\left(1 - 2\ \frac{x}{c}\right)$ … (12)

At $x = 0\ m:\ \theta_0 = \ cos^{-1}\left(1 - 2\ \frac{0}{5.279411}\right) = \ 0\ rad.$

At $x = 0.002206\ m:\ \theta_0 = \ cos^{-1}\left(1 - 2\ \frac{0.002206}{5.279411}\right) = 0.041\ rad$ … (13)

$\because x = \frac{C}{2}\ (1 - \ cos\theta_0) = \frac{5.279411}{2}\ (1 - \ cos\theta_0) = 2.639706\ (1 - \ cos\theta_0)$ … (14)

Substitute equation (13) in equation (14):

$\frac{dz}{dx}(\theta_0) = -5.902\,[2.639706\,(1 - cos\theta_0)\,] + 0.250$ ... (15) $\quad for:\ 0 < \theta_0 \leq 0.041\,rad.$

The procedure has been repeated for $0 < \theta_0 \leq \pi\,rad.$, see the table (8):

Table 8. wing airfoil section equations

X limits	θ_0 limits	The derivation
$0 \leq X \leq 0.002206$	$0 < \theta_0 \leq 0.041$	$-5.902\,[2.639706\,(1 - cos\theta_0)\,] + 0.250$
$0.002206 < X \leq 0.036765$	$0.041 < \theta_0 \leq 0.167$	$-5.902\,[2.639706\,(1 - cos\theta_0)\,] + 0.195$
$0.036765 < X \leq 0.551471$	$0.167 < \theta_0 \leq 0.658$	$-0.006[2.639706\,(1 - cos\theta_0)\,] + 0.036$
$0.551471 < X \leq 2.205882$	$0.658 < \theta_0 \leq 1.406$	$-0.006[2.639706\,(1 - cos\theta_0)\,] + 0.015$
$2.205882 < X \leq 4.227941$	$1.406 < \theta_0 \leq 2.216$	$-0.006[2.639706\,(1 - cos\theta_0)\,] + 0.011$
$4.227941 < X \leq 5.279411$	$2.216 < \theta_0 \leq 3.142$	$-0.014[2.639706\,(1 - cos\theta_0)\,] + 0.055$

$$\alpha_{L=0} = -\frac{1}{\pi}\left\{\begin{array}{l} \int_0^{0.041}[-5.902\,[2.639706\,(1 - cos\theta_0)\,] + 0.250]\,(cos\theta_0 - 1)\,d\theta_0 \\ + \int_{0.041}^{0.167}[-5.902\,[2.639706\,(1 - cos\theta_0)\,] + 0.195]\,(cos\theta_0 - 1)\,d\theta_0 \\ + \int_{0.167}^{0.658}[-0.006[2.639706\,(1 - cos\theta_0)\,] + 0.036]\,(cos\theta_0 - 1)\,d\theta_0 \\ + \int_{0.658}^{1.406}[-0.006[2.639706\,(1 - cos\theta_0)\,] + 0.015]\,(cos\theta_0 - 1)\,d\theta_0 \\ + \int_{1.406}^{2.216}[-0.006[2.639706\,(1 - cos\theta_0)\,] + 0.011]\,(cos\theta_0 - 1)\,d\theta_0 \\ + \int_{2.216}^{3.142}[-0.014[2.639706\,(1 - cos\theta_0)\,] + 0.055]\,(cos\theta_0 - 1)\,d\theta_0 \end{array}\right\}$$

$$= -\frac{1}{\pi}\,(0.000 + 0.000 - 0.003 + 0.010 + 0.007 + 0.024)$$

$$\alpha_{L=0} = -0.012\ rad. = -0.687\ degree$$

The lift distribution has been estimated using the modified lifting line theory for the swept wings. This theory considers the 3D effect, it considers the induced angle of attack which a reduction in the geometric angle of attack due to the down wash. But, theory has a limitation that the line where the lift is taken on must be straight.

The lift had been taken along the aerodynamic line which is a straight line mostly. At the interval $-5.51 \leq y_{ac}'' \leq 0.19$, the aerodynamic centers line is a straight line sweptback by 35 degrees and its coordinates are given as follows:

At $y_{ac}'' = -1.54$ $\quad \Rrightarrow x_{ac}'' = 0.77$

At $y_{ac}'' = -5.51$ $\quad \Rrightarrow x_{ac}'' = 0.23$

Thus,

$0.14\, y_{ac}'' + 0.99 = x_{ac}''$ ... (16)

At the interval $0.31 \geq y_{ac} \geq -0.12$, the aerodynamic centers line is straight line sweptback by 35 degrees also, but shifted upward than the first aerodynamic centers line by 0.23m. for simplicity purpose, this line is shifted down by 0.23m to be extension for the first line. And it given by the equation (16) above.

The interval $0.96 \geq y_{ac}'' \geq 0.19$ has been ignored; since it has a small area and the its aerodynamic centers points corresponding to unique y' point (forming a line connecting between the right end of the first aerodynamic centers line and the left end of the second one, for the left side of the wing). This point was not chosen as control point.

The tip aerodynamic center is a discrete point at $x_{ac} = 0.54$ and for accuracy, this point (tip) is not considered. The last interval $-5.51 \geq y_{ac}'' \geq -6.05$ has been divided into two parts, $C_1 < 0.54$ at the interval $-5.51 \geq y_{ac}'' \geq -5.88$ which is also a straight line sweptback by 15 degrees. This line has a small length comparing with the first aerodynamic centers line. Thus it has been rotated anticlockwise by 20 degrees. The second part at $C_1 \geq 0.54$ at the interval $-5.88 \geq y_{ac}'' \geq -6.05$, the aerodynamic centers line is a point corresponding to the tip aerodynamic center and it treated as the tip. See figure (43).

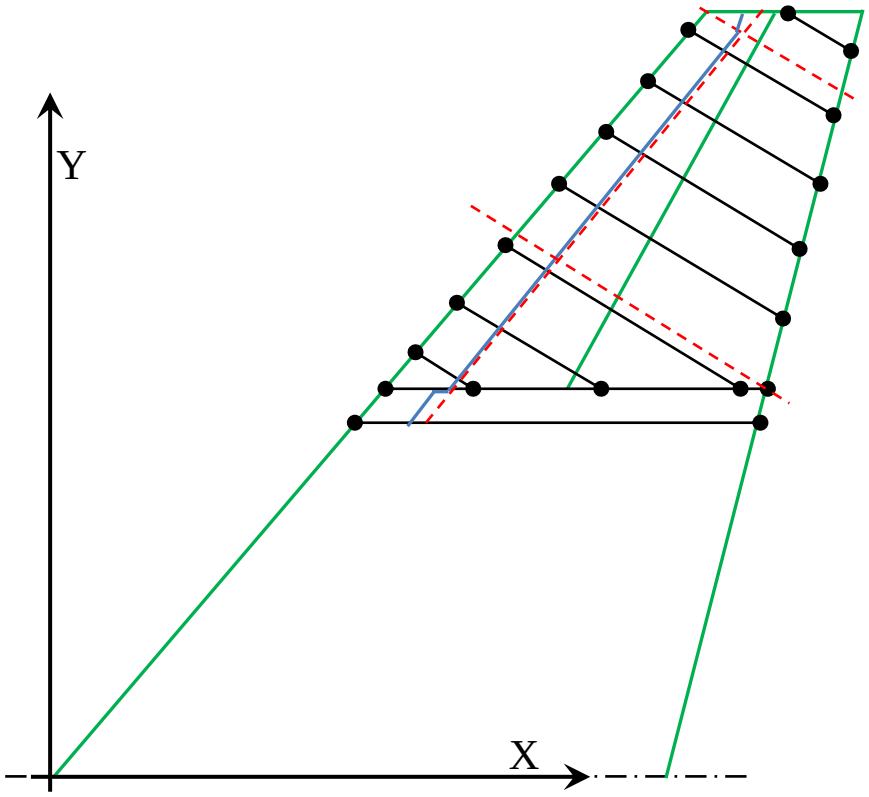

Figure 43. aerodynamic line (blue)

The lift distribution is given by equation (17) below.

$$L_1'(y) = \rho\, V_\infty\, \Gamma(y) \ldots (17)$$

At near root section and the tip section, the rib is parallel to the aircraft longitudinal axes. Thus, the velocity equal to the free stream velocity V_∞ while for the sections between them, the ribs are perpendicular over the middle spar which sweptback by 29 degrees thus, the velocity which produce the lift is $V_\infty \cos 29$.

Using the modified lifting line theory: the lifting line is placed one the aerodynamic centers line. Once the wing is sweptback, the lifting line is also swept back by an angle equal to the aerodynamic centers line sweep angle Λ_{ac}. Series of bound vortices are coincided to the lifting line and a two free trailing vortices trail from the two ends of each bound vortex to infinity $+\infty$. The airfoil sections which incline by 61 degrees (180 -90 – 29 = 61) from the Y axis build the lift with a velocity of $V_\infty \cos 29$. See figures (44) and (45).

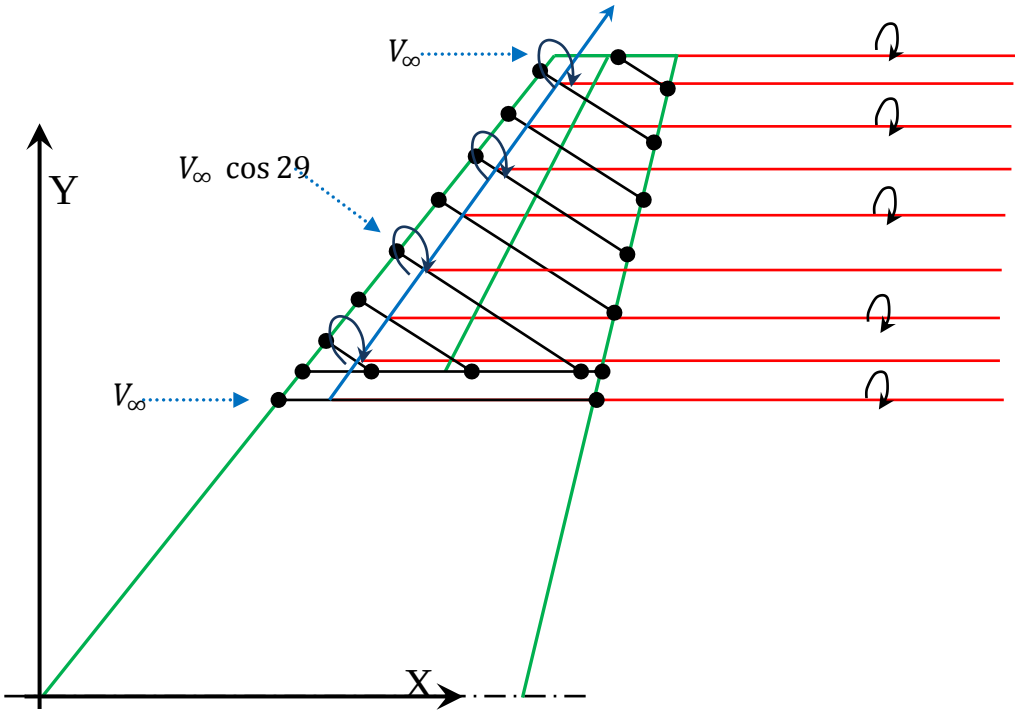

Figure 44. modified lifting line theory 1

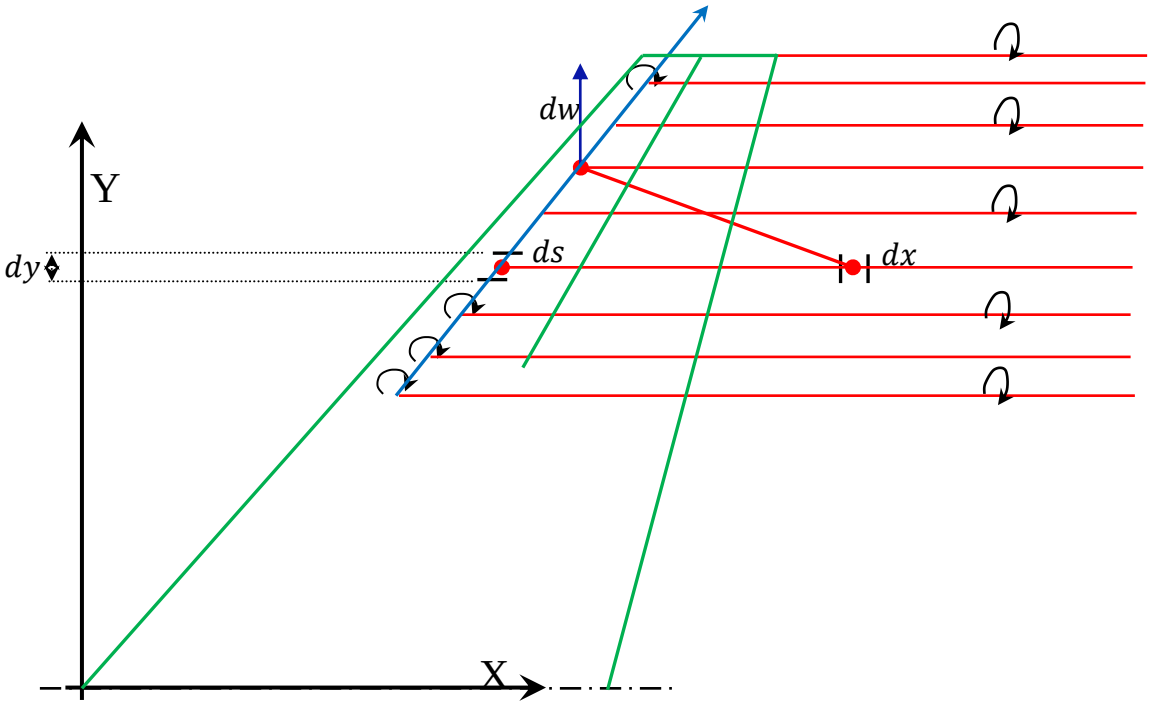

Figure 45. modified lifting line theory 2

When the velocity V_∞ and $V_\infty \cos 29$ interact with the vortices on the bound vortex, lift will be generated along the bound vortex (the lifting line). Thus, this simulate the local values of the lift in the aerodynamic centers. While the downwash generated by the tip vortices effect is simulated by the free trailing vortices which form a sheet along the span. See figure (46).

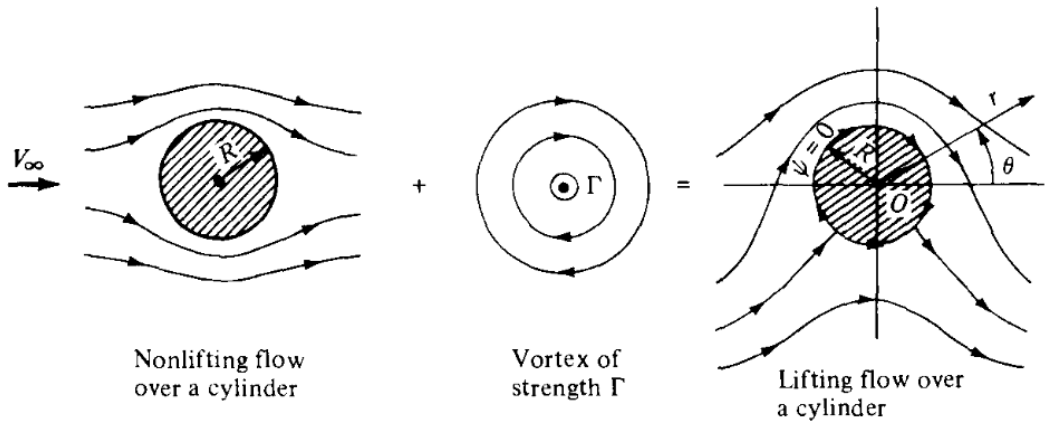

Figure 46. lift simulation using models

The lift which generated by the element ds of the lifting line is given by

$$dL_1 = \rho V_\infty \cos\Lambda_2 \ \Gamma \, \mathrm{ds} = \rho V_\infty \cos\big(\Lambda_{ac} - (\Lambda_{ac} - \Lambda_2)\big) \ \Gamma \, \mathrm{ds} \ \ldots (18)$$

$$\Lambda_{ac} - \Lambda_2 = 35 - 29 = 6 \, degrees$$

$$\cos(\Lambda_{ac} - 6) = \cos\Lambda_{ac} \cos(6) + \sin\Lambda_{ac} \sin(6) \ \ldots (19)$$

$$\therefore dL_1 = \rho V_\infty \left[\cos\Lambda_{ac} \cos(6) + \sin\Lambda_{ac} \sin(6)\right] \Gamma \, \mathrm{ds} \ \ldots (20)$$

$$dL_1 = \rho V_\infty \left[\cos\Lambda_{ac} \cos(6)\right]\Gamma \, \mathrm{ds} + \rho V_\infty \left[\sin\Lambda_{ac} \sin(6)\right]\Gamma \, \mathrm{ds} \ \ldots (21)$$

$$\because dy = ds \cos\Lambda_{ac} \qquad \Rightarrow ds = \frac{dy}{\cos\Lambda_{ac}}$$

$$\therefore dL_1 = \rho V_\infty \cos(6) \, \Gamma \, \mathrm{dy} + \rho V_\infty \sin 35 \sin(6) \, \Gamma \frac{\mathrm{dy}}{\cos 35} \ \ldots (22)$$

$$\therefore dL_1 = 0.99 \, \rho V_\infty \, \Gamma \, \mathrm{dy} + 0.07 \, \rho V_\infty \, \Gamma \, \mathrm{dy} \ \ldots (23)$$

$$\therefore dL_1 = 1.06 \ \rho V_\infty \, \Gamma \, \mathrm{dy} \ \ldots (24)$$

If Line1 is defined as the lifting line (the aerodynamic centers line) while Line2 defined as the projection of Line1 in the Y axis (for $-\frac{b}{2} \leq y \leq \frac{b}{2}$), the lift produced by Line1 is higher by 6% than the lift produced by Line2. And that is expected; because the sweepback increases the wing loadings.

The classical lifting line theory is applicable to the lifting line Line2:

The circulation which generated by element vortex (dx) from the free trailing vortex on the lifting line Line2 at $y = y_0$ is given by Biot-Savart law for semi-infinite straight vortex filament:

$$dw\,(y_0) = \frac{d\Gamma}{4\pi h} \quad \ldots (25)$$

$$h = y - y_0$$

The downwash at y_0 due to all the trailing vortices sheet from the root to the tip for both sides of the wing:

$$w\,(y_0) = -\frac{1}{4\pi}\left[\int_{y_r}^{b/2} \frac{\left(\frac{d\Gamma}{dy}\right)}{y - y_0} dy + \int_{-b/2}^{-y_r} \frac{\left(\frac{d\Gamma}{dy}\right)}{y - y_0} dy\right] \quad \ldots (26)$$

The change in the circulation has been estimated as follow: for the general lift distribution and thus general circulation distribution, the circulation distribution has been approximated using Fourier sine series:

$$\Gamma(\vartheta) = 2bV_\infty \sum_1^N A_n \sin n\vartheta \quad \ldots (27)$$

$$\Rrightarrow \frac{d\Gamma}{dy} = \frac{d\Gamma}{d\theta}\frac{d\vartheta}{dy} = 2bV_\infty \sum_1^N n\,A_n \cos n\vartheta \frac{d\vartheta}{dy} \quad \ldots (28)$$

$$y = -\frac{b}{2}\cos\vartheta \qquad \Rrightarrow \vartheta = \cos^{-1}\left(\frac{-2y}{b}\right) \quad \ldots (29)$$

$$\Rrightarrow w\,(\vartheta_0) = -\frac{V_\infty}{\pi}\left[\int_{\vartheta_r}^{0} \frac{\sum_1^N n\,A_n \cos n\vartheta}{\cos\vartheta - \cos\vartheta_0} d\vartheta + \int_{\pi}^{(180 - \vartheta_r)} \frac{\sum_1^N n\,A_n \cos n\vartheta}{\cos\vartheta - \cos\vartheta_0} d\vartheta\right] \quad \ldots (30)$$

$$\alpha = \alpha_{eff} + \alpha_i - i_w \quad \ldots (31)$$

$\because C_{l_0} = 2\pi(\alpha_{eff} - \alpha_{L=0}) \qquad \Rightarrow \alpha_{eff} = \frac{C_{l_0}}{2\pi} + \alpha_{L=0}$ … (32)

$\because L'_1(y_0) = \frac{1}{2}\rho V_\infty{}^2 C(y_0)C_{l_0}(y_0) = \rho V_\infty \Gamma(y_0)$ … (33)

$\Rightarrow C_{l_0}(y_0) = \frac{2\Gamma(y_0)}{V_\infty + C(y_0)}$ … (34)

$\Rightarrow \alpha_{eff} = \frac{\Gamma(y_0)}{\pi V_\infty C(y_0)} + \alpha_{L=0}$ … (35)

$\alpha_i = -\frac{w}{V_\infty}$ … (36)

$i_w = 1\ deg. = 0.02\ rad.$

Substitute equations (35) and (36) in equation (31):

$\alpha = \frac{\Gamma(y_0)}{\pi V_\infty C(y_0)} + \alpha_{L=0} - \frac{w}{V_\infty} - 0.02$ … (37)

α is constant along the wing span; because there is no geometric twist.

Substitute equations (27) and (30) in equation (37):

$$\alpha = \frac{2b}{\pi C(\vartheta_0)} \sum_1^N A_n \sin n\vartheta_0 + \alpha_{L=0} + \frac{1}{\pi}\left[\int_{\vartheta_r}^{0} \frac{\sum_1^N n A_n \cos n\vartheta}{\cos\vartheta - \cos\vartheta_0} d\theta + \int_{\pi}^{(180-\vartheta_r)} \frac{\sum_1^N n A_n \cos n\vartheta}{\cos\vartheta - \cos\vartheta_0} d\theta\right] - 0.02 \quad \ldots (38)$$

For simplification of equation (38) above:

$\because \int_0^\pi \frac{\cos n\vartheta}{\cos\vartheta - \cos\vartheta_0} d\vartheta = \frac{\pi \sin n\vartheta_0}{\sin\vartheta_0}$

Equation (37) has been applied for the integration:

$$\left[\int_{\vartheta_r}^{0} \frac{\sum_1^N n A_n \cos n\vartheta}{\cos\vartheta - \cos\vartheta_0} d\vartheta + \int_{\pi}^{(180-\vartheta_r)} \frac{\sum_1^N n A_n \cos n\vartheta}{\cos\vartheta - \cos\vartheta_0} d\vartheta\right]$$

$$\alpha = \frac{2b}{\pi C(\vartheta_0)} \sum_1^N A_n \sin n\vartheta_0 + \alpha_{L=0} + \sum_1^N n A_n \frac{\sin n\vartheta_0}{\sin\vartheta_0} - 0.02 \quad \ldots (39)$$

Equation (39) can be rewritten as:

$$\sum_1^N \left[\left(\frac{2b}{\pi\, C(\vartheta_0)} + \frac{n}{\sin\vartheta_0}\right)\sin n\vartheta_0\right] A_n = \alpha - \alpha_{L=0} + 0.02 \ldots (40)$$

Take,

$$C_C(\vartheta_0, n) = \left(\frac{2b}{\pi\, C(\vartheta_0)} + \frac{n}{\sin\vartheta_0}\right)\sin n\vartheta_0 \ldots (41)$$

$$A(n) = A_n$$

$$D = \alpha - \alpha_{L=0} + 0.02 \ldots (42)$$

Then,

$$\sum_1^N C(\theta_0, n)\, A(n) = D \ldots (43)$$

The wing has been divided to a 30 equally spaced intervals along the span from $n = 1, 2, 3 \ldots, N$ from the left wing tip until the right wing tip. Each interval has a control point (k) at the mid of it where $k = 1, 2, 3 \ldots, N$ and the coordinate of k is given by equation (44). $k's$ have not include the wing tips or $y = 0$; because equation (43) is already satisfied at these points.

$$N = 14$$

$$y(k) = y_k = -\frac{b}{2}\left(1 - \frac{2k-1}{N}\right) \quad \ldots (44)$$

$$\Rightarrow \vartheta(k) = \vartheta_k = \cos^{-1}\left(-\frac{2y_k}{b}\right) = \cos^{-1}\left(1 - \frac{2k-1}{N}\right) \ldots (45)$$

Thus, equation (43) can be rewritten as function in k and n:

$$\sum_1^N C_c(k, n)\, A(n) = D \ldots (46)$$

Since the control points are symmetrical about the line at which $y = 0$:

$$\vartheta(k) = \vartheta(N + 1 - k) \ldots (47)$$

Also, the values of Fourier amplitudes (A_n's) all zero for even index (n). And since N is an even number, it can be written as: $N = 2M$. Then, the even values of the index n will

be relative to $n = 2m$ where $m = 1, 2, 3 \ldots, M$. After this, it has been possible to separate the even index (n) terms than the odd ones in equation (48).

$\sum_{m=1}^{M} C_c(k, 2m-1)\, A(2m-1) + \sum_{m=1}^{M} C_c(\theta_0, 2m)\, A(2m) = D$ … (48)

$\sum_{m=1}^{M} C_c(k, 2m-1)\, A(2m-1) + 0 = D$ … (49)

$\sum_{m=1}^{M} C_c(k, 2m-1)\, A(2m-1) = D$ … (50)

The lift which generated is symmetrical about the line at which $y = 0$: $L(k) = L(N + 1 - k)$. Thus, equation (50) has been applied for the half left side wing: $k = 1, 2, 3 \ldots, (N/2) = 1, 2, 3 \ldots, M$.

The chord distribution from the root until the tip for the left side of the wing at the aerodynamic centers points using the systems of axes: $(X, Y\ and\ Z)$ and $(X'', Y''\ and\ Z'')$.

For the interval: $-0.12 \leq y_{ac} \leq 0.31$,

At $y_{ac} = -0.12$ $\Rightarrow C = 5.50\ m$

At $y_{ac} = 0.31$ $\Rightarrow C = 5.24\ m$

Using a linear equation $Ay + B = C$:

$A(-0.12) + B = 5.50$

$A(0.31) + B = 5.24$

Solving the two equation together:

$-0.60\ y_{ac} + 5.43 = C$ … (51)

Equation (51) has been represented as function in y_{ac}'' as follows:

$y_{ac}'' = \frac{-y_{ac} + x_{ac}'' \sin 29}{\cos 29}$ … (52)

$y_{ac} = -0.81\ y_{ac}'' + 0.48$ … (53)

Substitute equation (53) in equation (51),

$C = 0.49\, y_{ac}'' + 5.14,$ ... (54) $for: 0.74 \geq y_{ac}'' \geq 0.21$

<u>For the interval: $-1.54 \geq y_{ac}'' \geq -5.51,$</u>

At $y_{ac}'' = -1.54$ $\Rightarrow C = 4.04\, m$

At $y_{ac}'' = -5.51$ $\Rightarrow C = 2.16\, m$

Using the linear equation $Ay + B = C$, and by solving the two resultant equations:

$0.47\, y_{ac}'' + 4.76 = C$ … (55)

For the two tringles the chord is not completed. Thus, it has been considered as not a straight airfoil section, see figure (47).

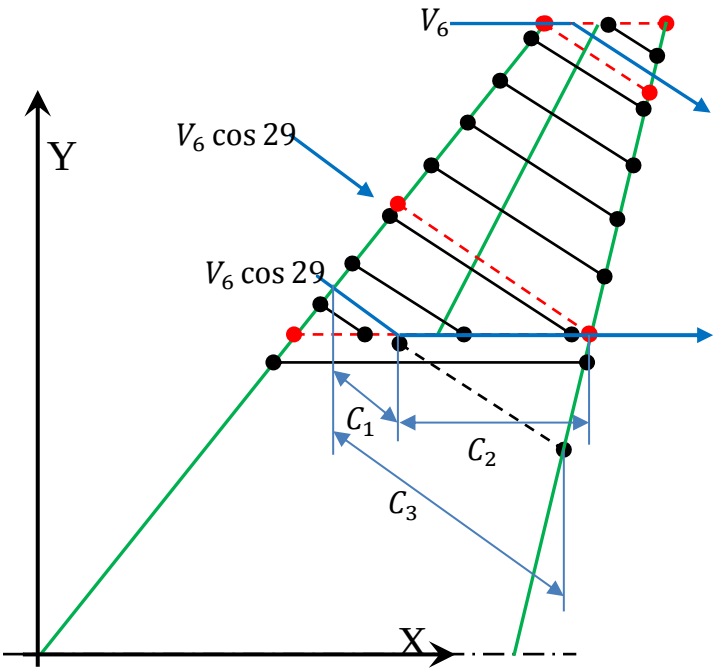

Figure 47. modified lifting line theory 3

Then:

$C = C_1 + C_2$

The resultant chord length (C) is exactly equal to the chord length (C_3) while it equal to (C_{tip}) for the tip tringle.

For the interval: $0.19 \geq y_{ac}'' \geq -1.54$,

At $y_{ac}'' = -1.54$ $\Rightarrow C_1 = 4.04\ m$

At $y_{ac}'' = 0.19$ $\Rightarrow C_1 = 1.17\ m$

Using the linear equation $Ay + B = C$, and by solving the two resultant equations:

$-1.66\ y_{ac}'' + 1.48 = C_1$ … (56)

At $y_{ac}'' = -1.54$ $\Rightarrow C_2 = 0\ m$

At $y_{ac}'' = 0.19$ $\Rightarrow C_2 = 2.73\ m$

Using the linear equation $Ay + B = C$, and by solving the two resultant equations:

$1.58\ y_{ac}'' + 2.43 = C_2$ … (57)

$-0.08\ y_{ac}'' + 3.91 = C$ … (58)

For the interval: $-5.51 \geq y_{ac}'' \geq -5.88$

The aerodynamic centers line is very small line inclines by 20 degrees than the

At $y_{ac}'' = -5.51$ $\Rightarrow C_1 = 0\ m$

At $y_{ac}'' = -5.88$ $\Rightarrow C_1 = 0.77\ m$

Using the linear equation $Ay + B = C$, and by solving the two resultant equations:

$-2.08\ y'' - 11.46 = C_1$ … (59)

At $y'' = -5.51$ $\Rightarrow C_2 = 2.16\ m$

At $y'' = -5.88$ $\Rightarrow C_2 = 1.39\ m$

Using the linear equation $Ay + B = C$, and by solving the two resultant equations:

$2.08\ y'' + 13.62 = C_2$ … (60)

$C = 2.16 = constant$

$$C(y_{ac}'') = \begin{cases} 0.49\, y_{ac}'' + 5.14 & 0.74 \geq y_{ac}'' \geq 0.21 \\ 0.47\, y_{ac}'' + 4.76 & -1.54 \geq y_{ac}'' \geq -5.51 \\ -0.08\, y_{ac}'' + 3.91 & 0.19 \geq y_{ac}'' \geq -1.54 \\ 2.16 & -5.51 \geq y_{ac}'' \geq -5.88 \end{cases}$$

The systems of axes $(X'', Y''\ and\ Z'')$ has been transformed to the system $(X', Y'\ and\ Z')$ using equation (61) below.

$$y_{ac}'' = \frac{\left(y_{ac}' - (-2.28)\right) + x_{ac}''\ \sin 29}{\cos 29} \quad \ldots (61)$$

$$y_{ac}'' = \frac{y_{ac}' + 2.76}{0.81} \quad \ldots (62)$$

Thus,

$$C(y_{ac}') = \begin{cases} 0.60 y_{ac}' + 6.8 & -2.16 \geq y_{ac}' \geq -2.59 \\ 0.58\, y_{ac}' + 6.36 & -4.01 \geq y_{ac}' \geq -7.22 \\ -0.10\, y_{ac}' + 3.63 & -2.61 \geq y_{ac}' \geq -4.01 \\ 2.16 & -7.22 \geq y_{ac}' \geq -7.52 \end{cases}$$

Note:

The system of the algebraic equations has been solved using Gauss-Seidle method for the algebraic equations system.

A MATLAB code has been written, see Appendix (A) to estimate the lift distribution.

4.3.5 L_2 estimation

For the near root section *(i=1),* the section upper surface has been divided into 17 panels *(j).* Each panel has a control point *(k)* at the middle where the pressure is estimated due to the effect of the all 35 panels. A vortex sheet of strength $\lambda\ (s)$ per unit length is placed on the wing upper surface. This sheet reacts with the uniform flow at station by induce potential velocity distribution around the wing. This velocity distribution changes the directions and the values of the uniform velocity and thus simulate the velocity distribution around the wing. and simulate the flow around the wing.

For the upper surface: $V_6 = \Delta V_6$

The induced potential velocity at the control points around the wing is given by:

$$\phi(k) = \sum_{j=1}^{N} \frac{\lambda_j}{2\pi} \int_j \ln r_{Pj} \; ds_j \quad \ldots (63)$$

$$r_{Pj} = \sqrt{\left(x_k - x_j\right)^2 + \left(z_k - z_j\right)^2} \qquad \textit{for x=0:1} \quad \ldots (64)$$

A MATLAB code has been used, see Appendix (B) to estimate the pressure coefficient.

4.3.6 The total lift coefficient and the lift curve slope

$$C_L = C_{L1} + C_{L2} \ldots (65)$$

To consider the 3D wing effect in the local lift coefficient, replace α by the effective angle of attack:

Using Kuchemann formula for swept wings, the wing lift curve slope has been estimated:

$$a = \frac{a_o \cos \Lambda_{c/2}}{\sqrt{1 + \left(\frac{a_o \cos \Lambda_{c/2}}{\pi e AR}\right)^2} + \left(\frac{a_o \cos \Lambda_{c/2}}{\pi e AR}\right)} \quad \ldots (66)$$

$$= \frac{2\pi \cos(30.01)}{\sqrt{1 + \left(\frac{2\pi \cos(30.01)}{\pi(0.742)(3.658)}\right)^2} + \left(\frac{2\pi \cos(30.01)}{\pi(0.742)(3.658)}\right)} = 2.981 \; per \; rad.$$

Where:

The tapper ratio of SU-35S: $\lambda = \frac{C_t}{C_r}$ = 0.28, using figure (), the induced drag factor $\delta =$ 0.016, the span efficiency factor e_0:

$$e_0 = \frac{1}{1+\delta} = 0.984 \quad \ldots (67)$$

Then, the Oswald efficiency factor which is for swept wings is given by the Hörner formula:

$$e = e_o \cos \Lambda_{L.E.} \quad \ldots (68)$$

$= 0.984 \times \cos 42 = 0.742$

4.3.7 The moment around the aerodynamic center

The aerodynamic moment around the aerodynamic center: this moment is caused by the lift force. Once the lift force changes due to the wing tip vortex effect, this must be represented in the equation besides the compressibility effect. The location of the aerodynamic center for the wing section that the wing lift resultant effects has been estimated:

$$\bar{x}_{ac}(y) = -\frac{\frac{dC_{m,c/4}}{d\alpha}}{a_0} + \frac{1}{4} \quad \ldots (69)$$

Using the thin airfoils theory:

$$C_{m,c/4} = \frac{\pi}{4}(A_2 - A_1) \quad \ldots (70)$$

Where:

$$A_1 = \frac{2}{\pi}\int_0^{\pi} \frac{dz}{dx}\cos\theta_0 \, d\theta \quad \ldots (71)$$

$$A_2 = \frac{2}{\pi}\int_0^{\pi} \frac{dz}{dx}\cos 2\theta_0 \, d\theta \quad \ldots (72)$$

"A_1 and A_2 depended only on the shape of the camber line and do not involve the angle of attack"." Thus, the quarter-chord point is the theoretical location of the aerodynamic center for a cambered airfoil".

$$\frac{dC_{m,c/4}}{d\alpha} = \frac{\pi}{4}\frac{d(A_2 - A_1)}{d\alpha} = 0 \quad \ldots (73)$$

$$\bar{x}_{ac}(y) = \frac{1}{4}$$

To estimate the aerodynamic line sweep angle:

$$\Lambda_{ac} = 35 \; degrees$$

The moment around the aerodynamic center:

$$C_{m,ac} = C_{m,c/4} = \frac{\pi}{4}(A_2 - A_1) = \text{constant} \quad \ldots (74)$$

$$A_1 = \frac{2}{\pi}\left\{\begin{array}{l} \int_0^{0.041}[-5.902\,[2.639706\,(1 - cos\theta_0)\,] + 0.250]\,cos\theta_0\,d\theta_0 \\ + \int_{0.041}^{0.167}[-5.902\,[2.639706\,(1 - cos\theta_0)\,] + 0.195]\,cos\theta_0\,d\theta_0 \\ + \int_{0.167}^{0.658}[-0.006[2.639706\,(1 - cos\theta_0)\,] + 0.036]\,cos\theta_0\,d\theta_0 \\ + \int_{0.658}^{1.406}[-0.006[2.639706\,(1 - cos\theta_0)\,] + 0.015]\,cos\theta_0\,d\theta_0 \\ + \int_{1.406}^{2.216}[-0.006[2.639706\,(1 - cos\theta_0)\,] + 0.011]\,cos\theta_0\,d\theta_0 \\ + \int_{2.216}^{3.142}[-0.014[2.639706\,(1 - cos\theta_0)\,] + 0.055]\,cos\theta_0\,d\theta_0 \end{array}\right\}$$

$$= \frac{2}{\pi}(0.010 + 0.013 + 0.018 + 0.004 + 0.002 + 0.012) = 0.035$$

$$A_2 = \frac{2}{\pi}\left\{\begin{array}{l} \int_0^{0.041}[-5.902\,[2.639706\,(1 - cos\theta_0)\,] + 0.250]\,cos2\theta_0\,d\theta_0 \\ + \int_{0.041}^{0.167}[-5.902\,[2.639706\,(1 - cos\theta_0)\,] + 0.195]\,cos2\theta_0\,d\theta_0 \\ + \int_{0.167}^{0.658}[-0.006[2.639706\,(1 - cos\theta_0)\,] + 0.036]\,cos2\theta_0\,d\theta_0 \\ + \int_{0.658}^{1.406}[-0.006[2.639706\,(1 - cos\theta_0)\,] + 0.015]\,cos2\theta_0\,d\theta_0 \\ + \int_{1.406}^{2.216}[-0.006[2.639706\,(1 - cos\theta_0)\,] + 0.011]\,cos2\theta_0\,d\theta_0 \\ + \int_{2.216}^{3.142}[-0.014[2.639706\,(1 - cos\theta_0)\,] + 0.055]\,cos2\theta_0\,d\theta_0 \end{array}\right\}$$

$$= \frac{2}{\pi}(0.011 + 0.012 + 0.021 - 0.003 + 0.005 - 0.008) = 0.024$$

$$C_{m,ac} = \frac{\pi}{4}(0.024 - 0.035) = -0.009$$

Note:

$$cos2\theta_0 = \cos\theta_0{}^2 - 1$$

$$M_{ac} = \frac{1}{2}\rho(V_\infty \cos 29)^2 S\bar{C}C_{m,ac} \quad \ldots (74)$$

$$\bar{C} = \frac{2}{3}(C_r)_{y=-0.12}\left(\frac{\lambda^2+\lambda+1}{\lambda+1}\right) \quad \ldots (75)$$

$$(C_r)_{(y=-0.12)} = -0.60 \times -0.12 + 5.43 = 5.502m$$

$$\bar{C} = \frac{2}{3} \times 5.502\left(\frac{0.28^2+0.28+1}{0.28+1}\right) = 3.893m$$

$M_{ac} = \frac{1}{2}\rho(V_\infty \cos 29)^2 \times 62 \times 3.893 \times -0.009 = -0.822\rho {V_\infty}^2$

The drag produced by the wing,

$C_D = C_{D,0} + C_{D,i} + C_{D,w}$ … (76)

Since the maneuver such that the wing will receive a velocity below the critical Mach number; there is no wave drag over the wing:

$\therefore C_{D,w}$ = zero

$\therefore \boldsymbol{C_D = C_{D,0} + C_{D,i}}$ … (77)

$C_{D,i} = k_3 {C_L}^2$ … (78)

where: $k_3 = \frac{1}{\pi AR} = \frac{1}{\pi(3.776)} = 0.0842$ … (79)

$C_{D,i} = 0.0842\ {C_L}^2$ … (80)

$C_{D,0} = C_{D,e_0} + \Delta C_{D,0} = C_{D,e_0} + k_1 {C_L}^2$ … (81)

$k_1 = \frac{1}{3} k_3 = \frac{0.0842}{3} = 0.028$ … (82)

Where $\Delta C_{D,0}$ is an increment in the zero lift drag due the separation happens by the increasing in the angle of attack to increase the lift coefficient.

$C_D = 0.02 + (0.028 + 0.0842){C_L}^2 = 0.02 + 0.112\ {C_L}^2$ … (83)

The total drag has been assumed to effect through the same point where the total lift effect, for simplicity of calculations. (the total lift effect at the point of the second moment of area point of the lift distribution shape along the semi-span, thus no need to estimate the drag distribution if the drag effect at the same point).

4.4 SU-35S stability model

It is important during maneuver to achieve a longitudinal stability to be sure the aircraft fly vertically not to pitch around its center of gravity (CG). the main contributors are:

- The wing-body
- The horizontal tail
- The engines nacelles
- The prop-fans
- The addition sliding part.

The shifting in the CG due to the sliding part and the prop-fans combinations:

$\Delta CG = \frac{M_{PF} \times arm + M_{SP} \times arm}{M_{PF} + M_{SP}}$, this value estimated at the last stage of the design procedure.

At level flight, assume a condition where the CG between the most forward and rearward locations $x_{cg} = \frac{1.98+2.12}{2} = 2.05m$

Then the new CG location = $x_{cg} + \Delta CG$ = $\underline{2.05 + \Delta CG}$ … (83)

Since SU-35S has a small wing-span-to-body-diameter ratio, the mutual interference between the wing and the fuselage is considerable. For such configuration we evaluate the wing-body together.

$C_{m_{\alpha,wb}} = \left(\bar{x}_{cg} - \bar{x}_{ac_{wb}}\right) C_{L_{\alpha,wb}}$ … (84)

Note:

The measurement datum is the Y-axis. Also the used chord is the mean aerodynamic chord.

$\bar{C} = 3.893m$ at: y= $\frac{5.43-C}{0.6} = \frac{5.43-3.893}{0.6} = 2.561$

$\bar{x}_{ac_{wb}} = \bar{x}_{ac} + \frac{y \tan 42}{\bar{C}} = 0.25 + \frac{2.561 \times \tan 42}{3.893} = 0.842$ … (85)

$$\bar{x}_{cg} = \frac{x_{cg}}{\bar{C}} = \frac{2.05 + \Delta CG}{3.893} = 0.53 + 0.26\Delta CG\_\ldots \text{ (86)}$$

To estimate the lift curve slope for the wing body combination:

$$C_{L_{\alpha WB}} = \left[K_N + K_{W(B)} + K_{B(W)}\right] C_{L,\alpha e} \left(\frac{S_{exp}}{S}\right) \quad \ldots (87)$$

$C_{L,\alpha e} = \frac{2.981}{\sqrt{1 - {M_6}^2}}$, … (88) considering the compressibility effects.

$S = 90\ m^2$

$S_{exp} = 62\ m^2$

$\frac{S_{exp}}{S} = 0.69$

$$K_N = \left(\frac{C_{L_{\alpha,N}}}{C_{L_{\alpha,e}}}\right) \left(\frac{S_{exp}}{S}\right) \quad \ldots (89)$$

For subsonic speeds:

$$C_{L_{\alpha,N}} = \frac{2\,(k_2 - k_1)\, S_{B,max.}}{S} \quad \ldots (90)$$

Using SU-35S data:

$S_{B,max.} = 3.6351\ m^2$ at station number No.8.

$b_{f,max.} = 4.57\ m$

$b = 15.3 - 2 \times 0.12 = 15.06m$ (without tips features).

$l_f = 21.9\ m$

Using figure (48) at fineness ratio: $\frac{l_f}{b_{f,max.}}$ = 4.79, the value of $k_2 - k_1 = 0.83$.

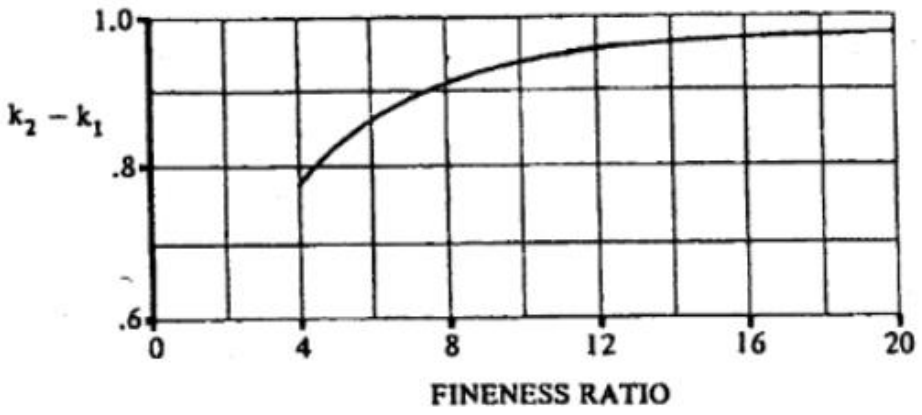

Figure 48. fuselage apparent mass coefficient

$$C_{L_{\alpha,N}} = \frac{2 \times 0.83 \times 3.6351}{90} = 0.067 \text{ per rad.}$$

$$K_N = \left(\frac{0.0973}{2.981}\right)(0.69) = 0.02$$

$$\frac{b_{f,max.}}{b} = 0.3$$

$$K_{W(B)} = 0.1714\left(\frac{b_{f,max.}}{b}\right)^2 + 0.8326\left(\frac{b_{f,max.}}{b}\right) + 0.9974 = 1.26 \quad \ldots (91)$$

$$K_{B(W)} = 0.7810\left(\frac{b_{f,max.}}{b}\right)^2 + 1.1976\left(\frac{b_{f,max.}}{b}\right) + 0.0088 = 0.44 \quad \ldots (92)$$

$$C_{L_{\alpha WB}} = [0.02 + 1.26 + 0.44]\frac{2.981}{\sqrt{1 - {M_6}^2}}(0.69)$$

$$C_{L_{\alpha WB}} = \frac{3.536}{\sqrt{1 - {M_6}^2}} \quad \ldots (93)$$

To estimate the value of $\bar{x}_{ac_{wb}}$:

$$\bar{x}_{ac_{wb}} = \frac{x_{ac_{wb}}}{C_{re}} \times \frac{C_{re}}{\bar{C}} \quad \ldots (94)$$

$$\left(\frac{x_{ac_{wb}}}{C_{re}}\right) = \frac{\left(\frac{x_{ac}}{C_{re}}\right)_N C_{L_{\alpha,N}} + \left(\frac{x_{ac}}{C_{re}}\right)_{W(B)} C_{L_{\alpha,W(B)}} + \left(\frac{x_{ac}}{C_{re}}\right)_{B(W)} C_{L_{\alpha,B(W)}}}{C_{L_{\alpha,WB}}} \quad \dots (95)$$

Where:

C_{re}: exposed root chord

$$C_{L_{\alpha,W(B)}} = C_{L_{\alpha,e}} K_{W(B)} \left(\frac{S_{exp}}{S}\right) = 2.981 \times 1.26 \times (0.69) = 2.59 \quad \dots (96)$$

$$C_{L_{\alpha,B(W)}} = C_{L_{\alpha,e}} K_{B(W)} \left(\frac{S_{exp}}{S}\right) = 2.981 \times 0.44 \times (0.69) = 0.78 \quad \dots (97)$$

For subsonic speeds:

$$\left(\frac{x_{ac}}{C_{re}}\right)_N = -\left(\frac{1}{C_{re}\, S_{B,max.}}\right) \int_0^{x_0} \frac{dS_b(x)}{dx} (l_N - x)\, dx \quad \dots (98)$$

$C_{re} = 5.43\, m$

$l_N = 3.01\, m$

The nose sectional area is circular: $S_b(x) = \frac{\pi}{4} {D_N}^2$ where $D_N = f(x)$. Using the geometrical data of SU-35S:

Table 9. SU-35S nose diameter distribution

X	D_N
0	0
1.2 m	0.90 m
3.01 m	1.38 m

It's clear that the, the diameter of the nose is change in a second order equation related to the change in x:

$Ax^2 + Bx + C = D_N(x)$ … (99)

At $x = 0 \Rightarrow C = D_N(0) = 0$

At $x = 1.2 \Rightarrow A(1.2)^2 + B(1.2) = 0.9$ … (100)

At $x = 3.01 \Rightarrow A(3.01)^2 + B(3.01) = 1.38$ … (101)

Solving equation (100) and (101):

B = 0.943

A = - 0.161

$D_N(x) = -0.161\,x^2 + 0.943\,x$ … (102)

$S_b(x) = \frac{\pi}{4}\,{D_N}^2 = \frac{\pi}{4}\,[-0.161\,x^2 + 0.943\,x]^2$

$= \frac{\pi}{4}\,[(-0.161\,x^2)^2 - 2 \times 0.161\,x^2 \times 0.943\,x + (0.943\,x)^2]$

$= \frac{\pi}{4}\,(0.026\,x^2 - 0.304\,x^3 + 0.889\,x^2)$ … (103)

$\frac{dS_b(x)}{dx} = \frac{\pi}{4}\,(0.026\,x^4 - 0.304\,x^3 + 0.889\,x^2) = \frac{\pi}{4}(0.104\,x^3 - 0.912\,x^2 + 1.778\,x)$
… (104)

$\left(\frac{x_{ac}}{C_{re}}\right)_N = -\left(\frac{1}{5.43 \times 3.6351}\right) \int_0^{3.01} \left[\frac{\pi}{4}(0.104\,x^3 - 0.912\,x^2 + 1.778\,x)\right] (3.01 - x)\,dx$

$= -\left(\frac{\pi}{4 \times 5.41 \times 3.6351}\right) \left\{\int_0^{3.01}(0.313\,x^3 - 2.745\,x^2 + 5.352\,x)\,dx - \int_0^{x_0}(0.104\,x^4 - 0.912\,x^3 + 1.778\,x^2)\,dx\right\}$

$= -0.040\,\left[\left(\frac{0.313 \times 3.01^4}{4} - \frac{2.745 \times 3.01^3}{3} + \frac{5.352 \times 3.01^2}{2}\right) - \left(\frac{0.104 \times 3.01^5}{5} - \frac{0.912 \times 3.01^4}{4} + \frac{1.778 \times 3.01^3}{3}\right)\right]$

$\left(\frac{x_{ac}}{C_{re}}\right)_N = -0.125$

For SU-35S, the exposed aspect ratio:

$A_e = \frac{b^2}{S_{exp}} = \frac{15.06^2}{62} = 3.658$

$\beta = \sqrt{1 - M^2} < 1$

$\Rightarrow \beta A_e > 1$

Since $\beta A_e > 1$:

$$\left(\frac{x_{ac}}{C_{re}}\right)_{B(W)} = \frac{1}{4} + \left(\frac{b - b_{f,max.}}{2C_{re}}\right) \chi \tan \Lambda_{c/4} \quad \ldots (105)$$

$\tan \Lambda_{c/4} = 0.67$

The value of the parameter χ had been found from figure (49): $\chi = 0.266$

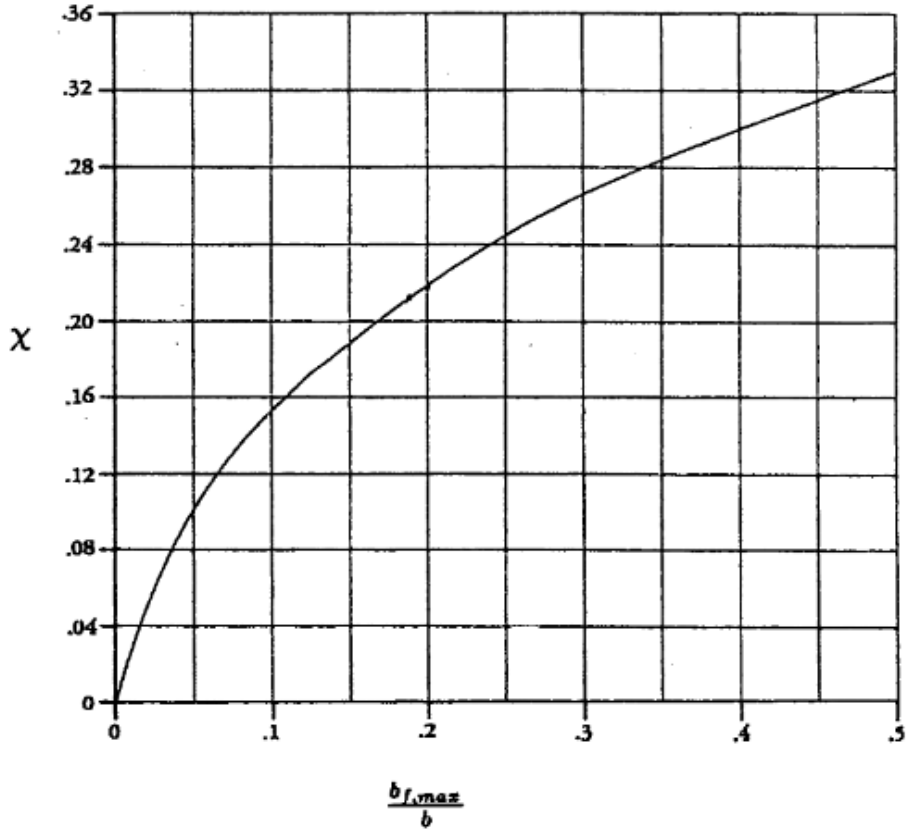

Figure 49. subsonic wing-lift carryover parameter

$$\left(\frac{x_{ac}}{C_{re}}\right)_{B(W)} = \frac{1}{4} + \left(\frac{15.06 - 4.57}{2 \times 5.43}\right) \times 0.266 \times 0.67 = 0.422$$

Since the effect of the body in the wing aerodynamic center is small and can be neglected:

$$\left(\frac{x_{ac}}{C_{re}}\right)_{W(B)} = \left(\frac{x_{ac}}{C_{re}}\right)_{W} = 0.25$$

$$\left(\frac{x_{ac_{wb}}}{C_{re}}\right) = \frac{1}{\sqrt{1-M_6{}^2}} \frac{(-0.125\times 0.0973+ 0.25 \times 2.23+ 0.422\times 0.78)}{\frac{3.037}{\sqrt{1-M_6{}^2}}} = 0.288$$

$$\bar{x}_{ac_{wb}} = 0.288 \times \frac{5.430}{3.893} = 0.401$$

$$C_{m_{\alpha,wb}} = \left((0.53 + 0.26\Delta CG) - 0.401\right)\frac{3.52}{\sqrt{1-M_6{}^2}} \quad \ldots (106)$$

$$C_{m_{0,wb}} = C_{m_{0,w}} = -0.009 < 0$$

The tail is extremely impressed in the wing wake; thus the tail will receive high velocity as well as the wing even at the low aircraft speed. This makes the tail capable to trim the aircraft.

$$C_{m_{\alpha,t}} = -a_t\left(1 - \frac{d\epsilon}{d\alpha}\right)\eta_t V_t \quad \ldots (107)$$

The fuselage side flow (down wash) on the horizontal tail is small and can be neglected; because of the presence of the vertical tail as a wall prevent the fuselage side flow to reach the horizontal tail. In the other hand the wing is very close to the horizontal tail and affect it by considerable down wash.

Since as motioned before, the maneuver will be achieved in high subsonic speeds, we used the empirical formula for subsonic speeds to estimate:

$$\frac{d\epsilon}{d\alpha} = 4.44\left[k_A k_\lambda k_H \left(\cos\Lambda_{1/4}\right)^{1/2}\right]^{1.19} \quad \ldots (108)$$

$$\cos\Lambda_{1/4} = 0.83$$

$$k_A = \frac{1}{AR} - \frac{1}{1+ AR^{1.7}} = \frac{1}{3.658} - \frac{1}{1+ 3.658^{1.7}} = 0.174 \ldots (109)$$

$$k_\lambda = \frac{10-3\lambda}{7} = \frac{10-(3\times 0.28)}{7} = 1.309 \quad \ldots (110)$$

$$l_h = 4.81\, m$$

$h_H = -0.6\,m$

$k_H = \frac{1-\frac{h_H}{b}}{\sqrt[3]{\frac{2l_h}{b}}} = \frac{1-\frac{-0.6}{15.06}}{\sqrt[3]{\frac{2\times4.81}{15.06}}} = \frac{1.040}{0.861} = 1.208$ … (111)

$\frac{d\epsilon}{d\alpha} = 4.44\left[0.174 \times 1.309 \times 1.208 \times (0.83)^{1/2}\right]^{1.19} = 0.856$

As the vertical tail presence keep the fuselage cross flow away from the horizontal tail, the value of the tail lift curve slope is equal to the value of lift curve slope for isolated horizontal tail.

Since the maneuver had been achieved at subsonic speeds we used the Datcom below to estimate the dynamic pressure ration:

$\eta_t = 1 - \frac{\Delta q}{q}$ … (112)

$l_{h1} = 2.467\,m$

$\lambda_t = 0.33 \Rrightarrow \delta_t = 0.017 \Rrightarrow e_0 = \frac{1}{1+0.33} = 0.75 \Rrightarrow e = e_o \cos\Lambda_{L.E.} = 0.751\ \cos 45 = 0.531$

$\frac{\Delta q}{q} = \frac{2.42\sqrt{C_{D_{o,w}}}}{\frac{l_{h1}}{\bar{C}}+0.30} = \frac{2.42\sqrt{0.02+(0.028)C_L{}^2}}{\frac{2.467}{3.893}+0.30} = 2.602\sqrt{0.02+(0.028)C_L{}^2}$ … (113)

$\eta_t = 1 - 2.602\sqrt{0.02+(0.028)C_L{}^2}$ … (114)

$V_h = \frac{S_h\, l_h}{S\,\bar{C}} = \frac{S_h\, l_h}{62\times 3.893}$ … (115)

S_h have been approximated as twice of the projection of the area on the X-Y plane.

$S_h = 12.424m^2$

$l_h = 7.761 - (2.05 + \Delta CG) = 5.711 - \Delta CG$ … (116)

$V_h = \frac{12.424\times(5.711-\Delta CG)}{62\times 3.893} = 0.291 - 0.051\Delta CG$

$AR = 3.92$

$$a_t = \frac{a_o \cos \Lambda_{c/2}}{\sqrt{1+\left(\frac{a_o \cos \Lambda_{c/2}}{\pi e AR}\right)^2}+\left(\frac{a_o \cos \Lambda_{c/2}}{\pi e AR}\right)} = \frac{2\pi \cos(32.38)}{\sqrt{1+\left(\frac{2\pi \cos(32.38)}{\pi(0.751)(3.92)}\right)^2}+\left(\frac{2\pi \cos(32.38)}{\pi(0.751)(3.92)}\right)} = 3.08\ per\ rad.$$

Considering the compressibility effect:

$$a_t = \frac{3.08}{\sqrt{1-(\eta_t M_\infty)^2}} = \frac{3.08}{\sqrt{1-\left\{\left[1-2.602\sqrt{0.02+(0.028){C_L}^2}\right] M_6\right\}^2}} \quad \dots (117)$$

$$C_{m_{\alpha,t}} = -\frac{0.444}{\sqrt{1-\left\{\left[1-2.602\sqrt{0.02+(0.028){C_L}^2}\right] M_6\right\}^2}} \left[1-2.602\sqrt{0.02+(0.028){C_L}^2}\right](0.291 - 0.051\Delta CG) \quad \dots (118)$$

Since the tail has a thin and symmetrical airfoil section:

$$C_{m_{0,t}} = C_{m_{0,c/4}} = 0 \quad \dots (119)$$

The trust produced by the two turbo-fan engine is relatively small during the maneuver to keep low forward speed; thus, it is acceptable to ignore the nacelles contribution.

The prop-fans effect in the longitudinal stability consist of:

- **Effect of thrust line vertical location related to the CG line**

  The prop-fan thrust effect through the thrust line in the direction of airflow. When a vertical distance separate between the thrust line and the CG line a pith down moment will produced around the aircraft CG. Once the distance between the CG line and the thrust line of the prop-fans is very small and the thrust produced by them approximately equal to zero.

  $M_{CG.propeller} = T_P . h_p \dots (120)$

  Divide equation (120) by qSC to estimate the moment coefficient around the CG:

  $$C_{m_{CG.P.F}} = \frac{T_P}{q.s}\frac{h_p}{C} \quad \dots (121)$$

$C_{m_{\alpha.P.F}}$ = zero … (122)

The moment produced by the propeller forward thrust don't affected by the local flow angle of attack. This shows that, the effect of propeller thrust location relative to the location of the CG has neutral contribution in the aircraft stability.

- **Effect of the normal force**

The normal force is the vertical component of the thrust when the prop-fans experience a local freestream with angle of attack (α_p) and it produces pitch up moment around the CG for puller configuration (Destabilizing).

$M_{CG.RS} = N_P . l_p$ … (123)

Divide equation ((123)) by q.S.C to estimate the moment coefficient around the CG:

$C_{m_{CG.SR}} = \frac{N_P}{q.S} \frac{l_p}{C}$ … (124)

$C_{N_P} = \frac{N_P}{q.S_P}$ … (125)

$C_{m_{CG.RS}} = \frac{C_{N_P} . q . S_P}{q . S} \frac{l_p}{C} = \frac{C_{N_P} . S_P}{S} \frac{l_p}{C}$ … (126)

$C_{m_{\alpha.P.F.}} = \frac{S_P}{S} \frac{l_p}{C} \frac{\partial C_{N_P}}{\partial \alpha_P} \frac{\partial \alpha_P}{\partial \alpha}$ … (127)

Once the prop-fans feed the wing with axial flow (no down or up wash) $\frac{\partial \alpha_P}{\partial \alpha} = 1$. Also, $\frac{S_P}{S} = 0.5 \; or \; 1$ since the total upper surface of the wing is impressed in the prop-fans wake while the lower surface can be impressed in the prop-fans wake or not. For the case of just the upper surface impressed in the prop-fans flow: $\frac{S_P}{S} = 0.5$

$\frac{\partial C_{N_P}}{\partial \alpha_P} = 0.02$

$C_{m_{\alpha.P.F.}} = 0.5 \times \frac{l_p}{3.893} \times 0.02 = 0.003 l_p$ … (128)

Since there are many prop-fans, this contribution is estimated for N prop-fan and the value of (l_p) depends on the prop-fan location.

The normal force affected by the local flow angle of attack even at small angle of attacks. So, it has a contribution in the aircraft $C_{m_{0,SP}}$ and in $\frac{\partial C_{m_{CG.SP}}}{\partial \alpha}$.

- **Effect of the slipstream (wake)**

  The propeller slipstream pass over the wing and the horizontal tail. "the wing sections exposed to the propeller slipstream experience a high dynamic pressure and hence develop higher local lift and drag force". This increment in lift and drag is local (2-D lift and drag) and it make a distortion to the lift and thus drag distribution over the wing leading to increase in the aerodynamic forces. This effect is small and can be neglected. But the tail is affected more than the wing because the propeller slipstream effect the tail efficiency (η) (the tail will experience much turbulent air flow if there a propeller than if there is no propeller and the tail angle of attack will increase) and also the downwash (ε), thus the horizontal tail lift to trim will be affected more.

  Due to the increment in the wing lift by ΔL due to the prop-fans axial wake, additional moment around the aircraft center of gravity will be produced but the value of $C_{m_{\alpha,wb}}$ is the same as if there is no prop-fan axial wake.

A MATLAB code had been written to estimate the stability model results, see Appendix (C).

4.5 SU-35S structural model

4.5.1 Introduction

The structural model of SU-35S wing had been approximated using the idealization theory.

4.5.2 The objectives of the model

This model aimed to achieve one objective: to be sure for the produced air loads, the wing bending stiffness and torsional stiffness are capable to be counteracted (resisted) these loads by considering the structural model in the optimization as constraints.

4.5.3 Assumptions

1. The skin and the webs have been assumed to be fully effective in resisting the shear stresses.
2. The flanges and the stringers have been assumed to be fully effective in resisting the direct stresses.
3. Due to the lack of the data about the internal structure of the fighter SU-35S, the dimensions of the stringers and the three spars are approximated using a closer model of fighters. The stringers area chosen to be $900\ mm^2$ at the near root section N_1 while the spars flanges are chosen to be $1200\ mm^2$ for the same section. The area decreases linearly even reach $600\ mm^2$ and $900\ mm^2$ at the tip for the stringers and the flanges respectively. Also, since it's so difficult to manufacture a variable thickness stringers or spars, the thickness of the them have been taken to be constant which means, the dimensions of the stringer or the spar are change along its length. The skin thickness has been chosen to be $0.8\ in$ and it's constant.
4. Since the dimensions of the wing internal structural element (such as a stringer section) are small, it's fair to take the moment of inertia for the section, $I_G = 0$.
5. No axial constraint effects (neglect the weapons, their fixations … etc.).

4.5.4 Case definition

4.5.4.1 Air loads definitions

The wing is a complex closed sections and it is affected by two main force and a moment. The forces as follow, the lift distribution resultant which effect at distance y_L in the Z-axis direction and the drag distribution resultant which effect parallel to the wing ribs (at the most of the wing) and normal to Spar No.2 which swept back by 29 degrees. Thus, it divided into two components: one parallel to the X-axis and the other parallel to the Y-axis. The moment is the aerodynamic moment produced by the transition of the lift resultant from the center of pressure of the airfoil section where the lift actually effects into the aerodynamic center of the same section. Both lift and drag forces incline by the angle of attack and the wing setting angle from the X-Y plane, thus both of them have contribution in the loads that affect the wing parallel to the X, Y and the Z axes.

Note, the wing total lift don't affect by the induced angle of attack.

- The load in the X direction ≡ $S_x = L\sin(\alpha + i_w) + D_x\cos(\alpha + i_w)$ … (129)
- The load in the Y direction ≡ $S_y = D_y$ … (130)
- The load in the Z direction ≡ $S_z = L\cos(\alpha + i_w) - D_x\sin(\alpha + i_w)$ … (131)

Where:

$D_x = D\cos 29$ … (132)

$D_y = D\sin 29$ … (133)

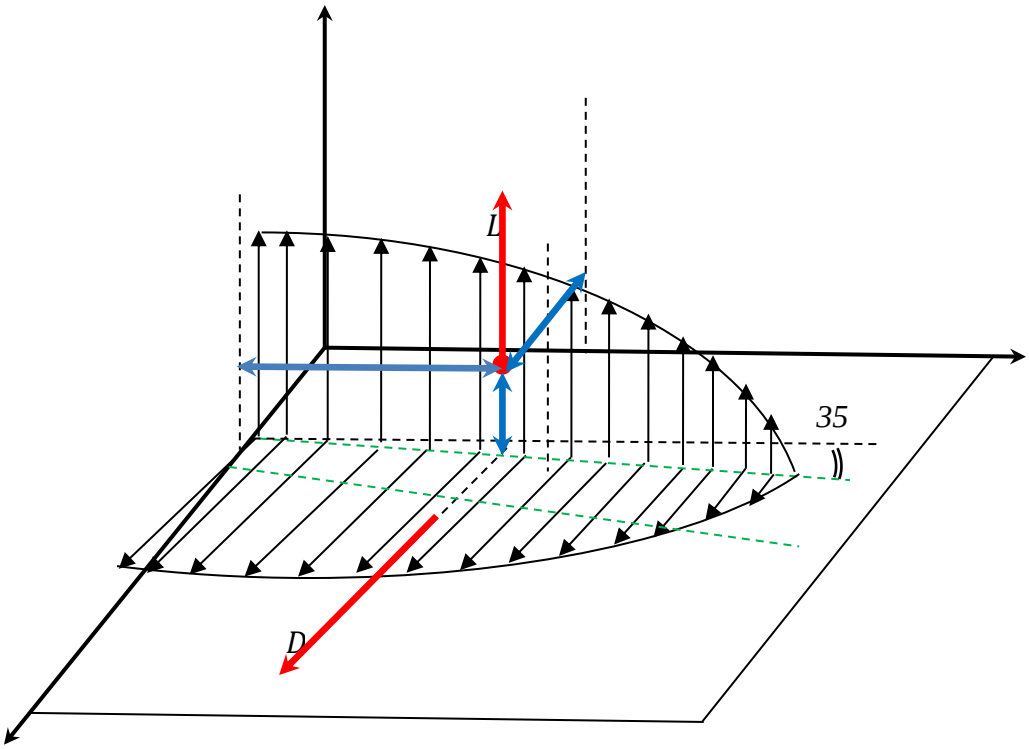

Figure 50. force distribution

The lift resultant effect at a point (x_R, y_R, z_R) lays on somewhere in the aerodynamic centers line. The first two coordinates are the most important and they depend on the center of area of the lift distribution. Along the aerodynamic center, the lift resultant locates at distance $(\bar{a})$ from the root:

$$\bar{a} = \frac{\sum\left[L(a)\Delta a\left(\frac{\Delta a}{2}\right)\right]}{\sum[L(a)\Delta a]} \quad \ldots (134)$$

$$y = a\cos 35 \;\Rightarrow a = y\ \sec 35$$

$$L(a) = L(y) \quad \ldots (135)$$

$$\bar{a} = \frac{\sum\left[L(y)\Delta y\ \sec 35\left(\frac{\Delta y\ \sec 35}{2}\right)\right]}{\sum[L(y)\Delta y\ \sec 35]} = \frac{\sec 35}{2}\frac{\int[\int L(y)\ dy]dy}{\int L(y)\ dy} \quad \ldots (136)$$

$$x_R = root\ a.c + \bar{a}\sin 35 = \frac{5.50}{4} + \bar{a}\sin 35 \quad \ldots (137)$$

$$y_R = \bar{a}\cos 35 \quad \ldots (138)$$

The force S_z bends the wing around the X-axis, produce a shear flow in the wing internal structure once it doesn't pass through the shear center of the wing sections (twisting) and it twists the wing about the Y-axis (that is because the wing is sweptback and thus the aerodynamic line where the lift distribution effects through sweptback also relative to the Y-axis, thus this force produce a moment in a plane parallel and pass through the sweptback aerodynamic line, this moment con be divided into two components: the first around the X-axis, bending while the other around the Y-axis, twisting) which produce additional shear flow in the wing structure. The force S_x and S_y exert an ignorable bending moment on the wing around the Z-axis and a considerable shear flow in the wing internal structure because they don't pass through the shear center of the wing sections (twisting).

The moment around the aerodynamic center has two components: the first twist the wing around the Y-axis producing a shear flow while the other bends the wing around the X-axis.

4.5.4.2 Setup (geometrical definition)

The spars

The wing consists of three I-section spars: the front, the middle and the rear spars or spar No.1, No.2 and No.3 respectively. Spar No.2 is a straight line while spar No.1 consists of three straight lines and spar No.3 consists of two straight lines. The spars coordinates are given as follows:

Spar No.1

$y = 0 \qquad \Rightarrow x_{S1} = 1.58$

$y = 3.08 \qquad \Rightarrow x_{S1} = 3.47$

$\therefore\ x_{S1} = 0.61y + 1.58, \quad \ldots (139) \qquad 0 \leq y \leq 3.08$

$y = 3.08 \qquad \Rightarrow x_{S1} = 3.47$

$y = 3.85 \qquad \Rightarrow x_{S1} = 4.10$

$\therefore\ x_{S1} = 0.82y + 0.94, \quad \ldots (140) \qquad 3.08 < y \leq 3.85$

$y = 3.85 \qquad \Rightarrow x_{S1} = 4.10$

$y = 5.24 \qquad \Rightarrow x_{S1} = 4.85$

$\therefore\ x_{S1} = 0.54y + 2.02, \quad \ldots (141) \qquad 3.85 < y \leq 5.24$

Spar No.2

$y = 0 \qquad \Rightarrow x_{S2} = 2.73$

$y = 5.24 \qquad \Rightarrow x_{S2} = 5.58$

$\therefore\ x_{S2} = 0.54y + 2.73 \quad \ldots (142)$

Spar No.3

$y = 0 \qquad \Rightarrow x_{S3} = 4.24$

$y = 2.31 \qquad \Rightarrow x_{S3} = 4.84$

$\therefore\ x_{S3} = 0.26y + 4.24, \quad \ldots (143) \qquad 0 \leq y \leq 2.31$

$y = 2.31 \qquad \Rightarrow x_{S3} = 4.84$

$y = 5.24 \qquad \Rightarrow x_{S3} = 6.27$

$\therefore\ x_{S3} = 0.48y + 3.73, \quad \ldots (144) \qquad 2.31 < y \leq 5.24$

The booms area decreases linearly from $1200mm^2$ at the intersection of the three spars with the rib N_1 even reach $900mm^2$ at the intersection of the three spars with the tip rib.

Using the transformations:

$$x'' = -(x - 2.73)\cos 29 + y \sin 29 \quad \ldots (145)$$

$$y'' = -(x - 2.73)\sin 29 - y \cos 29 \quad \ldots (146)$$

Spar No.1

$i = 01$: $x = 1.58$, $y = 0.00$ $\Rightarrow x'' = 1.00$, $\beta = 1200mm^2$

$i = 20$: $x = 4.85$, $y = 5.24$ $\Rightarrow x'' = 0.67$, $\beta = 900mm^2$

Thus the boom area changes with respect to x, y by equation (147) below.

$$\beta(x'') = 909.09x'' + 290.91$$

$$\beta(x, y) = 909.09[-(x - 2.73)\cos 29 + y \sin 29\ ] + 290.91$$

$$= -908.22\, x + 436.36\, y + 2450.09 \quad \ldots (147)$$

β: $in\ mm^2$

The booms number are 1 for the upper surface and 34 for the lower surface.

Spar No.2

This spar entirely at $x'' = 0.00$,

$i = 01$: $x = 2.73$, $y = 0.00$ $\Rightarrow y'' = 0.00$, $\beta = 1200mm^2$

$i = 20$: $x = 5.58$, $y = 5.24$ $\Rightarrow y'' = -5.93$, $\beta = 900mm^2$

Thus the boom area changes with respect to x, y by equation (148) below.

$$\beta(y'') = 50.59\, y'' + 1200$$

$\beta(x,y) = 50.59[-(x-2.73)\sin 29 - y\cos 29\,] + 1200 = -24.28\,x - 44.01\,y + 1266.29$ … (149)

β: $in\ mm^2$

The booms number are 9 for the upper surface and 26 for the lower surface.

Spar No.3

$i = 01$: $x = 4.24,$ $y = 0.00$ $\Rrightarrow x'' = -1.31\,,$ $\beta = 1200mm^2$

$i = 20$: $x = 6.27,$ $y = 5.24$ $\Rrightarrow x'' = -0.56\,,$ $\beta = 900mm^2$

Thus the boom area changes with respect to x, y by equation (150) below.

$\beta(x'') = -400\,x'' + 676$

$\beta(x,y) = -400[-(x-2.73)\cos 29 + y\sin 29\,] + 676 = 348\,x - 192\,y + 274.04$ … (150)

β: $in\ mm^2$

The booms number are 17 for the upper surface and 18 for the lower surface.

$$\beta(x,y,n) = \begin{cases} -908.22\,x + 436.36\,y + 2450.09 & n = 1\ and\ 34 \quad \dots (151) \\ -24.28\,x - 44.01\,y + 1266.29 & n = 9\ and\ 26 \quad \dots (152) \\ 348\,x - 192\,y + 274.04 & n = 17\ and\ 18 \quad \dots (153) \end{cases}$$

The stringers

The stringers are divided into two groups separated by a support:

Group No.1:

Between *i=2* and *i=9*. There are 28 stringers, 14 for the upper surface, 14 for the lower surface. For the surface (upper or lower surface): 7 between spar No.1 and spar No.2, 7 between spar No.2 and spar No.3. The stringers are equally spaced along the surface. The two ribs at *i=3* and *i=4* have less stringers due to their position.

Group No.2:

For *i=11* and *i=12* there are 20 stringers, 10 for the upper surface, 10 for the lower surface. For the surface (upper or lower surface): 5 between spar No.1 and spar No.2, 5 between spar No.2 and spar No.3. The stringers are equally spaced along the surface.

Between *i=13* and *i=19*. There are 16 stringers, 8 for the upper surface, 8 for the lower surface. For the surface (upper or lower surface): 4 between spar No.1 and spar No.2, 4 between spar No.2 and spar No.3. The stringers are equally spaced along the surface. The rib at *i=19* has less stringers due to its position.

The booms were numbered as follows:

For i=2:9:

Table 10. booms distribution

	Spar No.1	between	Spar No.2	between	Spar No.3
Upper surface	1	2:8	9	10:16	17
Lower surface	34	27:33	26	19:25	18

For i=11:12:

Table 11. booms distribution

	Spar No.1	between	Spar No.2	between	Spar No.3
Upper surface	1	4:8	9	10:14	17
Lower surface	34	27:31	26	21:25	18

For i=11:12:

Table 12. booms distribution

	Spar No.1	between	Spar No.2	between	Spar No.3
Upper surface	1	5:8	9	10:13	17
Lower surface	34	27:30	26	22:25	18

Booms coordinates estimation

For any section i parallel to the X-axis, once the stringers are equally spaced between the spar No.1 and the spar No.2, the space is given by equation (154) while the X-coordinate of each stringer is given by equation (155).

$$\text{The space} = \frac{P_{S2,S1}}{\text{the stringers number between the two spars}} \quad \dots (154)$$

For i=2:9:

$$(x_i)_n = (x_i)_{34-n+1} = (x_{S1})_i + (n-1)\left(\frac{P_{S2,S1}}{7}\right)_i \quad \dots (155)$$

Once the airfoil between the fist spar and the third spar is approximately flat for both the upper and the lower surfaces, the space can have approximated as distance along the chord:

$$\left(\frac{P_{S2,S1}}{7}\right)_i = \left(\frac{x_{S2}-x_{S1}}{7}\right)_i$$

$$\Rightarrow \boldsymbol{(x_i)_n = (x_i)_n = (x_i)_{34-n+1} = (x_{S1})_i + \frac{(n-1)}{7}(x_{S2} - x_{S1})_i} \quad \dots (156)$$

The same thing between the second and the third spar,

$$\boldsymbol{(x_i)_n = (x_i)_{34-n+1} = (x_{S2})_i + \frac{(n-9)}{7}(x_{S3} - x_{S2})_i} \quad \dots (157)$$

For the i sections parallel to the X'' axis: the section inclines by 29 degrees than the Y-axis.

For i=2:9:

$$(x_i'')_n = (x_{S1}'')_i - \frac{(n-1)}{7}(x_{S2}'' - x_{S1}'')_i = [1 + 0.14\,(n-1)]\,(x_{S1}'')_i \quad \dots (158)$$

$$(x_i'')_{\beta i} = (x_{S2}'')_i + \frac{(n-9)}{7}(x_{S3}'' - x_{S2}'')_i = 0.14\,(n-9)(x_{S3}'')_i \quad \dots (159)$$

$i = 2$:

Substitute $(y = 0.31)$ in equations (139),(142) and (143):

$(x_{S1})_2 = 0.61 \times 0.31 + 1.58 = 1.77$

$(x_{S2})_2 = 0.54 \times 0.31 + 2.73 = 2.90$

$(x_{S3})_2 = 0.26 \times 0.31 + 4.24 = 4.32$

Substitute the values of $(x_{S1})_2, (x_{S2})_2$ and $(x_{S3})_2$in the equations (158) and (159):

$\Rightarrow (x_2)_n = 1.77 + 0.16\ (n -$
1) ... (160) *between spar No.1 and spar No.2*

$\Rightarrow (x_2)_n = 2.90 + 0.2(n -$
9) ... (161) *between spar No.2 and spar No.3*

$\underline{i = 9}$:

$y'' = -2.62 \Rightarrow y = -(0.55x - 4.52)$ ... (162)

The spar No.1 at $y = 2.73$, thus: $(x_{S1})_9 = 0.61 \times 2.73 + 1.58 = 3.25$

The spar No.3 at $y = 1.94$, thus: $(x_{S3})_9 = 0.26 \times 1.94 + 4.24 = 4.74$

Using the transformation (145):

$(x_{S1}'')_9 = 0.86$

$(x_{S3}'')_9 = -0.82$

Then, using equations (156) and (157) and then the transformation (146) at $y = -(0.55x - 4.52)$:

Between spars No.1 and No.2:

$(x_9'')_n = 0.86\ [1 + 0.14(n - 1)]$ … (163)

$\Rightarrow (x_9)_n = -0.76[1 + 0.14(n - 1)] + 4.03$ … (164)

Between spars No.2 and No.3:

$(x_9'')_n = -0.11\ (n - 9)$ … (165)

$\Rightarrow (x_9)_n = 0.10(n-9) + 4.03$ … (166)

By substitute $(x_i)_n$ in $(y_i)_n$, $(y_i)_n$ has been estimated as function in the boom number.

Between spar No.1 and spar No.2:

$i = 2: (y_2)_n = 0.31 \qquad (x_2)_n = 1.77 + 0.16(n-1)$ … (167)

$i = 9: (y_9)_n = 0.06 + 2.72(n-1)$ … (168)

$(x_9)_n = -0.76[1 + 0.14(n-1)] + 4.03$ … (169)

Between spar No.2 and spar No.3:

$i = 2: (y_2)_n = 0.31 \qquad (x_2)_n = 2.90 + 0.2(n-9)$ … (170)

$i = 9: (y_9)_n = -0.06(n-9) + 2.30$ … (171)

$(x_9)_n = 0.10(n-9) + 4.03$ … (172)

By solving two linear equations for *i=2* and *i=9* between spar No.1 and spar No.2 once and between spar No.2 and spar No.3, the x-coordinate as a function in the boom number has been estimated:

$$x = \begin{cases} \frac{-0.01(n-1)^2+(n-1)(0.27y-0.59)-3.8-1.5y}{-0.06(n-1)-2.41} & spar\ No.1\ and\ spar\ No.2 \quad \dots (173) \\ \frac{0.01(n-9)^2+(n-9)(0.10y-0.26)-5.42-1.13y}{0.06(n-9)-1.99} & spar\ No.2\ and\ spar\ No.3 \quad \dots (174) \end{cases}$$

<u>For i=11:12:</u>

$(x_i'')_n = (x_{S1}'')_i - \frac{(n-3)}{5}(x_{S2}'' - x_{S1}'')_i = [1 + 0.20(n-3)]\,(x_{S1}'')_i$ … (175)

$(x_i'')_{\beta i} = (x_{S2}'')_i + \frac{(n-9)}{5}(x_{S3}'' - x_{S2}'')_i = 0.20(n-9)(x_{S3}'')_i$ … (176)

<u>$i = 11$:</u>

$y'' = -3.35 \Rightarrow y = -(0.55x - 5.36)$ … (177)

The spar No.1 at $y = 3.29$, thus: $(x_{S1})_{11} = 0.82 \times 3.29 + 0.94 = 3.64$

The spar No.3 at $y = 2.60$, thus: $(x_{S3})_{11} = 0.48 \times 2.60 + 3.73 = 4.98$

Using the transformation (145):

$(x_{S1}'')_{11} = 0.79$

$(x_{S3}'')_{11} = -0.71$

Then, using equations (156) and (157) and then the transformation (146) at $y = -(0.55x - 5.36)$:

Between spars No.1 and No.2:

$(x_{11}'')_n = 0.79[1 + 0.20(n - 3)]$ … (178)

$\Rightarrow (x_{11})_n = -0.70[1 + 0.20(n - 3)] + 4.38$ … (179)

Between spars No.2 and No.3:

$(x_{11}'')_n = -0.14(n - 9)$ … (180)

$\Rightarrow (x_{11})_n = 0.12\,(n - 9) + 4.38$ … (181)

$\underline{i = 12:}$

$y'' = -3.68 \Rightarrow y = -(0.55x - 5.74)$ … (182)

The spar No.1 at $y = 3.65$, thus: $(x_{S1})_{12} = 0.82 \times 3.65 + 0.94 = 3.93$

The spar No.3 at $y = 2.89$, thus: $(x_{S3})_{12} = 0.48 \times 2.89 + 3.73 = 5.12$

Using the transformation (145):

$(x_{S1}'')_{12} = 0.71$

$(x_{S3}'')_{12} = -0.69$

Then, using equations (156) and (157) and then the transformation (146) at $y = -(0.55x - 5.74)$:

Between spars No.1 and No.2:

$(x_{12}'')_n = 0.71\,[1 + 0.20(n-3)]$ … (183)

$\Rrightarrow (x_{12})_n = -0.63[1 + 0.20(n-3)] + 4.55$ … (184)

Between spars No.2 and No.3:

$(x_{12}'')_n = -0.14\,(n-9)$ … (185)

$\Rrightarrow (x_{12})_n = 0.12\,(n-9) + 4.55$ … (186)

$y(n) =$

$$\begin{cases} i = 11 & \begin{cases} 0.08(n-3) + 3.34 & \text{Between spars No. 1 and No. 2} \quad \dots (187) \\ -0.07(n-9) + 2.95 & \text{Between spars No. 2 and No. 3} \quad \dots (188) \end{cases} \\ i = 12 & \begin{cases} 0.07(n-3) + 3.59 & \text{Between spars No. 1 and No. 2} \quad \dots (189) \\ -0.07(n-9) + 3.24 & \text{Between spars No. 2 and No. 3} \quad \dots (190) \end{cases} \end{cases}$$

As same as before by solving a two linear equations represent the variation of $(x_i)_n$ as function in (n) once between spar No.1 and spar No.2 and once between spar No.2 and spar No.3 both for *i=11:12*, a general form has been estimated:

$$x = \begin{cases} \frac{(n-3)(-0.01y+0.13)-0.12-0.24y}{0.01(n-3)-0.25} & spar\ No.1\ and\ spar\ No.2 \quad \dots (191) \\ 0.59y + 0.16(n-9) + 2.64 & spar\ No.2\ and\ spar\ No.3 \quad \dots (192) \end{cases}$$

<u>For i=12:20:</u>

<u>$i = 20$:</u>

$y = 5.24$

$(\boldsymbol{x_{S1}})_{\boldsymbol{20}} = 0.54 \times 5.24 + 2.02 = 4.85$

$(\boldsymbol{x_{S2}})_{\boldsymbol{20}} = 0.54 \times 5.24 + 2.73 = 5.56$

$(\boldsymbol{x_{S3}})_{\boldsymbol{20}} = 0.48 \times 5.24 + 3.73 = 6.25$

$(x_{20})_n = (x_{S1})_{20} + \frac{(n-4)}{4}(x_{S2} - x_{S1})_{20} = 4.85 + 0.18(n-$

$4)$ … (193) $spars\ No.1\ and\ No.2$

$$(x_{20})_n = (x_{S2})_{20} + \frac{(n-9)}{4}(x_{S3} - x_{S2})_{20}$$

$$= 5.56 + 0.17(n9) \ldots (194) \ spars\ No.2\ and\ No.3$$

$$x = \begin{cases} \frac{0.01(n-3)(n-4)+(n-3)(-0.13y+1.02)+(n-4)(-0.18y+0.64)-3.13-0.93y}{0.07(n-3)-1.65} \ldots (195) \\ \frac{-0.01(n-3)^2+(n-9)(-0.05y-0.47)-5.83-1.01y}{-0.07(n-9)-2.00} \ldots (196) \end{cases}$$

<u>Booms (stringers) areas estimation</u>

The booms area decrease linearly between the section at $i = 2$ and the section at $i = 9$, from 900 mm^2even 600 mm^2.

Between spar No.1 and spar No.2:

$i = 2: (y_2)_n = 0.31$ $, \beta = 900\ mm^2$

$i = 9: (y_9)_n = 0.06(n-1) + 2.72$ ... (197) $, \beta = 600\ mm^2$

Between spar No.2 and spar No.3:

$i = 2: (y_2)_n = 0.31$ $, \beta = 900\ mm^2$

$i = 9: (y_9)_n = -0.06(n-9) + 2.30$ ... (198) $, \beta = 600\ mm^2$

Thus, solving the linear equation $(A(y_i)_n + B = \beta)$:

$$\beta(n,y) = \begin{cases} 900 + \frac{-300y_n+93}{2.41+0.06(n-1)} \ldots (199) \quad between\ spar\ No.1\ and\ spar\ No.2 \\ 900 + \frac{300y_n-93}{-1.99+0.06(n-9)} \ldots (200) \quad between\ spar\ No.1\ and\ spar\ No.2 \end{cases}$$

$\beta\ in\ mm^2$

As same as, the booms areas decrease between *i=11* and *i=20* from 600 mm^2 e ven 300 mm^2.

Between spar No.1 and spar No.2:

$i = 11: (y_{11})_n = 0.08(n-3) + 3.34$ ... (201) $, \beta = 600\ mm^2$

$i = 20: (y_{20})_n = 5.24$ $, \beta = 300\ mm^2$

Between spar No.2 and spar No.3:

$i = 11: (y_{11})_n = -0.07(n-9) + 2.95$ … (202) $, \beta = 600\ mm^2$

$i = 20: (y_{20})_n = 5.24$ $, \beta = 300\ mm^2$

$$\beta(n,y) = \begin{cases} 300 + \frac{300y_n - 1572}{-1.90 + 0.08(n-3)} \ \ldots (203) & between\ spar\ No.1\ and\ spar\ No.2 \\ 300 + \frac{300y_n - 1572}{-2.29 - 0.07(n-9)} \ \ldots (204) & between\ spar\ No.1\ and\ spar\ No.2 \end{cases}$$

$\beta\ in\ mm^2$

The z coordinate estimation

The z coordinates of the booms for the upper and the lower surfaces have been estimated as follows:

The wing consists of the same airfoil but with a different chord length. Simply it is scaled from the section $i = 1$ by a percentage equal to the chord ratio $\left(\frac{C_i}{C_1}\right)$.

Nevertheless, due to the tapering of the wing upper surface in the Y-axis direction, the leading edge line is inclined downward than the X-axis by an angle ψ.Thus, the leading point of each section is shifted down by a distance ζ. This shift appears as decreasing in z_{u_i} and increasing in z_{l_i} than their value if $\psi = 0$. Thus,

$$z_{u_i} = \frac{C_i}{C_i} \times z_{u_1} - \zeta_i \quad \ldots (205)$$

$$z_{l_i} = \frac{C_i}{C_1} \times z_{l_1} - \zeta_i \quad \ldots (206)$$

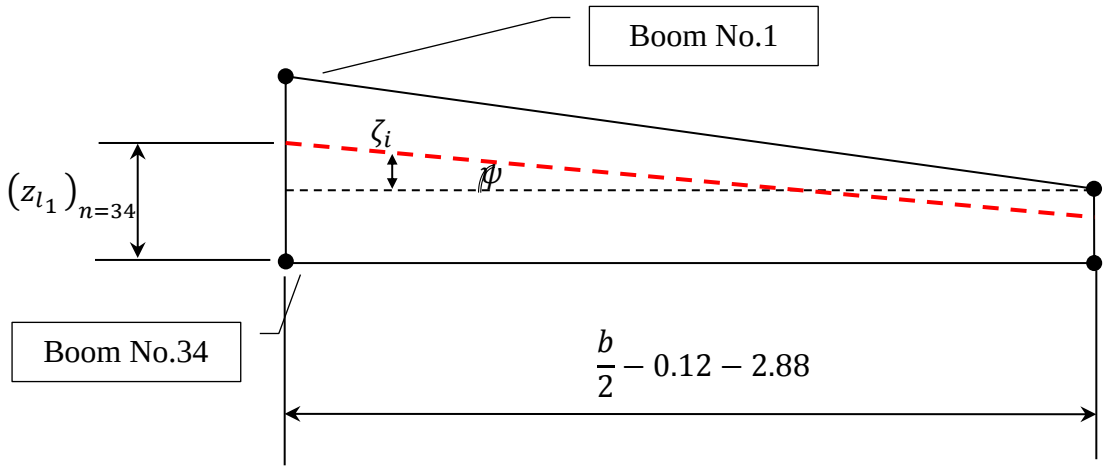

Figure 51. wing tapering

$$\psi = \tan^{-1}\left[\frac{(z_{l_1})_{n=34} - \left(\frac{c_{20}}{c_1}\right)(z_{l_1})_{n=34}}{\frac{b}{2} - 0.12 - 2.28}\right] \quad \ldots (207)$$

$$(x_1)_{n=34} = (x_{S1})_1 + \frac{(34-n)}{7}(x_{S2} - x_{S1})_1 \quad \ldots (208)$$

$$x_1 = 1.58$$

$$(z_{l_1})_{n=34} = 0.010(1.58)^2 - 0.050 \times 1.58 - 0.060 = -0.114$$

$$\Rightarrow \psi = \tan^{-1}\left[\frac{-0.114 - \left(\frac{2.16}{5.43}\right)(-0.114)}{\frac{15.3}{2} - 0.12 - 2.28}\right] = -0.748\ degrees$$

Thus, at certain section i, the shift down equal to:

$$\zeta_i = \sqrt{x^2 + y^2}\tan\psi = 0.013\sqrt{x^2 + y^2} \quad \ldots (209)$$

The shift value is small. Thus it ignored. And the all L. E's have been taken to be at the same level.

For the section i=1, the upper and the lower surface coordinated between spar No.1 and spar No.2 are given as follows:

Table 13. near root airfoil equations for the upper surface

The interval	$\mathbf{z_{u_1}}$
$x_{S1} \leq x \leq 1.84$	$-0.030x^2 + 0.140x + 0.030$ … (210)
$1.84 < x \leq 3.68$	$-0.030x^2 + 0.130x + 0.045$ … (211)
$3.68 < x \leq x_{S3}$	$-0.070x + 0.370$ … (212)

Table 14. near root airfoil equations for the lower surface

The interval	$\mathbf{z_{l_1}}$
$x_{S1} \leq x \leq 2.21$	$0.010x^2 - 0.050x - 0.060$ … (213)
$2.21 < x \leq x_{S3}$	$0.010x^2 - 0.030x - 0.110$ … (214)

The chords distribution is given by equations (215) and (216).

$C(y) = -0.60\,y + 5.43,$ ... (215) $0.31 \geq y \geq -0.12$

$C(y'') = 0.47\,y'' + 4.76,$ ... (216) $0.96 \geq y'' \geq -6.45$

$C(y) = 2.16$ $y = 5.24$

Using the transformation (145) to represent equation (146) as function in y.

Then, at any point (x, y) the chord of the section which include this point is given by equation () below:

$$C(x,y) = \begin{cases} -0.60\,y + 5.43, & \text{... (217)} \quad 0.31 \geq y \geq -0.12 \\ -0.41\,y - 0.23x + 5.38, & \text{... (218)} \quad 5.24 > y \geq 0.31 \\ 2.16 & \qquad\qquad y = 5.24 \end{cases}$$

4.5.4.3 Shear centers estimation

To estimate the shear center of each section: the shear center has coordinates (ξ_s, η_s) the first in the $x$direction and the second in the z direction for a certain section at y. Case of zero twist and shear load effect through the shear center had been assumed. The

moments around the leading edge of the section had been taken and equated with the internal moments due to the shear flow produced by this shear load.

Note: the shear centers have been estimated for sections all parallel to the X-axis.

To estimate ξ_s, unknown shear load S_z applied through the shear center.

The shear flow distribution due to any shear force S_z :

$$q_s = q_b + q_{s,o} \quad \dots (219)$$

$$q_b = -\left(\frac{-S_z I_{xz}}{I_{xx} I_{zz} - I_{xz}^2}\right) \left(\sum_{r=1}^{n} \beta_r x_r\right) - \left(\frac{S_z I_{zz}}{I_{xx} I_{zz} - I_{xz}^2}\right) \left(\sum_{r=1}^{n} \beta_r z_r\right) \dots (220)$$

For a certain element of the wing internal structure lays between two booms *r* and *r+1*, the basic shear flow contribution is given as:

$$q_b = -\left(\frac{-S_z I_{xz}}{I_{xx} I_{zz} - I_{xz}^2}\right) \beta_r x_r - \left(\frac{S_z I_{zz}}{I_{xx} I_{zz} - I_{xz}^2}\right) \beta_r z_r \quad \dots (221)$$

Where:

The moment of inertia $I_{xx} = \sum \Delta I_{xx} = \sum_{r=1}^{N} \beta_r (\bar{z} - z)^2$ … (222)

The moment of inertia $I_{zz} = \sum \Delta I_{zz} = \sum_{r=1}^{N} \beta_r (\bar{x} - x)^2$ … (223)

The moment of inertia $I_{xz} = \sum \Delta I_{xz} = \sum_{r=1}^{N} \beta_r (\bar{x} - x)(\bar{z} - z)$ … (224)

Where:

$$\bar{z} = \frac{\Sigma(\beta . z)}{\Sigma\beta} \quad \dots (225)$$

$$\bar{x} = \frac{\Sigma(\beta . x)}{\Sigma\beta} \quad \dots (226)$$

Since the shear load working line pass through the section shear center, the rate of twist equal to zero (no torque generated) then the shear flow in the five cuts $q_{S,O,R}$ is given as:

The rate of twist is given by equation (227) below:

$$\frac{d\theta}{dy} = \frac{1}{2A_R}\oint_R q\frac{ds}{t} = \frac{1}{2A_R}\oint_R \left(q_{S,O,R} + q_b\right)\frac{ds}{t} = 0 \quad \ldots (227)$$

For cell No.1:

$$0 = q_{S,O,1}\left(\frac{ds_{1,34c}}{t_{1,34c}} + \frac{ds_{1,34}}{t_{1,34}}\right) - q_{S,O,2}\frac{ds_{1,34}}{t_{1,34}} + 0 \times q_{S,O,3} + 0 \times q_{S,O,4} + \oint_{R1} q_b\frac{ds}{t} \quad \ldots (228)$$

For cell No.2:

$$0 = -q_{S,O,1}\frac{ds_{1,34}}{t_{1,34}} + q_{S,O,2}\left(\frac{ds_{1,34}}{t_{1,34}} + \frac{ds_{1,9}}{t_{1,9}} + \frac{ds_{34,26}}{t_{34,26}} + \frac{ds_{9,26}}{t_{9,26}}\right) - q_{S,O,3}\frac{ds_{9,26}}{t_{9,26}} + 0 \times q_{S,O,4} + \oint_{R2} q_b\frac{ds}{t} \quad \ldots (229)$$

For cell No.3:

$$0 = 0 \times q_{S,O,1} - q_{S,O,2}\frac{ds_{9,26}}{t_{9,26}} + q_{S,O,3}\left(\frac{ds_{9,26}}{t_{9,26}} + \frac{ds_{9,17}}{t_{9,17}} + \frac{ds_{26,18}}{t_{26,18}} + \frac{ds_{17,18}}{t_{17,18}}\right) - q_{S,O,4}\frac{ds_{17,18}}{t_{17,18}} + \oint_{R3} q_b\frac{ds}{t} \quad \ldots (230)$$

For cell No.4:

$$0 = 0 \times q_{S,O,1} + 0 \times q_{S,O,2} - q_{S,O,3}\frac{ds_{17,18}}{t_{17,18}} + q_{S,O,4}\left(\frac{ds_{17,18}}{t_{17,18}} + \frac{ds_{17,18,c}}{t_{17,18,c}}\right) + \oint_{R4} q_b\frac{ds}{t} \quad \ldots (231)$$

The cell area has been approximated as follows:

$$A_1 = \left(\int_{L.E}^{x_{s1}} z_u\,dx - \int_{L.E}^{x_{s1}} z_l\,dx\right) \times chord\ ratio \quad \ldots (232)$$

$$= \left\{\int_0^{0.01}(-188.88x^2 + 3.75x)\,dx + \int_{0.01}^{0.04}(-2.85x^2 + 0.67x + 0.01)\,dx + \int_{0.04}^{1.58}(-0.03x^2 + 0.14x + 0.03)\,dx - \left[\int_0^{0.01}(472.04x^2 - 7.21x)\,dx + \int_{0.01}^{0.15}(0.12x^2 - 0.18x - 0.026)\,dx + \int_{0.15}^{0.55}(0.12x^2 - 0.18x - 0.02)\,dx + \int_{0.55}^{1.58}(0.01x^2 - 0.05x - 0.06)\,dx\right]\right\} \times chord\ ratio$$

$$= 0.36 \times chord\ ratio\ m^2$$

$$A_2 = \left(\int_{x_{s1}}^{x_{s2}} z_u \, dx - \int_{x_{s1}}^{x_{s2}} z_l \, dx\right) \times chord\ ratio \ \ldots (233)$$

$$= \left\{\int_{1.58}^{1.84}(-0.03x^2 + 0.14x + 0.03)\, dx + \int_{1.84}^{2.73}(-0.03x^2 + 0.13x + 0.045)\, dx - \left[\int_{1.58}^{2.21}(0.01x^2 - 0.05x - 0.06)\, dx + \int_{2.21}^{2.73}(0.01x^2 - 0.03x - 0.11)\, dx\right]\right\} \times chord\ ratio$$

$$= 0.35 \times chord\ ratio\ m^2$$

$$A_3 = \left(\int_{x_{s2}}^{x_{s3}} z_u \, dx - \int_{x_{s2}}^{x_{s3}} z_l \, dx\right) \times chord\ ratio \quad \ldots (234)$$

$$= \left[\int_{2.73}^{3.68}(-0.03x^2 + 0.13x + 0.045)\, dx + \int_{3.68}^{4.24}(-0.07x + 0.37)\, dx - \int_{273}^{4.24}(0.01x^2 - 0.03x - 0.11)\, dx\right] \times chord\ ratio$$

$$= 0.34 \times chord\ ratio\ m^2$$

$$A_4 = \left(\int_{x_{s3}}^{T.E} z_u \, dx - \int_{x_{s3}}^{T.E} z_l \, dx\right) \times chord\ ratio \quad \ldots (235)$$

$$= \left[\int_{4.24}^{5.43}(-0.07x + 0.37)\, dx - \left[\int_{4.24}^{4.60}(0.01x^2 - 0.03x - 0.11)\, dx + \int_{4.60}^{5.43}(-0.02x^2 + 0.25x - 0.76)\, dx\right]\right] \times chord\ ratio$$

$$= 0.07 \times chord\ ratio\ m^2$$

ds has been approximated as:

$$ds = \sqrt{\left(z_{\beta_{n+1}} - z_{\beta_n}\right)^2 + \left(x_{\beta_{n+1}} - x_{\beta_n}\right)^2} \quad \ldots (236)$$

By solving the four equations using the Gauss Seidel iteration method (MATLAB code), the values of the shear flow in the cuts have been estimated. Then the first coordinate for the shear center is given from the moment equation around the L.E:

$$S_z\xi = \sum_{R=1}^{4} M_{q,R} = \sum_{R=1}^{4} \oint_R q_b p ds + \sum_{R=1}^{4} 2A_R q_{S,O,R} \quad \ldots (237)$$

The airfoil section is approximately flat between the first and the third spars. Thus, for simplicity the moment arm assumed to be equal to the z coordinate.

η_s has been estimated in a same manner but with applying unknown shear load S_x through the shear center. Then, the same procedure repeated.

The basic shear flow distribution due to the shear force S_x:

$$q_b = -\left(\frac{S_x I_{xx}}{I_{xx}I_{zz} - I_{xz}^2}\right)\left(\sum_{r=1}^{n} \beta_r x_r\right) - \left(\frac{-S_x I_{xz}}{I_{xx}I_{zz} - I_{xz}^2}\right)\left(\sum_{r=1}^{n} \beta_r z_r\right) \quad \ldots (238)$$

The moments taken around the leading edge of the section:

$$S_x \eta_s = \sum_{R=1}^{4} M_{q,R} = \sum_{R=1}^{4} \oint_R q_b p ds + \sum_{R=1}^{4} 2A_R q_{S,O,R} \quad \ldots (239)$$

4.5.5 The structural analysis

4.5.5.1 Introduction

Both S_z and S_x produce moment, the bending moment produced by S_x is around the Z-axis and it usually neglected. Since SU-35S has high sweep, the force S_z produces two moment components: the first is a bending moment and it is around the X-axis call it M_{x1} and the other around the Y-Axis call it M_{y1} and it twist the wing down (torsion).

$$M_{y1} = S_z x_R \quad \ldots (240)$$

$$M_{x1} = S_z y_R \quad \ldots (241)$$

The moment around the aerodynamic center has two components: the first around the X-axis (bending moment) and the second around the Y-axis (torsion). This torque generates a shear flow in the wing sections. This shear flow has a constant value for each cell of the section.

$$M_{y2} = M_{ac} \cos \Lambda_{ac} = M_{ac} \cos 35 \quad \ldots (242)$$

$$M_x 2 = M_{ac} \sin \Lambda_{ac} = M_{ac} \sin 35 \quad \ldots (243)$$

The shear loads don't necessary path through the shear centers of the wing sections, thus as the aerodynamic load which generate the shear forces transferred from the section aerodynamic center, a torque T must be considered to compensate this transformation. This torque distributes in the cells and generates additional shear flow $(q_{,R})$. Nevertheless, it twists the section with a certain rate which assumed to be constant for the section here.

R = 1,2, …4 since SU-35S has three main spars.

$$T(y) = \sum_{R=1}^{4} 2A_R q_R = 2A_1 q_1 + 2A_2 q_2 + 2A_3 q_3 + 2A_4 q_4 \quad \ldots (244)$$

4.5.5.2 bending moment M_x

M_x is distributed along the semi-span between the wing root and the tip. The bending moment at any section is given by:

$$M_x = M_{x1} + M_{x2} = S_z\,(y_R - y) + M_{ac} \sin 35$$

$$= [L\cos(\alpha + 1) - D\sin(\alpha + 1)\,](y_R - y) + M_{ac} \sin 35 \quad \ldots (245)$$

This bending moment generate direct stresses in the booms (stringers, the spar and ribs flanges). The direct stresses effects on the internal structural elements of the wing had been estimated for each element not for each section as follow:

The wing upper surface is tapered in two directions: $\alpha_u \neq 0 = 2$ and $\alpha_{L.E} \neq 0 = 42$ while the lower surface is tapered in one direction: $\alpha_l = 0$ and $\alpha_{T.E} \neq 0 = -14$. This tapering effects the stresses transmitting through the internal structural elements of the wing. The lower surface of the wing is not tapered in the y-axis direction. Thus, $\alpha_l = 0$ while $\alpha_u \neq 0$.

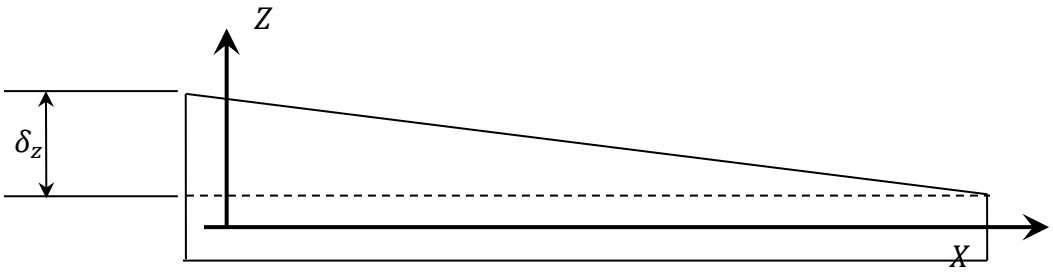

Figure 52. wing tapering

Each boom will experience an axial force p_r: for the upper surface booms of the wing this axial force p_{r_u}has tree components: p_{r_x} , p_{r_y} , and p_{r_z}. p_{r_y} cause the direct stress σ normal to the boom area while p_{r_z} and p_{r_x}cause a shear stresses tangentially to the boom area. For the lower surface booms, the axial force p_{r_l} has two components: p_{r_x} , p_{r_y}. p_{r_y} cause the direct stress σ normal to the boom while p_{r_x} cause a shear stress in the boom area.

❖ **direct stresses in booms**

The direct stress at a section locates at distance y and has a moment of inertia I_{xx} due to the bending moment value at the section:

$$\sigma_{y_r} = \frac{M_x(y)}{I_{xx}} z_r \quad \dots (246)$$

The max. σ_{y_r} along the boom length must be less than the yield stress of the boom material to prevent permanent deformation of the booms. Thus,

$$\sigma_{y_n} < \sigma_{yield} \quad \dots (247)$$

❖ **Shear stress in walls and webs**

The shear loads S_z and S_x produce shear flow in the walls and the webs besides the shear forces p_{r_z} and p_{r_x} at the booms:

$S_{x,w}$ is the shear flow resultant of the skin.

$S_{z,w}$ is the shear flow resultant of the webs.

$$S_x = S_{x,w} + \sum_{r=1}^{n} p_{x,r} \quad \Rrightarrow S_{x,w} = S_x - \sum_{r=1}^{n} p_{x,r} \quad \dots (248)$$

$$p_{r_x} = \sigma_{y_r} \beta, r \frac{\delta_{xr}}{\delta_y} \quad \dots (249)$$

$$S_z = S_{z,w} + \sum_{r=1}^{n} p_{z,r} \quad \Rrightarrow S_{z,w} = S_z - \sum_{r=1}^{n} p_{z,r} \quad \dots (249)$$

$$p_{r_z} = \sigma_{y_r} \beta, r \frac{\delta_{zr}}{\delta_y}$$

$$\frac{\delta_{xr}}{\delta_y} = \frac{\delta_{zr}}{\delta_y} = \begin{cases} \tan 2 = 0.03 & for\ the\ upper\ surface\ booms \\ 0.00 & for\ the\ lower\ surface\ booms \end{cases}$$

The basic shear flow in the skin and the web due to the action of $S_x$and S_z:

$$q_b = -\left(\frac{S_{x,w}\, I_{xx} - S_{z,w}\, I_{xz}}{I_{xx} I_{zz} - {I_{xz}}^2}\right)\left(\int_0^s t_D\ x\ ds + \sum_{r=1}^{n} \beta_r\, x_r\right) -$$

$$\left(\frac{S_{z,w}\, I_{zz} - S_{x,w}\, I_{xz}}{I_{xx} I_{zz} - {I_{xz}}^2}\right)\left(\int_0^s t_D\ z\ ds + \sum_{r=1}^{n} \beta_r\, z_r\right) \quad \ldots (250)$$

$$\int_0^s t_D\ x\ ds = \int_0^s t_D\ z\ ds = 0$$

$$q_b = -\left(\frac{S_{x,w} I_{xx} - S_{z,w}\, I_{xz}}{I_{xx} I_{zz} - {I_{xz}}^2}\right)\left(\sum_{r=1}^{n} \beta_r\, x_r\right) - \left(\frac{S_{z,w}\, I_{zz} - S_{x,w}\, I_{xz}}{I_{xx} I_{zz} - {I_{xz}}^2}\right)\left(\sum_{r=1}^{n} \beta_r\, z_r\right) \quad \ldots (251)$$

Because the booms have a variable cross-section are along their length additional shear value is added to the shear flow. This value is given as the change in the load p_{z_r} between two section separated by 35 even 70 cm. here, 50 cm has been taken

$$\Delta p = \frac{(p_{z_r})_y - (p_{z_r})_{y-0.5}}{y-(y-0.5)} = \frac{1}{2}\left[(p_{z_r})_y - (p_{z_r})_{y-0.5}\right] \quad \ldots (252)$$

To predict the value of $q_{S,OR}$: the external moments due to the shear loads must be totally resisted by the internal moments produced by the internal shear flow. The moment due to the shear loads is taken around the leading edge:

$$S_{x,w}\eta - S_{z,w}\xi = \sum_{R=1}^{4} \oint_R\ q_b\, p_0\, ds\ + \sum_{R=1}^{4} 2\, A_R\, q_{s,o,R}\ - \sum_{r=1}^{n} p_{z_r}\xi_r + \sum_{r=1}^{n} p_{x_r}\eta_r \quad \ldots (253)$$

This equation is function in $(q_{s,o,R})$ for 4 cells and it is solved with other four equations represent the twist rate due to that, the shear loads don't pass through the section shear center to estimate the shear flow in the cuttings. Assume constant rate of twist:

$$\frac{d\theta}{dy} = \frac{1}{2A_R}\oint_R\ q\,\frac{ds}{t} = \frac{1}{2A_R}\oint_R\ (q_{S,O,R} + q_b)\frac{ds}{t} = \text{constant} \ldots (254)$$

$$\frac{d\theta}{dy} = \frac{1}{2A_1}\left[q_{S,O,1}\,\frac{ds_{1,34,c}}{t_{1,34,c}} + (q_{S,O,1} - q_{S,O,2})\frac{ds_{1,34}}{t_{1,34}} + \oint_{R1} q_b\,\frac{ds}{t}\right] \quad \ldots (255)$$

$$\frac{d\theta}{dy} = \frac{1}{2A_2}\left[-q_{S,O,1}\frac{ds_{1,34}}{t_{1,34}} + q_{S,O,2}\left(\frac{ds_{1,34}}{t_{1,34}} + \frac{ds_{1,9}}{t_{1,9}} + \frac{ds_{34,26}}{t_{34,26}} + \frac{ds_{9,26}}{t_{9,26}}\right) - q_{S,O,3}\frac{ds_{9,26}}{t_{9,26}} + \oint_{R2} q_b \frac{ds}{t}\right] \ldots (256)$$

$$\frac{d\theta}{dy} = \frac{1}{2A_3}\left[-q_{S,O,2}\frac{ds_{9,26}}{t_{9,26}} + q_{S,O,3}\left(\frac{ds_{9,26}}{t_{9,26}} + \frac{ds_{9,17}}{t_{9,17}} + \frac{ds_{26,18}}{t_{26,18}} + \frac{ds_{17,18}}{t_{17,18}}\right) - q_{S,O,4}\frac{ds_{17,18}}{t_{17,18}} + \oint_{R3} q_b \frac{ds}{t}\right] \ldots (257)$$

$$\frac{d\theta}{dy} = \frac{1}{2A_4}\left[\left(q_{S,O,4} - q_{S,O,3}\right)\frac{ds_{17,18}}{t_{17,18}} + q_{S,O,4}\frac{ds_{17,18,c}}{t_{17,18,c}} + \oint_{R4} q_b \frac{ds}{t}\right] \quad \ldots (258)$$

By subtract equation j from j+1 four equation have been generated and solved using Gauss Seidel iteration method

For cell No.1: $q_{S,O,1}$ calculated

$$0 = q_{S,O,1}\left[\frac{1}{A_1}\frac{ds_{1,34,c}}{t_{1,34,c}} + \frac{ds_{1,34}}{t_{1,34}}\left(\frac{1}{A_1} + \frac{1}{A_2}\right)\right]$$

$$-q_{S,O,2}\left[\frac{ds_{1,34}}{t_{1,34}}\left(\frac{1}{A_1} + \frac{1}{A_2}\right) + \left(\frac{ds_{1,34}}{t_{1,34}} + \frac{ds_{1,9}}{t_{1,9}} + \frac{ds_{34,26}}{t_{34,26}} + \frac{ds_{9,26}}{t_{9,26}}\right)\left(\frac{1}{A_2}\right)\right]$$

$$+q_{S,O,3}\frac{1}{A_2}\frac{ds_{9,26}}{t_{9,26}}$$

$$+\frac{1}{A_1}\oint_{R1} q_b \frac{ds}{t} - \frac{1}{A_2}\oint_{R2} q_b \frac{ds}{t} \quad \ldots (259)$$

For cell No.2: $q_{S,O,2}$ calculated

$$0 = -q_{S,O,1}\frac{1}{A_2}\frac{ds_{1,34}}{t_{1,34}}$$

$$+q_{S,O,2}\left[\frac{ds_{9,26}}{t_{9,26}}\left(\frac{1}{A_2} + \frac{1}{A_3}\right) + \left(\frac{ds_{1,34}}{t_{1,34}} + \frac{ds_{1,9}}{t_{1,9}} + \frac{ds_{34,26}}{t_{34,26}} + \frac{ds_{9,26}}{t_{9,26}}\right)\left(\frac{1}{A_2}\right)\right]$$

$$-q_{S,O,3}\left[\frac{ds_{9,26}}{t_{9,26}}\left(\frac{1}{A_2} + \frac{1}{A_3}\right) + \left(\frac{ds_{9,17}}{t_{9,17}} + \frac{ds_{26,18}}{t_{26,18}} + \frac{ds_{17,18}}{t_{17,18}}\right)\left(\frac{1}{A_2}\right)\right]$$

$$+q_{S,O,4}\frac{1}{A_3}\frac{ds_{17,18}}{t_{17,18}}$$

$$+\frac{1}{A_2}\oint_{R2} q_b \frac{ds}{t} - \frac{1}{A_3}\oint_{R3} q_b \frac{ds}{t} \quad \dots (260)$$

For cell No.3: $q_{S,O,3}$ calculated

$$0 = -q_{S,O,2}\frac{1}{A_3}\frac{ds_{9,26}}{t_{9,26}}$$

$$+q_{S,O,3}\left[\frac{ds_{17,18}}{t_{17,18}}\left(\frac{1}{A_3}+\frac{1}{A_4}\right)+\left(\frac{ds_{9,26}}{t_{9,26}}+\frac{ds_{9,17}}{t_{9,17}}+\frac{ds_{26,18}}{t_{26,18}}\right)\left(\frac{1}{A_2}\right)\right]$$

$$-q_{S,O,4}\left[\frac{ds_{17,18}}{t_{17,18}}\left(\frac{1}{A_3}-\frac{1}{A_4}\right)-\frac{ds_{17,18,c}}{t_{17,18,c}}\left(\frac{1}{A_4}\right)\right]$$

$$+\frac{1}{A_3}\oint_{R3} q_b \frac{ds}{t} - \frac{1}{A_4}\oint_{R4} q_b \frac{ds}{t} \quad \dots (261)$$

For cell No.4: $q_{S,O,4}$ calculated

$$0 = \frac{1}{A_1}\left[q_{S,O,1}\left(\frac{ds_{1,34,c}}{t_{1,34,c}}+\frac{ds_{1,34}}{t_{1,34}}\right)-q_{S,O,2}\frac{ds_{1,34}}{t_{1,34}}\right]$$

$$-\frac{1}{A_4}\left[-q_{S,O,3}\frac{ds_{17,18}}{t_{17,18}}+q_{S,O,4}\left(\frac{ds_{17,18}}{t_{17,18}}+\frac{ds_{17,18,c}}{t_{17,18,c}}\right)\right]$$

$$+\frac{1}{A_1}\oint_{R1} q_b \frac{ds}{t} - \frac{1}{A_4}\oint_{R4} q_b \frac{ds}{t} \quad \dots (262)$$

4.5.5.3 The torsion

$$T(y) = M_{y1} + M_{y2}$$

$$= S_z\,(x_R - x) + M_{ac}\cos 35$$

$$= [L\cos(\alpha+1) - D\sin(\alpha+1)](x_R - x) + M_{ac}\cos 35$$

$$T(y) = \sum 2A_R q_R = [L\cos(\alpha+1) - D\sin(\alpha+1)](x_R - x) + M_{ac}\cos 35 \quad \dots (263)$$

Equation (263) above solved with four equation represent the twist rate to estimate the additional sear flow.

The rate of twist is given by:

$$\frac{d\theta}{dy} = \frac{1}{2A_R}\oint_R q\frac{ds}{t} = \frac{1}{2A_R}\oint_R (q_R + q_b)\frac{ds}{t} = \text{constant}$$

$$\frac{d\theta}{dy} = \frac{1}{2A_1}\left[q_1\frac{ds_{1,34,c}}{t_{1,34,c}} + (q_1 - q_2)\frac{ds_{1,34}}{t_{1,34}} + \oint_{R1} q_b\frac{ds}{t}\right] \quad \dots (264)$$

$$\frac{d\theta}{dy} = \frac{1}{2A_2}\left[-q_1\frac{ds_{1,34}}{t_{1,34}} + q_2\left(\frac{ds_{1,34}}{t_{1,34}} + \frac{ds_{1,9}}{t_{1,9}} + \frac{ds_{34,26}}{t_{34,26}} + \frac{ds_{9,26}}{t_{9,26}}\right) - q_3\frac{ds_{9,26}}{t_{9,26}} + \oint_{R2} q_b\frac{ds}{t}\right] \quad \dots (265)$$

$$\frac{d\theta}{dy} = \frac{1}{2A_3}\left[-q_2\frac{ds_{9,26}}{t_{9,26}} + q_3\left(\frac{ds_{9,26}}{t_{9,26}} + \frac{ds_{9,17}}{t_{9,17}} + \frac{ds_{26,18}}{t_{26,18}} + \frac{ds_{17,18}}{t_{17,18}}\right) - q_4\frac{ds_{17,18}}{t_{17,18}} + \oint_{R3} q_b\frac{ds}{t}\right] \quad \dots (266)$$

$$\frac{d\theta}{dy} = \frac{1}{2A_4}\left[(q_4 - q_3)\frac{ds_{17,18}}{t_{17,18}} + q_4\frac{ds_{17,18,c}}{t_{17,18,c}} + \oint_{R4} q_b\frac{ds}{t}\right] \quad \dots (267)$$

By subtract equation j from j+1 four equation have been generated and solved using Gauss Seidel iteration method

For cell No.1: q_1 calculated

$$0 = q_1\left[\frac{1}{A_1}\frac{ds_{1,34,c}}{t_{1,34,c}} + \frac{ds_{1,34}}{t_{1,34}}\left(\frac{1}{A_1} + \frac{1}{A_2}\right)\right]$$

$$-q_2\left[\frac{ds_{1,34}}{t_{1,34}}\left(\frac{1}{A_1} + \frac{1}{A_2}\right) + \left(\frac{ds_{1,34}}{t_{1,34}} + \frac{ds_{1,9}}{t_{1,9}} + \frac{ds_{34,26}}{t_{34,26}} + \frac{ds_{9,26}}{t_{9,26}}\right)\left(\frac{1}{A_2}\right)\right]$$

$$+q_3\frac{1}{A_2}\frac{ds_{9,26}}{t_{9,26}}$$

$$+\frac{1}{A_1}\oint_{R1} q_b\frac{ds}{t} - \frac{1}{A_2}\oint_{R2} q_b\frac{ds}{t} \quad \dots (268)$$

For cell No.2: q_2 calculated

$$0 = -q_1\frac{1}{A_2}\frac{ds_{1,34}}{t_{1,34}}$$

$$+q_2\left[\frac{ds_{9,26}}{t_{9,26}}\left(\frac{1}{A_2} + \frac{1}{A_3}\right) + \left(\frac{ds_{1,34}}{t_{1,34}} + \frac{ds_{1,9}}{t_{1,9}} + \frac{ds_{34,26}}{t_{34,26}} + \frac{ds_{9,26}}{t_{9,26}}\right)\left(\frac{1}{A_2}\right)\right]$$

$$-q_3\left[\frac{ds_{9,26}}{t_{9,26}}\left(\frac{1}{A_2} + \frac{1}{A_3}\right) + \left(\frac{ds_{9,17}}{t_{9,17}} + \frac{ds_{26,18}}{t_{26,18}} + \frac{ds_{17,18}}{t_{17,18}}\right)\left(\frac{1}{A_2}\right)\right]$$

$$+q_4\frac{1}{A_3}\frac{ds_{17,18}}{t_{17,18}}$$

$$+\frac{1}{A_2}\oint_{R2} q_b\frac{ds}{t}-\frac{1}{A_3}\oint_{R3} q_b\frac{ds}{t} \quad \dots (269)$$

For cell No.3: q_3 calculated

$$0=\ -q_2\frac{1}{A_3}\frac{ds_{9,26}}{t_{9,26}}$$

$$+q_3\left[\frac{ds_{17,18}}{t_{17,18}}\left(\frac{1}{A_3}+\frac{1}{A_4}\right)+\left(\frac{ds_{9,26}}{t_{9,26}}+\frac{ds_{9,17}}{t_{9,17}}+\frac{ds_{26,18}}{t_{26,18}}\right)\left(\frac{1}{A_2}\right)\right]$$

$$-q_4\left[\frac{ds_{17,18}}{t_{17,18}}\left(\frac{1}{A_3}-\frac{1}{A_4}\right)-\frac{ds_{17,18,c}}{t_{17,18,c}}\left(\frac{1}{A_4}\right)\right]$$

$$+\frac{1}{A_3}\oint_{R3} q_b\frac{ds}{t}-\frac{1}{A_4}\oint_{R4} q_b\frac{ds}{t} \quad \dots (270)$$

For cell No.4: q_4 calculated

$$0=\ \frac{1}{A_1}\left[q_1\left(\frac{ds_{1,34,c}}{t_{1,34,c}}+\frac{ds_{1,34}}{t_{1,34}}\right)-q_2\frac{ds_{1,34}}{t_{1,34}}\right]$$

$$-\frac{1}{A_4}\left[-q_3\frac{ds_{17,18}}{t_{17,18}}+q_4\left(\frac{ds_{17,18}}{t_{17,18}}+\frac{ds_{17,18,c}}{t_{17,18,c}}\right)\right]$$

$$+\frac{1}{A_1}\oint_{R1} q_b\frac{ds}{t}-\frac{1}{A_4}\oint_{R4} q_b\frac{ds}{t} \quad \dots (271)$$

The shear stress effect the internal component must be below the yield shear stress of the components material.

$$\tau=\ \frac{q}{t} \quad \dots (272)$$

$$\tau<\tau_{yeild} \quad \dots (273)$$

A MATLAB code had been written to calculate the structural mode results, see Appendix (D)

4.6 NASA STF fan model

4.6.1 Introduction

NASA STF fan had been used as a prop-fan to accelerate the air into the wing at low aircraft speed (flight speeds) with the axial x-momentum equal or less than the drag produced by the fan. This fan is followed by stator stage to discharge the follow axially. This model approximates the axial momentum produced by the prop-fans per second ($M_x{}'$).

4.6.2 The axial momentum

As the air flow sweep into and out of the prop-fan a reaction face ($\bar{F}$) pushes the aircraft forward and this force proportion to the time rate of change of the momentum produced by the prop-fan as formulated by newton's third and second laws.

$F = \frac{d}{dt}\ (m_{air} \times V_{air})$ … (274) where: $\bar{F} = -F$

The negative sine refers to the opposite direction to F. The force that increase the aircraft velocity in the X-direction is the X-momentum component.

The model configuration

The model used is a finite control volume fixed in the space with the fluids moves through it. The control volumes are bended to be parallel to the cylindrical hub so that assumption number two below can be used. Also, the rear part of the rotor control volume is inclines by angle corresponding to the out flow angle to capture the out flow. The depth of both control volumes in the radius direction is the unit length of the blade. See figure ().

The objective of this model is to estimate the increment in the X-momentum component $\left(\frac{dM_x}{dt}\right)$ as a function in its variables (equation). Using the X-component in the integral form of Navier-Stokes equation:

$\iiint_v \frac{\partial(\rho u)}{\partial t} dv + \oiint_S (\rho u.dS)\, u = -\oiint_S pdS + \oiint_S \tau_{xx} dS + \oiint_S \tau_{yx} dS + \oiint_S \tau_{zx} dS + \iiint_v \rho g dv$ … (275)

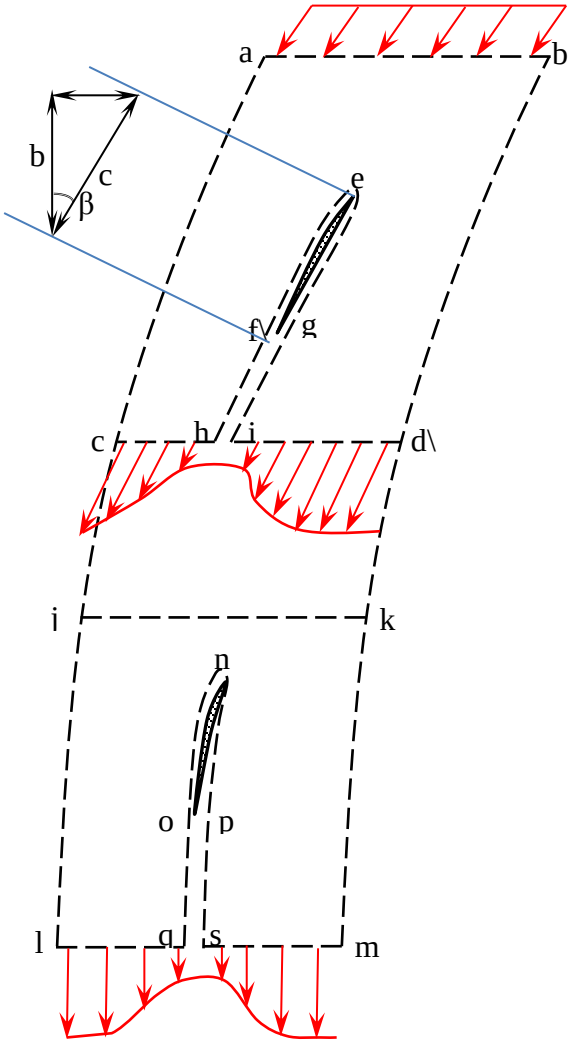

Figure 53. prop-fan control volume

Assumptions

1. No separation at the rotor and stator blade trailing edge (the air flow particulars kinetic energy more than zero even the trailing edge).
2. The rotor receives a uniform flow along a certain radius ⇒ $u_3 = f(r)$
3. The fans are near to each other. Thus a wing receives uniform mass flow rate along it semi-span.
4. Assume the condition of steady operation ⇒ $N = constant$.
5. The mass flow through the side walls equal to zero.

6. Assume the flow moves absolutory parallel to the fan axis. Thus there is no Z-component $\omega = 0$.
7. The prop-fan will be operated bellow the sonic Mach number and it has thin airfoil, the heat change inside the control volume can be neglected. Thus,

$$\oiint_S (\rho u dS)\, u = -\oiint_S pdS + \oiint_S \tau_{xx} dS + \oiint_S \tau_{yx} dS + \oiint_S \tau_{zx} dS + \oiiint_v \rho g dv + \bar{R}_x \quad \ldots (276)$$

Where:

$\oiint_S (\rho u dS)\, u = M_x{}'$ ≡ the net flow of the momentum in the x-direction out of one prop fan.

The prop fans are scaled to be suitable for the design but the velocity tringle which illustrated in the data sheet of the original NASA STF fan is kept the same by decreasing the velocities: c_a, w and U with the ***same percentage*** (E). Thus, the angle of attack and the blade inlet and outlet angles are the same as in the data sheet velocity tringle.

$E = 0.4$

The variation in the axial velocity with the radius at station No.2

Using second order equation:

$$Az'''^2 + Bz''' + C = M = 20.04\sqrt{T}u \quad \ldots (277)$$

Where: $z''' = r$.

Hub: $A(r_h)^2 + Br_h + C = 2E \quad \ldots (278)$

Mid.: $A(r_m)^2 + Br_m + C = 2E \quad \ldots (279)$

Tip: $A(r_t)^2 + Br_t + C = 2.01E \quad \ldots (280)$

By solving the three equation together and substituting for:

$r_t - r_h = l$

$$r_m + r_h = \frac{l}{2} l + D_h$$

$$r_m + r_t = -\frac{l}{2} l + D_t$$

$$r_t - r_m = r_m - r_h = \frac{l}{2} l$$

$$u_2 = \frac{0.001E}{\sqrt{T} l^2} \left[z'''^2 + (r_h - z''') \left(\frac{l}{2} l + D_h \right) - {r_h}^2 \right] + 2E \quad \ldots (281)$$

$$\left(\frac{du}{dz'''} \right)_2 = \frac{0.001E}{\sqrt{T} l^2} \left[2z''' - \left(\frac{l}{2} l + D_h \right) \right] \quad \ldots (282)$$

The variation in the axial velocity at station No.3

The same procedure is done at station No.3:

Hub: $A(r_h)^2 + Br_h + C = 2.76E$ … (283)

Mid.: $A(r_m)^2 + Br_m + C = 2.57E$ … (284)

Tip: $A(r_t)^2 + Br_t + C = 2.51E$ … (285)

$$u_3 = \frac{0.012E}{\sqrt{T} l^2} \left[z'''^2 + (r_h - z''') \left(\frac{l}{2} l + D_h \right) - {r_h}^2 \right] + 2.76E \quad \ldots (286)$$

$$\left(\frac{du}{dz'''} \right)_3 = \frac{0.012E}{\sqrt{T} l^2} \left[2z''' - \left(\frac{l}{2} l + D_h \right) \right] \quad \ldots (287)$$

The variation in the inlet velocity at station No.2

Hub: $A(r_h)^2 + Br_h + C = 2.36E$ … (288)

Mid.: $A(r_m)^2 + Br_m + C = 2.54E$ … (289)

Tip: $A(r_t)^2 + Br_t + C = 2.70E$ … (290)

$$V_2 = \frac{-0.001E}{\sqrt{T} l^2} \left[z'''^2 + (r_h - z''') \left(\frac{l}{2} l + D_h \right) - {r_h}^2 \right] + 2.36E \quad \ldots (291)$$

$$\left(\frac{dV}{dz'''} \right)_2 = \frac{-0.001E}{\sqrt{T} l^2} \left[2z''' - \left(\frac{l}{2} l + D_h \right) \right] \quad \ldots (292)$$

The variation in the inlet velocity at station No.3

Hub: $A(r_h)^2 + Br_h + C = 3.11E$ … (293)

Mid.: $A(r_m)^2 + Br_m + C = 2.79E$ … (294)

Tip: $A(r_t)^2 + Br_t + C = 2.67E$ … (295)

$$V_3 = \frac{-0.001E}{\sqrt{T}l^2}\left[z'''^2 + (r_h - z''')\left(\frac{l}{2}l + D_h\right) - r_h{}^2\right] + 3.11E \quad \text{… (296)}$$

$$\left(\frac{dV}{dz'''}\right)_3 = \frac{-0.001E}{\sqrt{T}l^2}\left[2z''' - \left(\frac{l}{2}l + D_h\right)\right] \quad \text{… (297)}$$

The variation in the outlet velocity at station No.3

Hub: $A(r_h)^2 + Br_h + C = 2.75E$ … (298)

Mid.: $A(r_m)^2 + Br_m + C = 2.63E$ … (299)

Tip: $A(r_t)^2 + Br_t + C = 2.65E$ … (300)

$$u_{3,out} = \frac{0.007E}{\sqrt{T}l^2}\left[z'''^2 + (r_h - z''')\left(\frac{l}{2}l + D_h\right) - r_h{}^2\right] + 2.75E \quad \text{… (301)}$$

$$\left(\frac{du_{out}}{dz'''}\right)_3 = \frac{0.007E}{\sqrt{T}l^2}\left[2z''' - \left(\frac{l}{2}l + D_h\right)\right] \quad \text{… (302)}$$

The variation of the blade inlet angle at station No.2

Table 15. blade inlet angle at station No.2

	β
Hub	32.06
Mid.	38.06
Tip	41.89

Hub: $A(r_h)^2 + Br_h + C = 32.06$ … (303)

Mid.: $A(r_m)^2 + Br_m + C = 38.06$ … (304)

Tip: $A(r_t)^2 + Br_t + C = 41.89$ … (305)

$$\beta_2 = \frac{-2.17}{l^2}\left[z'''^2 + (r_h - z''')\left(\frac{l}{2}l + D_h\right) - {r_h}^2\right] + 32.06 \qquad \ldots (306)$$

The variation of the angle ε at station No.3

Table 16. the angle ε at station No.3

	$\boldsymbol{\varepsilon}$
Hub	-4.88
Mid.	12.26
Tip	18.71

Hub: $A(r_h)^2 + Br_h + C = -4.88$ … (307)

Mid.: $A(r_m)^2 + Br_m + C = 12.26$ … (308)

Tip: $A(r_t)^2 + Br_t + C = 18.71$ … (309)

$$\varepsilon_3(z''') = \frac{-10.69}{l^2}\left[z'''^2 + (r_h - z''')\left(\frac{l}{2}l + D_h\right) - {r_h}^2\right] - 4.88 \qquad \ldots (310)$$

Rotor control volume

To apply equation () to the air sweeps into the control volume which include the rotor, the forces effect on the air inside the control volume had been estimated. There are two forces effects there:

1. The surface forces: the pressure and the shear stress.
2. The potential energy due to the change in the altitude.

The surface forces

The shear force and the pressure force effect on the walls f,h and g,i

This two surfaces of the rotor control volume "are taken adjacent to each other; hence any shear stress or pressure distribution one is equal and opposite to that on the other" thus they cancel each other's.

The surface feg

The shear stress distribution and the pressure distribution over the blade wall effect this surface by a reaction force ($\bar{R}$) to the aerodynamic force R:

$$\bar{R}(z''') = -R(z''') = -\sqrt{L(z''')^2 + D(z''')^2} \quad \dots (311)$$

The lift is normal to the inlet velocity while the drag is parallel to it.

The x-component of this force has been considered:

$$\bar{R}_x(z''') = -\left(L(z''')\csc\beta(z''') - D(z''')\cos\beta(z''')\right) \quad \dots (312)$$

$$L'(z''') = \frac{1}{2}\rho V_2(z''')^2 C(z''') C_{l_0}(z''') \quad \dots (313)$$

$$D'(z''') = \frac{1}{2}\rho V_2(z''')^2 C(z''') C_{D_0}(z''') \quad \dots (314)$$

$$C_{D_0}(z''') = C_{D,0_0}(z''') + C_{D,i_0}(z''') + C_{D,w}(z''') \quad \dots (315)$$

Since the maneuver such that the wing will receive a velocity below the critical Mach number; there is no wave drag over the blade length.

$\therefore C_{D,w}(z''')$ = zero

$$C_{D,i_0}(z''') = k_3 C_{l_0}(z''')^2 \quad \text{where: } k_3 = \frac{1}{\pi e AR} \quad \dots (316)$$

The values of the aspect ratio and the span efficiency factor don't depend on the rescaling procedure.

$AR = 0.97$

$\lambda = 0.79$

Using figure (), the induced drag factor $\delta = 0.008$,

$$e_0 = \frac{1}{1+0.036} = 0.992$$

$$e = e_o \cos\Lambda_{L.E.} = 0.992\cos 1 = 0.992$$

$k_3 = 0.331$

$C_{D,0_0}(z''') = C_{D,e_0} + \Delta C_{D,0}(z''')$ … (317)

$C_{D,e_0} = 0.010$

$\Delta C_{D,0}(z''') = k_1 C_{l_0}(z''')^2$ … (318)

$k_1 = \frac{1}{3} k_3 = 0.110$

$C_{D_0}(z''') = 0.010 + 0.441\ C_{l_0}(z''')^2$ … (319)

$V_2(z''')$ is given by equation (291).

$\bar{R}_x(z''') = -\frac{1}{2}\rho V_2(z''')^2 C(z''')[C_{l_0}(z''')(\csc\beta(z''') - 0.441\cos\beta(z''')) - 0.010\cos\beta(z''')]$ … (320)

Where (β) is given by equation (306).

$\bar{R}_x = \int_{r_h}^{r_t} \bar{R}_x(z''')\, dz'''$ … (321)

Since the rotational speed of the prop-fan is constant, the angle of attack is constant also at certain radius. Thus the blade has a constant lift coefficient. The blade has a geometric and aerodynamic twist.

Using the classical thin airfoil theory for the root section, the zero lift angle of attack had been estimated:

$\alpha_{L=0} = -\frac{1}{\pi}\int_0^{\pi} \frac{dy}{dx}\,(cos\theta_0 - 1)\, d\theta_0$ … (322)

Root section

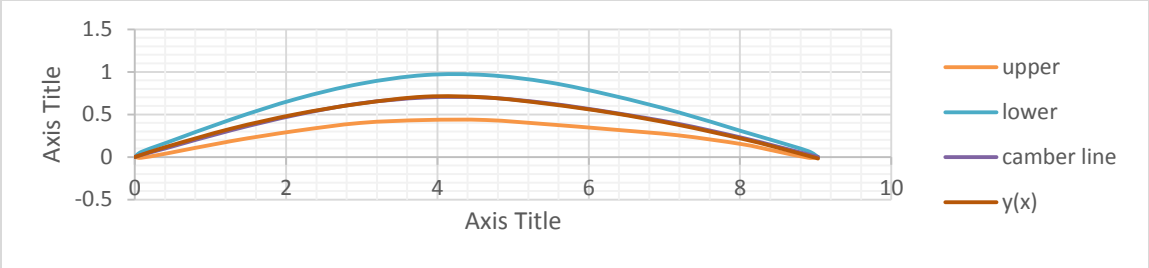

Figure 54. prop-fan rotor root section

Table 17. prop-fan rotor root section camber line

x real	y-lower	y-upper	cam.	Y(x)
0	0	0	0	0
0.0852	-0.00852	0.05964	0.02556	0.025342
0.426	0.0426	0.1704	0.1065	0.122356
1.278	0.18744	0.44304	0.31524	0.334401
2.13	0.30672	0.6816	0.49416	0.502893
2.982	0.40044	0.86052	0.63048	0.62783
3.834	0.43452	0.96276	0.69864	0.709213
4.6434	0.43452	0.96276	0.69864	0.699551
5.46984	0.3834	0.87756	0.63048	0.623299
6.3048	0.32376	0.7242	0.52398	0.518518
7.17384	0.2556	0.52824	0.39192	0.379843
8.0088	0.15336	0.30672	0.23004	0.21815
8.4348	0.07668	0.19596	0.13632	0.124911
8.9034	-0.00852	0.06816	0.02982	0.013963
9.0312	0	0	0	-0.01782

To estimate $\frac{dy}{dx}$ for the thin airfoil smooth camber line for the root section, a second order equation is solved for its coefficients A, B and C to estimate z(x). Then, the equation differentiated.

$$y(x) = \begin{cases} -0.03x^2 + 0.3x & 0 < x \leq 3.834 \\ -0.02x^2 + 0.11x + 0.62 & 3.834 < x \leq 9.031 \end{cases} \quad \ldots (323), (324)$$

$$\frac{dy}{dx} = \begin{cases} -0.060x + 0.300 & 0.000 < x \leq 3.834 \\ -0.040x + 0.110 & 3.834 < x \leq 9.031 \end{cases} \quad \ldots (325), (326)$$

$$x = 4.516\,(1 - \cos\theta_0) \quad \ldots (327)$$

$$\theta_0 = \cos^{-1}\left(1 - 2\,\frac{x}{c}\right) \quad \ldots (328)$$

$$\frac{dy}{dx}(\theta_0) = \begin{cases} -0.271(1 - \cos\theta_0) + 0.300 & 0.000 < \theta_0 \leq 1.419 \\ -0.181(1 - \cos\theta_0) + 0.110 & 1.419 < \theta_0 \leq \pi \end{cases} \quad \ldots (329), (330)$$

$$\alpha_{L=0} = -\frac{1}{\pi}\left\{ \begin{matrix} \int_0^{1.419}[-0.271(1 - \cos\theta_0) + 0.300](\cos\theta_0 - 1)d\theta_0 \\ + \int_{1.419}^{\pi}[-0.181(1 - \cos\theta_0) + 0.110](\cos\theta_0 - 1)d\theta_0 \end{matrix} \right\}$$

$$= -0.046\,rad. = -2.635\,deg.$$

Mid. section

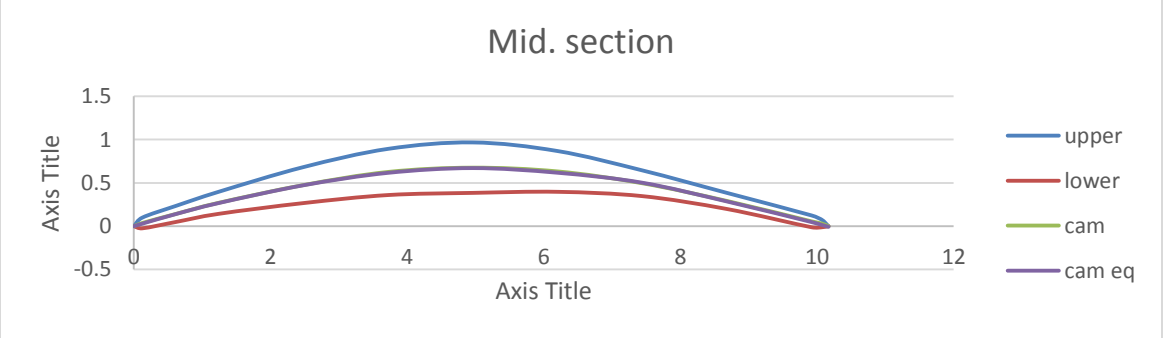

Figure 55. prop-fan rotor mid-section

Table 18. prop-fan rotor mid-section camber line

x real	y-lower	y-upper	cam.	cam
0	0	0	0	0
0.124	-0.0248	0.0992	0.0372	0.029452
0.62	0.0496	0.2356	0.1426	0.141112
1.24	0.1426	0.3968	0.2697	0.266848
2.48	0.2666	0.682	0.4743	0.472192

3.72	0.3596	0.8928	0.6262	0.616032
4.96	0.3844	0.9672	0.6758	0.670768
6.2	0.3968	0.868	0.6324	0.6172
7.44	0.3472	0.6448	0.496	0.502128
8.68	0.1984	0.3844	0.2914	0.285552
9.92	-0.0124	0.124	0.0558	0.047472
10.0688	-0.0124	0.0744	0.031	0.014769
10.168	0	0	0	-0.00752

$$y(x) = \begin{cases} -0.020x^2 + 0.240x + 0.000 & 0.000 < x \leq 3.720 \\ -0.020x^2 + 0.180x + 0.270 & 3.720 < x \leq 7.440 \\ -0.020x^2 + 0.180x + 0.230 & 7.440 < x \leq 10.168 \end{cases} \quad \ldots (331), (332), (333)$$

$$\frac{dy}{dx} = \begin{cases} -0.040x + 0.240 & 0.000 < x \leq 3.720 \\ -0.040x + 0.180 & 3.720 < x \leq 10.168 \end{cases} \quad \ldots (334), (335)$$

$$x = 5.084(1 - \cos\theta_0) \quad \ldots (336)$$

$$\theta_0 = \cos^{-1}\left(1 - 2\,\frac{x}{c}\right) \quad \ldots (337)$$

$$\frac{dy}{dx}(\theta_0) = \begin{cases} -0.203(1 - \cos\theta_0) + 0.240 & 0.000 < x \leq 3.720 \\ -0.203(1 - \cos\theta_0) + 0.180 & 3.720 < x \leq 10.168 \end{cases} \quad \ldots (338), (339)$$

$$\alpha_{L=0} = -\frac{1}{\pi}\left\{ \begin{array}{l} \int_0^{3.720}[-0.203(1 - \cos\theta_0) + 0.240](\cos\theta_0 - 1)d\theta_0 \\ + \int_{3.720}^{\pi}[-0.203(1 - \cos\theta_0) + 0.180](\cos\theta_0 - 1)d\theta_0 \end{array} \right\}$$

$$= -0.043\ rad. = 2.463\ deg.$$

Tip section

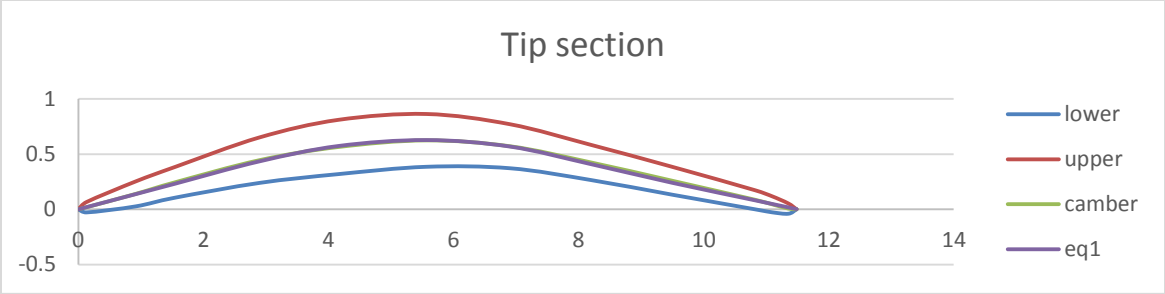

Figure 56. prop-fan rotor tip section

Table 19. prop-fan rotor tip section camber line

x real	y-lower	y-upper	cam.	cam
0	0	0	0	0
0.1328	-0.02789	0.0664	0.019256	0.01992
0.91632	0.02656	0.25232	0.13944	0.137448
1.55376	0.10624	0.38512	0.24568	0.233064
2.89504	0.23904	0.65072	0.44488	0.434256
4.15664	0.31872	0.81008	0.5644	0.573362
5.56432	0.38512	0.8632	0.62416	0.627376
6.9056	0.37184	0.77024	0.57104	0.568229
8.19376	0.2656	0.58432	0.42496	0.40981
9.4952	0.1328	0.38512	0.25896	0.240576
10.8232	0	0.17264	0.08632	0.081216
11.0888	-0.02656	0.11952	0.04648	0.049344
11.3544	-0.03984	0.05312	0.00664	0.017472
11.4872	0	0	0	0.001536

$$y(x) = \begin{cases} 0.150x & 0.000 < x \leq 2.895 \\ -0.030x^2 + 0.330x - 0.280 & 2.895 < x \leq 8.194 \\ -0.120x + 1.380 & 8.194 < x \leq 11.487 \end{cases} \quad \ldots (340), (341), (342)$$

$$\frac{dy}{dx} = \begin{cases} 0.150 & 0.000 < x \leq 2.895 \\ -0.060x + 0.330 & 2.895 < x \leq 8.194 \\ -0.120 & 8.194 < x \leq 11.487 \end{cases} \quad \ldots (343), (344), (345)$$

$$x = 5.744(1 - \ cos\theta_0) \quad \ldots (346)$$

$$\theta_0 = \ cos^{-1}\left(1 - 2\ \frac{x}{c}\right) \quad \ldots (347)$$

$$\frac{dy}{dx}(\theta_0) = \begin{cases} 0.150 & 0.000 < x \leq 1.052 \\ -0.345(1 - \ cos\theta_0) \ + 0.330 & 1.052 < x \leq 2.011 \\ -0.120 & 2.011 < x \leq \pi \end{cases} \quad \ldots (348), (349), (350)$$

$$\alpha_{L=0} = -\frac{1}{\pi}\left\{\begin{matrix} \int_0^{1.052} 0.150\ (cos\theta_0 - 1)d\theta_0 \\ + \int_{1.052}^{2.011} [-0.345(1 - \ cos\theta_0) \ + 0.330](cos\theta_0 - 1)d\theta_0 \\ + \int_{2.011}^{\pi} -0.120\ (cos\theta_0 - 1)d\theta_0 \end{matrix}\right\}$$

$$= -0.085\ rad.$$

The geometrical twist is included in the decrement in the blade angle of attack from the root to the tip:

Table 20. prop-fan sectional lift coefficients

	The angle of attack (degree)	$C_{l_0} = 2\pi\ (\alpha - \ \alpha_{L=0})$
Root angle of attack	7	1.056
Mid. section angle of attack	5	0.812
Tip angle of attack	4	0.972

Using second order equation to estimate the variation in the local lift coefficient along the blade radius:

Hub: $A(r_h)^2 + Br_h + C = 1.056$ … (351)

Mid.: $A(r_m)^2 + Br_m + C = 0.812$ … (352)

Tip: $A(r_t)^2 + Br_t + C = 0.972$ … (353)

$$C_{l_0}(z''') = \frac{0.404}{l^2}\left[{z'''}^2 + (r_h - z''')\left(\frac{l}{2}l + D_h\right) - {r_h}^2\right] + 1.056 \quad \ldots (354)$$

The surface ab and cd

The pressure force:

$P = \oiint_S pdS = P_2 - P_3$ … (355)

Due to the geometric twist of the fan blade there is a velocity gradient along the blade length and as result a pressure gradient at station No.2 and No.3 with the radius (see the velocity triangle in figure ()). Thus, the pressure force on the surface a, b given by:

$P_2(z''') \times t(z''') \times 1 = P_2(z''')\, t$ … (351)

Where:

$t(z''') = \frac{2\pi r(z''')}{z} = \frac{2\times 3.14\times r(z''')}{44} = 0.14r(z''')$ … (352)

$r(z''') = z'''$

$t(z''') = 0.14z'''$ … (353)

Applying Bernoulli's equation along the sliding part and the front cone between station 1 and 2 (since the Mach number is low value and there is no source action (addition or absorbing of work):

$\frac{1}{2}\,{u_1}^2 + P_1 = \frac{1}{2}\,u_2(z''')^2 + P_2(z''') \quad \Rrightarrow \quad P_2(z''') = \frac{1}{2}\,{u_1}^2 + P_1 - \frac{1}{2}\,u_2(z''')^2$ … (354)

Note: the pressure produced by the normal component of the velocity on the surface. In this case, it is u.

$u_1 = u_\infty$

$P_1 = P_\infty$

$P_2(z''') = \frac{1}{2}\,{u_\infty}^2 + P_\infty - \frac{1}{2}\,u_2(z''')^2$ … (355)

$u_2(z''')$ is given by equation (281).

The pressure force at the station No.3 has velocity gradient in both the z''' and y''' directions:

$$P_3(z''', y''') \times t(z''') = P_3(z''', y''') \times 0.14z''' \quad \dots (356)$$

The prop-fan pressure ratio $\pi' = \left(\frac{P_2}{P_3}\right) = 1.06$ is change as the rotational speed U changes. This value can be estimated from the off-design diagram illustrated in the data sheet of the fan.

The pressure force at station No.3:

$$P_3(z''', y''') \times 0.14z''' = 0.14z''' \frac{P_2(z''')}{1.06} \quad \dots (357)$$

The integration $\left(\oiint_S pdS\right)$ must be taken for the pressure effect on the control volume in the x-direction. Thus, it effects at the faces ab and cd:

$$\oiint_S pdS = 0.14z''' P_2(z''')\left(1 - \frac{1}{1.06}\right) = 0.14z'''\left(\frac{1}{2}u_\infty{}^2 + P_\infty - \frac{1}{2}u_2(z''')^2\right)\left(1 - \frac{1}{1.06}\right) \quad \dots (358)$$

The shear stress:

$$\oiint_S \tau_{xx} dS = \oiint_S \left[\lambda\left(\frac{\partial u}{\partial x'''} + \frac{\partial v}{\partial y'''}\right) + 2\mu \frac{\partial u}{\partial x'''}\right] dS = \left\{\left[\lambda\left(\frac{\partial u}{\partial x'''} + \frac{\partial v}{\partial y'''}\right) + 2\mu \frac{\partial u}{\partial x'''}\right] A\right\}_{cd} - \left\{\left[\lambda\left(\frac{\partial u}{\partial x'''} + \frac{\partial v}{\partial y'''}\right) + 2\mu \frac{\partial u}{\partial x'''}\right] A\right\}_{ab} \quad \dots (359)$$

The shear τ_{xx} is in the x-direction. It effects normal on the two faces ab and cd in the flow direction.

$$A_{ab} = A_{cd} = 1 \times t(z''') = 0.14z''' \quad \dots (360)$$

For air:

$$\mu = \mu_\infty \left(\frac{T}{T_\infty}\right)^{0.67} = 1.79 \times 10^{-6}\left(\frac{T}{288}\right)^{0.67} = 0.04 \times 10^{-6} \times T^{0.67}$$

$$\lambda = -\frac{2}{3}\mu = -0.027 \times 10^{-6} \times T^{0.67}$$

At the face ab:

The flow at a certain radius is uniform in the y''' direction because it is not effected by the blade yet.

$$\frac{\partial v}{\partial y'''} = 0 \quad \dots (361)$$

$\left(\frac{\partial u}{\partial x'''}\right)$ can be approximated for using a forward finite difference:

$$\frac{\partial u}{\partial x}(z''') = \frac{u_3(z''') - u_2(z''')}{b_r(z''')} \quad \dots (362)$$

Where b_r had been estimated in the design optimization of the sliding part.

At the face cd:

The face cd is behind the blade where the blade wake appears. The flow discharges through this surface with a velocity $V = ui + vj$. The velocity vectors are parallel. The change in the velocity component u in the x'''-direction is due to the spread of the wake. Once the distance between the blade trailing edge and the cd surface is small such that it is not enough to allow to the velocity to change greatly behind the blade. Thus:

$$\left(\frac{\partial u}{\partial x'''}\right)_{cd} = \left(\frac{\partial v}{\partial x'''}\right)_{cd} = 0 \quad \dots (363)$$

The velocity components: u and v change in the y'''- direction as V changes due to the present of the blade. This change had been estimated as follow:

$$\left(\frac{\partial v}{\partial y'''}\right)_{cd} \approx \left(\frac{\partial v}{\partial y'''}\right)_{T.E} \quad \dots (364)$$

From the KUTTA condition the flow leaves the blade trailing edge with a finite angle for cusp trailing edges, $V = ui + vj$. Thus: the shear stress at the wall at the trailing edge point is given by:

$$\tau_{w_{T.E}} = \mu \left(\frac{\partial u}{\partial y'''} + \frac{\partial v}{\partial x'''}\right)_{wall} = \mu \left(\frac{\partial u}{\partial y'''}\right)_{wall} \quad \dots (365)$$

$$\frac{\partial u}{\partial y'''} = \frac{\tau_{wT.E}}{\mu} = \frac{\frac{1}{2}\rho\, u_3 (z''')^2 c_f}{\mu} \quad \dots (366)$$

For incompressible laminar flow over flat plate:

$$c_f(z''') = \frac{0.664}{\sqrt{Re_x(z''')}} \quad \dots (367)$$

$$Re_x(z''') = \frac{\rho u x}{\mu} = \frac{\rho u_2(z''') c(z''')}{\mu} \quad \dots (368)$$

$u_2(z''')$ is given by equation (281).

$$\left(\frac{\partial v}{\partial y'''}\right)_{cd} = \frac{\partial v}{\partial z'''} \times \frac{\partial z'''}{\partial u'''} \times \frac{\partial u}{\partial y'''} \quad \dots (369)$$

The face cd is near station No.3:

$$\left(\frac{\partial v}{\partial z'''}\right)_{cd} = \left(\frac{\partial v}{\partial z'''}\right)_3 = \left(\frac{\partial u,out}{\partial z'''}\right)_3 \times \sin\varepsilon(z''') \quad \dots (370)$$

$$\left(\frac{\partial z'''}{\partial u'''}\right)_{cd} = \frac{1}{\left(\frac{\partial u}{\partial z'''}\right)_3} \quad \dots (371)$$

The surface ac and bd

The two surface are far enough from the blade and the mass flow through them equal to zero, thus there is no velocity gradient through them:

$$\tau_{ac_{yx}} = \tau_{bd_{yx}} = 0 \quad \dots (372)$$

$$\oiint_S \tau_{yx} dS = 0 \quad \dots (373)$$

$$\oiint_S p dS = 0 \quad \dots (374)$$

The surface abcd, tip and abcd, hub

The pressure force effect in this two surfaces are in the z''' direction and have no effects in the x-momentum.

The shear stress effects this surfaces are due to the gradient in the x-component of the velocity vector (u) in the z''' direction:

$$\oiint_S \tau_{zx} dS = \oiint_S \left[\mu\left(\frac{\partial u}{\partial z'''} + \frac{\partial \omega}{\partial x'''}\right)\right] dS = \left[\mu\left(\frac{\partial u}{\partial z'''} + \frac{\partial \omega}{\partial x'''}\right)\right]_{(abcd)} A + \left[\mu\left(\frac{\partial u}{\partial z'''} + \frac{\partial \omega}{\partial x'''}\right)\right]_{(abcd)'} A \quad \dots (375)$$

$$A(z''') = t(z''')\, b_r(z''') = 0.14 z''' b_r(z''') \quad \dots (376)$$

For both surfaces:

$$\omega = 0, \Rightarrow \quad \frac{\partial \omega}{\partial x} = 0 \quad \dots (377)$$

The value of $\left(\frac{\partial u}{\partial z'''}\right)$ has been taken as average between its value at station 2 and station 3 through the surfaces using forward difference:

$$\left\{\left(\frac{\partial u}{\partial z'''}\right)_{abcd} = \frac{1}{2}\left[\left(\frac{\partial u}{\partial z'''}\right)_2 + \left(\frac{\partial u}{\partial z'''}\right)_3\right]\right\}_{z'''=z'''} \quad \dots (378)$$

$$\left\{\left(\frac{\partial u}{\partial z'''}\right)_{(abcd)'} = \frac{1}{2}\left[\left(\frac{\partial u}{\partial z'''}\right)_2 + \left(\frac{\partial u}{\partial z'''}\right)_3\right]\right\}_{z'''=z'''+1} \quad \dots (379)$$

<u>The potential energy</u>

$$\iiint_v \rho g dv = 9.81 \rho \mathbf{V} = 9.81 \rho \pi \left[\frac{{D_t}^2 - {D_h}^2}{4}\right] b_r \quad \dots (380)$$

<u>A MATLAB code had been written to estimate the axial momentum produced by all prop-fans depending on the analysis done above. See Appendix (E).</u>

4.7 The consumed power

<u>The work</u>

Due to the rotational speed of the prop-fan, the flow in and outs the control volume un-axially. The mechanical work in the prop-fan shaft transmitted to the airflow in the control volume through the effect of the rotational speed in outflow direction, this work is directly proportion to $\Delta w_u$and Δc_a. Thus, two forces effect in the control volume: one in

the rotation direction and it don't affect the x-momentum and the other in the x-direction and produce besides the other forces effect in the x-direction the change in the axial velocity c_a. This force equal to the rate of change in the axial momentum.

$R_a = M_x{}' l$ … (381)

For simplicity the radial component is neglected.

The work to suck the air is given by:

$W = R_a \times (b_r + b_s) = 0.04\, \Delta p \times {l_b}^2 + \dot{m}\, \Delta c_u$ … (382)

The power consumed to suck the air:

$P = \dot{m}W = \dot{m}\big(R_a \times (b_r + b_s)\big)$ … (383)

A MATLAB code had been written to estimate the consumed power by all prop-fans. This step had been done after the design optimization. See Appendix (G).

5 Design optimization

5.1 The design of the sliding part

The airfoil which has been chosen for the sliding part is NACA 2412 and it is the same airfoil along the semi-span of the sliding part. The airfoils position of the sliding part is parallel to the original wing airfoils position (perpendicular on the middle spar (spar No.2)). To be sure when the sliding part in the extension position the sweep back at its leading edge is the same as the original wing leading sweep, the sliding part leading edge line is parallel to the original wing leading edge line. See figure (57).

In the choosing of the sliding part dimensions, two aspects had been considered:

1. The available space inside the original wing to store the sliding part without effect the original wing internal structure greatly.
2. The available extending trajectory out of the original wing.

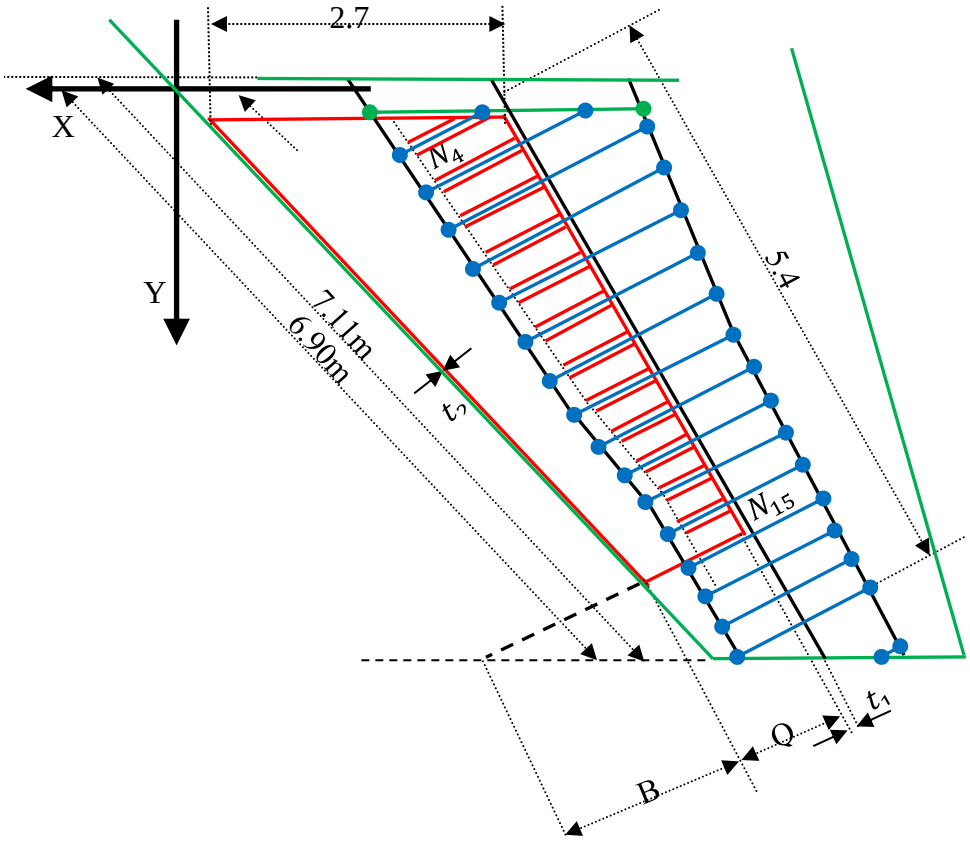

Figure 57. sliding part design 1

Cuttings in the internal structure of the original wing are necessary to pass the sliding part into the original wing as follow: the sliding part divided into two parts, the first has the airfoil cross-section and the second has a thinner rectangular cross-section. The first one included in the area between the original wing leading edge and the front spar (spar No.1) while the other pass through the front spar and the front part of the ribs (cuts). That is to decrease the cuttings cross-section area in the original wing internal structure.

After and while the sliding part extended out of the original wing, another two parts extend in a direction parallel to the original wing leading edge to fill the spaces between the new wing and the fuselage and the tip features and give a smooth shape. This parts are a thin wall parts which can stored in the two edges of the sliding part.

An optimization is achieved to maximize the exposed area of the sliding part using the MATLAB as follow:

The mathematical statement:

To maximize the exposed area of the sliding part (S_{exp})

$\Rightarrow (S_{exp})_{max.}$

The constraint

To be sure the sliding part tip section at the full extension position don't exceeds the wing tip section:

$Q \leq 0.8\,B$ … (384)

Suitable values have been chosen for t_1 and t_2:

$t_1 = 1cm$

$t_2 = 1cm$

The width of the sliding part is controlled by:

$y''_{N15} \geq y'' \geq y''_{N13}$ … (385)

$$\Rightarrow 4.62 \geq y'' \geq 3.58 \quad \dots (386)$$

Where:

$$Q = x''_{L.E}(y'') - t_1 - t_2 \quad \dots (387)$$

$$\therefore Q = 1.04 + 0.23(4.62 - y'') - t_1 - t_2 \quad \dots (388)$$

$$B = \frac{\left(y''_{tip} - y''_{Q}\right)_{S2}}{\tan 29} - t_1 - t_2 - Q = \frac{\left(5.93 - y''_{Q}\right)_{S2}}{\tan 29} - t_1 - t_2 - Q \quad \dots (389)$$

$$B = 10.78 - 1.82y''_{Q} - t_1 - t_2 - Q \quad \dots (390)$$

Note:

The length used from Q to fix the sliding part with the original wing is chosen to be 15% of Q.

The exposed area has been approximated as the projection of the sliding part on the X-Y plane:

$$g2 = \left(5.47 - \left(y''_{Q}\right)_{S2}\right)\cos 13 = 0.97\left(5.47 - \left(y''_{Q}\right)_{S2}\right) \quad \dots (391)$$

$$g1 = 1.62$$

$$\left(S_{exp}\right)_1 = 5.25\ m^2$$

$$\left(S_{exp}\right)_2 = \frac{1}{2}(0.85 \times 2.77)^2 \sin 58 \cos 58$$

$$+0.85Q\ (7.11 - g1 - g2)$$

$$+\frac{1}{2}(7.11 - g1 - g2)^2 \tan 13$$

$$\left(S_{exp}\right)_2 = 1.25 + 0.85Q\ (7.11 - g1 - g2) + +0.11(7.11 - g1 - g2)^2 \quad \dots (392)$$

$$\left(S_{exp}\right)_3 = \frac{1}{2}(g2)(0.85Q) = 0.43Q(g2) \quad \dots (393)$$

$$S_{exp} = \left(S_{exp}\right)_1 + \left(S_{exp}\right)_2 + \left(S_{exp}\right)_3 \quad \dots (394)$$

An actuator has been incorporated into the siding part inward side to rotate it by 13 degrees and thus increase the leading edge sweep be **13 degrees**. This will affect the generated lift and the aircraft stability during the maneuver when the sliding part extends out. See figure (58).

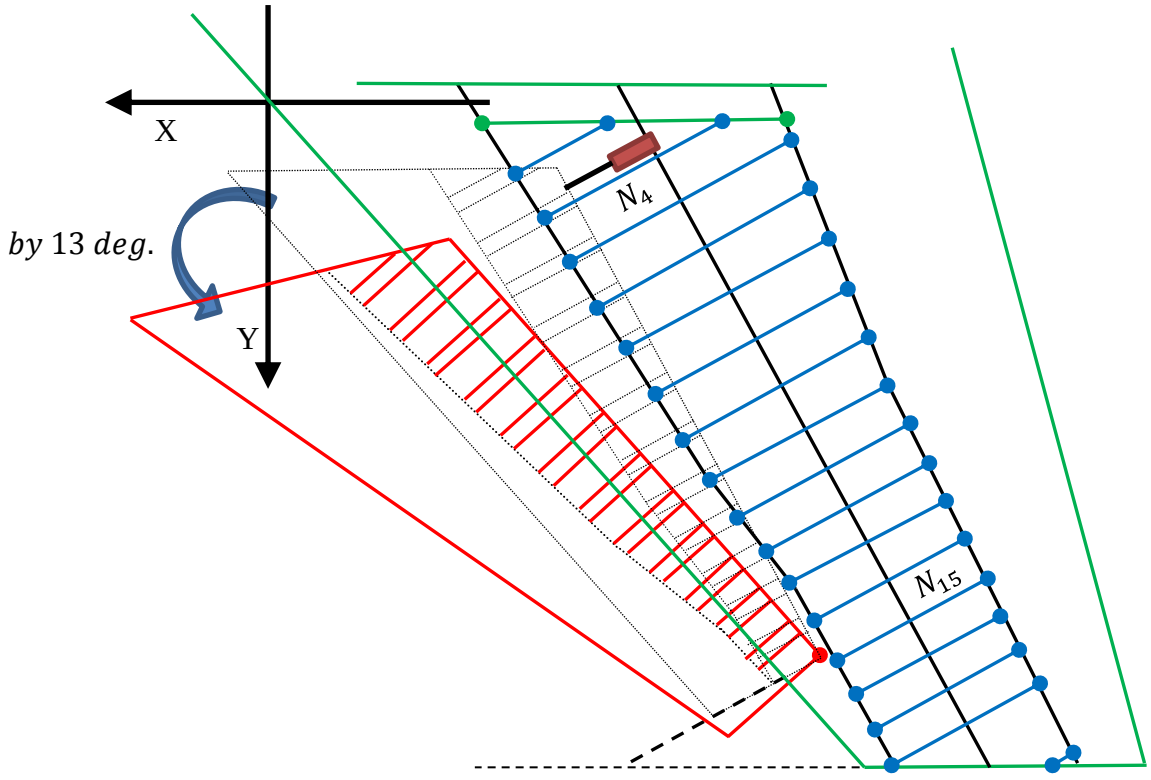

Figure 58. sliding part design 2

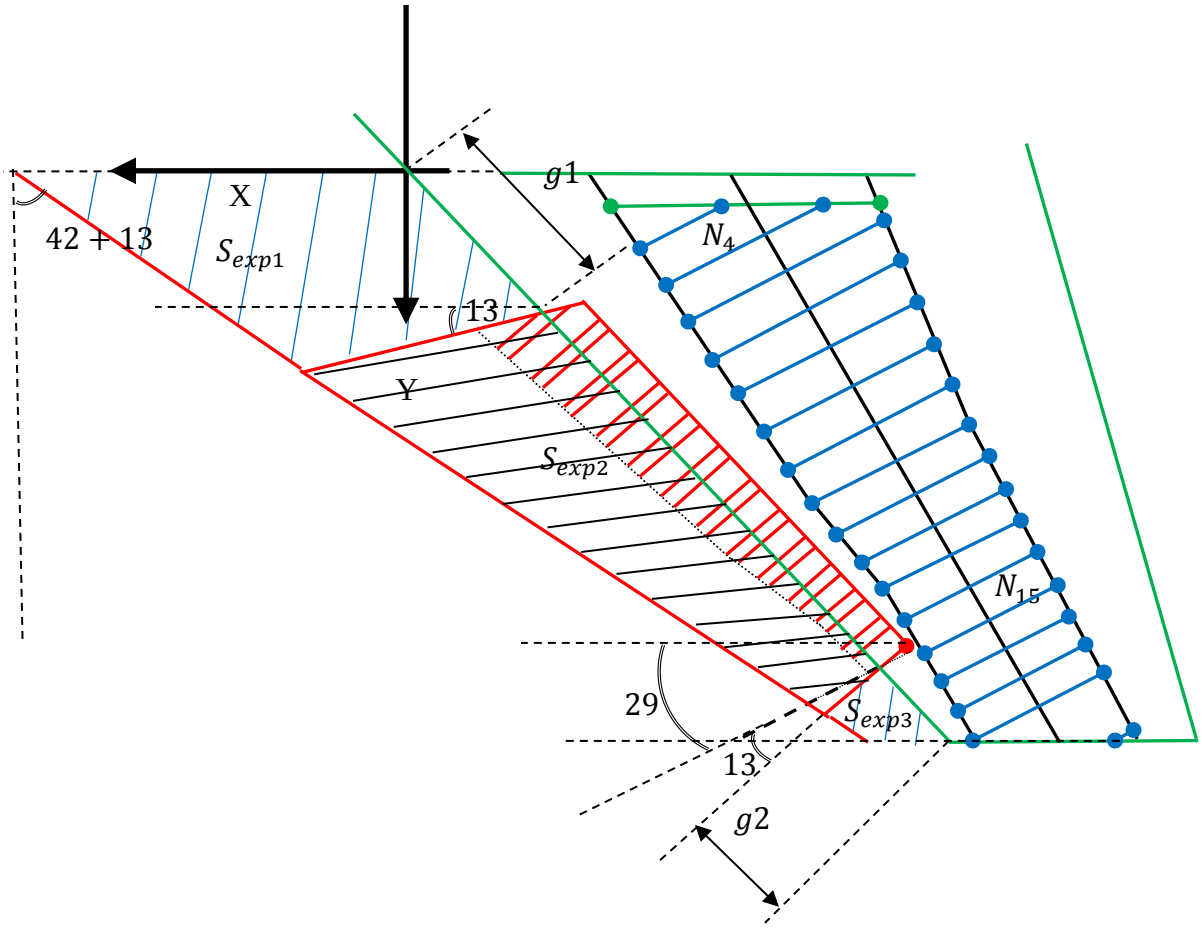

Figure 59. sliding part design 3

The slots design

When the slots are fully open:

$(A)_l = b \times h \times M$ … (395)

The slots are separated by 4cm while $b = 6cm$ and $h = 3cm$. Then:

$M = \frac{l_{L.E}}{b+0.03} = \frac{7.11}{0.06+0.04} \approx 71$ slot at each side. … (396)

$(A)_l = 0.06 \times 0.03 \times 71 = 0.13m^2$

The mass flow rate from the prop-fans to the lower surface is given as:

$\dot{m}_l = \rho V_6 (A)_l = 0.31 \rho V_6$ … (397)

The upper surface mass flow rate will decrease by $\dot{m}_l$ which effect the lift value.

5.2 The fan modification

The prop fans have been distributed along the semi-span of the sliding part and they are spaced by 15 cm from the tip even the root of the sliding part.

The fans diameter changes from the root into the tip (decreases) as well as the thickness of the wing is changes:

The rotor diameter equal to the stator diameter:

$$D_R(y'') = D_S(y'') = D_f(y'') \quad \dots (398)$$

To be sure the prop fan at certain section can be stored in the available volume, D_f must be less than the max. thickness of the sliding part section.

$$D_f < t_{max.} \quad \dots (399)$$

$C = 0.65Q =$ constant.

The fan width:

$$B_f(y'') = b_r(y'') + b_s(y'') + t(y'') + t_{cf}(y'') + t_{cr}(y'') \quad \dots (400)$$

Note: $b_r(y'')$ and $b_s(y'')$ here are for the blade tip; that is because the tip has the greater $b_r(y'')$ or $b_s(y'')$.

From the original NASA STF fan data sheet:

$$b_s = percentage\ (W) of\ b_r$$

$$\Rrightarrow b_s = W b_r \quad \dots (401)$$

$$W = \left(\frac{b_s}{b_r}\right)_{tip} = \frac{13.79cm}{10.62cm} = 1.30$$

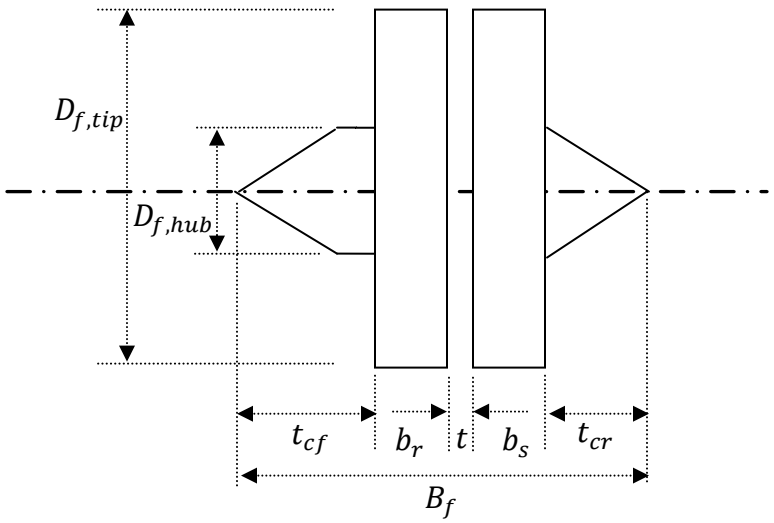

Figure 60. prop-fan dimensions

$B_f(y'') = (1 + W)b_r(y'') + t(y'') + t_{cf}(y'') + t_{cr}(y'')$ see figure (). … (402)

$b_r(y'') = 0.08$

t, t_{cf} and t_{cr} has been approximated from statistical data.

$t = 0.05b_r(y'')$ … (403)

$t_{cf} = t_{cr} = 2b_r(y'')$ … (404)

The thickness of the sliding part at a certain distance from its leading edge must be less than the thickness of the wing at the same distance from the wing leading edge.

$t(x'')_{S.P.} < t(x'')_{wing}$ … (405)

This width must be less than or equal to the thin rear part of the sliding part (which achieve no lift just serve as set for the fans). This length is chosen to be 20% of Q.

$l \geq B_f \quad \Rightarrow 0.2Q \geq B_f$ … (406)

The fan diameter is a percentage from the rotor disc width b_r (from the data sheet):

$b_r = KD_{f,tip}$ … (407)

For the full size NASA STF fan:

$$K = \frac{b_r}{D_{f,tip}} = \frac{10.62cm}{51cm} = 0.21$$

Also,

$$P = \frac{D_{f,hub}}{D_{f,tip}} = \frac{18cm}{51cm} = 0.35$$

$$\Rightarrow\ D_{f,hub} = \ 0.35\ D_{f,tip} \quad \ldots (408)$$

Note: b_r is taken at the tip because the fan blade chord increases from the root even the tip.

The prop fans are separated by distance T equal to:

$$T(i) = D_f(i) \ \ldots (409)$$

The number of prop-fans at one side is given as follows:

$$N_{P.F} = 7.11 - \sum D_f(i), \ \ldots (410) \quad \text{at each side}$$

The value of $N_{P.F}$ given from MATLAB (for) loop.

The new blade dimensions:

The three variables needed to be specified for the scaled prop-fans are: the length of the blades, their chords and the diameter of the hub.

For the full size NASA STF fan:

$$P = \frac{D_{f,hub}}{D_{f,tip}} = \frac{18cm}{51cm} = 0.35$$

$$\Rightarrow\ D_{f,hub} = \ 0.35\ D_{f,tip} \quad \ldots (411)$$

$D_{f,tip}$ has been calculated from the previous code.

The blade length is given by:

$$l_b = D_{f,tip} - D_{f,hub} \quad \ldots (412)$$

For the rotor and the stator blades:

$b = C\cos\beta \Rightarrow C = \frac{b}{\cos\beta}$ … (413)

Where β has been saved the same as in the velocity tringle illustrated by the data sheet of the real NASA STF fan; that is to make the using of the off-design diagram is possible.

β has been measured at three sections: at the tip, the mid. section and at the hub. Thus there are three chord values for the same blade at a certain y''. See table (15).

For real NASA STF fan:

$c_{tip} = 11.49\ cm$

$c_{hub} = 9.03\ cm$

$c_{mid} = 10.17$

$\therefore c_{hub} = 0.79\ c_{tip}$ … (414)

$\therefore c_{mid} = 0.89\ c_{tip}$ … (415)

A MATLAB code has been written for design optimization and prop-fan rescale, see Appendix (F)

6 Results and discussion

6.1 Modified lifting line theory code

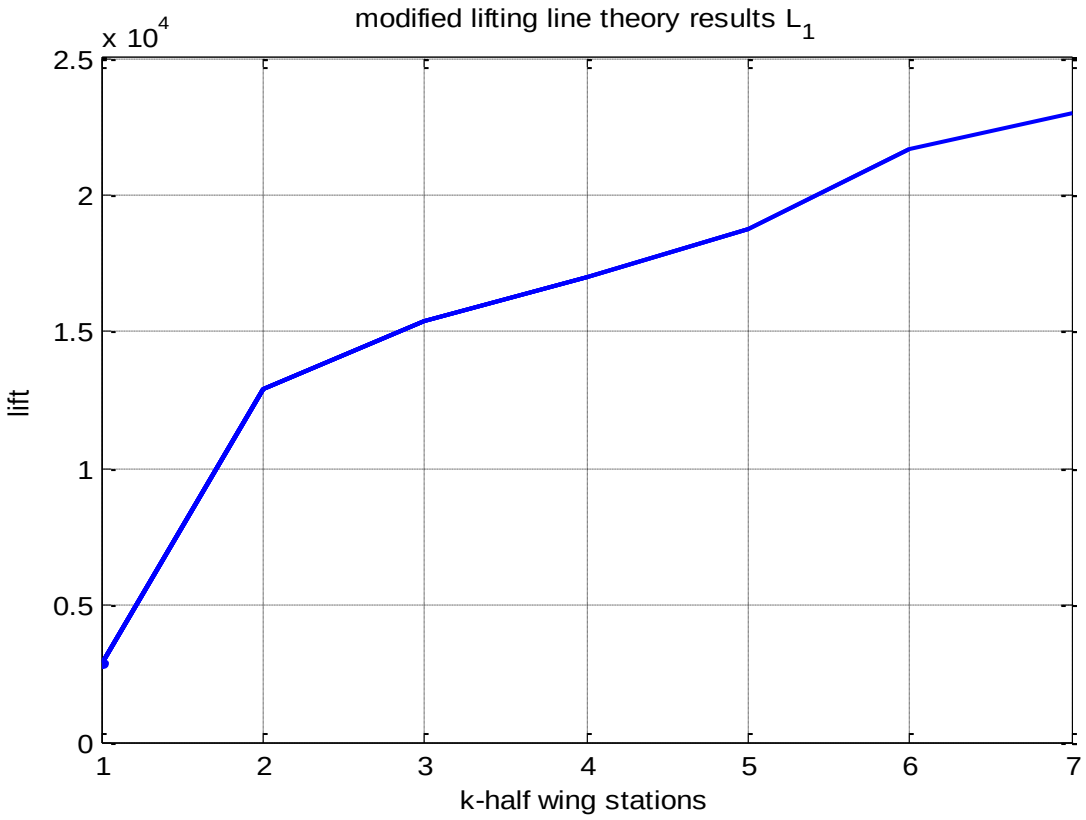

Figure 61. modified lifting theory results

Table 21. modified lifting line theory results

Lift coefficient _1	0.36
Lift _1	254150 N
Drag coefficient _1	0.03
Drag _1	24431 N

Figure (61) above shows that, the sectional lift value decreases from the root even the tip along the semi-span. When the prop-fans operated with a pressure ratio of 1.06, each prop-fan suck the air with 0.4 Mach and then accelerate the flow into the upper surface to 0.5 Mach. The lift and drag values which illustrated in table (21) are produce by the 0.4 Mach.

6.1.1 The upward acceleration

The lift value (L_1) results in upward acceleration (a) as follows:

$$a = \frac{L_1}{SU{-}35S\ mass} = \frac{254150}{18400} = 14\ m/s^2$$

SU-35S accelerates with $(14\ m/s^2)$ in the upward direction at zero forward speed and zero forward acceleration. This acceleration results in pure upward displacement in direction perpendicular over the aircraft wing. Additional acceleration values are results from the lift produced due to the difference in the velocity before and after the prop-fans (vortex panel code results (L_2)) and the lift generated by the sliding part due to the prop-fans suck velocity (0.4 Mach).

6.2 Panel method code results

For the near root section (N_1), the pressure coefficients distribution over the upper surface is given in figure (62). This pressure distribution is due the difference in the velocity between the upper and the lower surface of the wing section (0.1 Mach). The figure shows that the pressure decreases from value of 0.9 ear the leading edge even min. negative value of -2 then increase again even 0.9 near the trailing edge. This means that the upper surface produce additional lift due to the difference in the velocity.

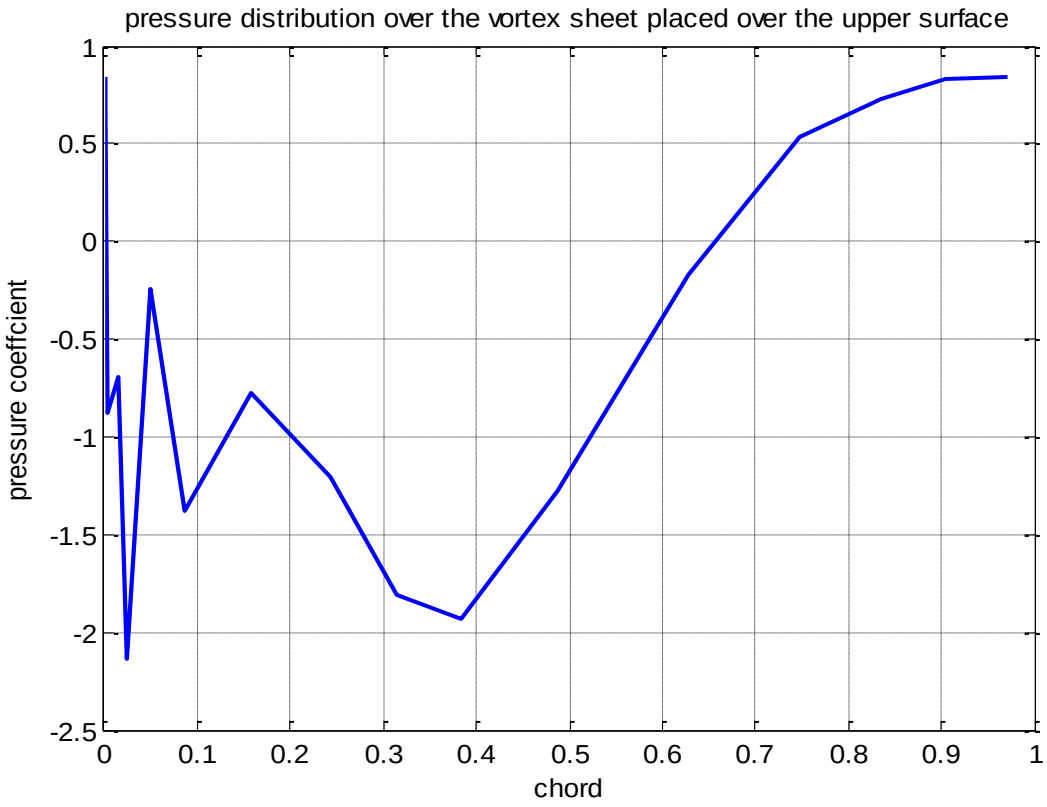

Figure 62. vortex panel code results

6.3 Design results

The maximum exposed area for the sliding pat equal to: 26.6019 m^2 for the half wing. This area is considerable in lift generation. The number of prop-fans is found to be 33 small prop-fans. All of the prop-fans are capable to be included inside the sliding part section and sliding part is also included inside the original wing volume. Some of the rescale results:

Table 22. design results

Prop-fan No.	Blade length (cm)	Total prop-fan width (cm)	Prop-fan diameter (cm)
1	8.41	17.26	12.94
2	8.04	16.49	12.36
3	7.68	15.75	11.81

4	7.33	15.05	11.28
5	7.01	14.38	10.78
6	6.69	13.73	10.30
7	6.39	13.12	9.84
8	6.11	12.53	9.40
9	5.84	11.97	8.98
10	5.56	11.44	8.58
33 prop-fan			

6.3.1 Sliding part design optimization, lift and upward acceleration

The design optimization procedure results in sliding part maximum exposed area of $(26.6019\ m^2)$ for half-wing. The airfoil NACA 2412 had been used because it illustrates good performance at the low speeds. Also, the code results illustrate that, the prop-fans are completely content inside the sliding part and the sliding part itself completely content inside the original wing.

$$L_{sp} = 0.5 \times 1.225 \times \left(20.04 \times 0.4 \times \sqrt{288}\right)^2 \times (26.6019 \times 2) \times 0.4 = 241222\ N$$

$$a = \frac{L_{sp}}{SU{-}35S\ mass} = \frac{241222}{18400} = 13\ m/s^2$$

As shown above the sliding part play an effective role in lift generation and the upward acceleration production.

6.4 Stability analysis results

Table 23. stability model results

Contribution	$C_{m,0}$	$C_{m,\propto}$	
Wing	-0.009	0.5456	Destabilizing
Tail	0	-0.0292	Stabilizing
Prop-fans	-	$33 \times 0.006 = 0.19$	Destabilizing

Table (23) shows that, the fighter SU-35S is not stable without the prop-fans effect. This result is expected because for fighters to increase the controllability (maneuverability) it must to have unstable aircraft (negative stability). Each prop-fan has small destabilizing contribution of 0.006. the total prop-fans contribution is that, they decrease the aircraft stability by 0.19.

6.5 Prop-fans axial momentum and consumed power codes results

6.5.1 Axial momentum

The code shows that, the prop-fans produce axial momentum value can't push the aircraft mass in the air in the forward direction. All prop-fans produce axial momentum of 1037 kg. m/sec. SU-35S has an empty mass of 18400 kg which means that it is needs a momentum of 18400 kg. m/sec. to move with 1m/sec. in the forward direction.

6.5.2 Consumed power

The consumed power code shows that, the consumed power by the all of the prop-fans equal to (649.6721 W) which much less than the power used to operate the turbojet engine in the thrust vectoring technique to achieve vertical takeoff which is more than (500 KW). Thus, it had been approved that the vertical flight technique normal to the aircraft wing and depending on the wing lift consumed less power than the other techniques (economical). This low consumed power is because of the very small dimension and weight of the prop-fans comparing with the turbo jet engine because the role of the turbo-jet engine is to produce thrust while the prop-fans role isn't thrust production but, accelerate thin layer of air over the wing upper surface.

7 Conclusion and recommendations

7.1 Conclusion

Most of the project objectives had been met. It was approved that, using the designed device the fixed wing aircraft become capable to perform vertical flight depending on the fixed wing lift itself sense a considerable amount of lift is generated. The stability model shows that; the aircraft is not stable during the vertical flight. But, it is expected result because for fighters the aircraft must be unstable to achieve the needed controllability (maneuverability). Due to the shortness of time, the structural analysis results is not completed. But it is expected that, there is no structural deformation because the applied load is less than the aircraft maximum load. The prop-fans model shows that, the axial momentum produced by the prop-fans is not enough to move (accelerate) the aircraft in the forward direction. The MATLAB design optimization and rescaling codes illustrate that, the prop-fans are extremely included inside the sliding part volume and the sliding part is completely included inside the original wing of the fighter SU-35S. The consumed power by all of the prop fans had been found much less than the power consumed to operate any turbo engine thus, the technique to achieve the vertical flight depending on the wing lift consumed much less power than all vertical takeoff technique which use the turbo-engines including the thrust vectoring technique.

7.2 Recommendations

It is better to apply this technique to achieve a vertical flight on the civil aircraft and to validate this theoretical results achieved in this projects using computational analysis. Also, it is preferred to complete the structural analysis by another team.

7.3 Future work

This technique will be applied on a simple straight wing aircraft prototype after much accurate analysis and depending on this research.

Referances

1. Anderson, J.D., *aircraft performance and design* 1999.
2. *http://en.m.wikipedia.org/wiki/Harriier_Jump_Jet*
3. *http://en.m.wikipedia.org/wiki/Ducted_Fan*.
4. William J. Fredericks , M.D.M.a.R.C.B., *Benefits of hybrid-electric propulsive to achieve 4x increase in cruise efficiency for VTOL aircrafts*.
5. Fredericks, W.J., *CONCEPTUAL DESIGN OF A VERTICAL TAKEOFF AND LANDING UNMANNED AERIAL VEHICLE WITH 24-HR ENDURANCE*.
6. ntrs.nasa.gov, *analysis of Mach 0.8 Turboprop slipstream wing*
7. *http://militaryrussia.ru/blog/topic-533.html*.
8. *https://en.wikipedia.org/wiki/Tiltrotor*.
9. *https://en.wikipedia.org/wiki/Powered_lift#Fan-in-wing*.
10. *https://en.wikipedia.org/wiki/Coand%C4%83_effect*
11. *https://en.wikipedia.org/wiki/V/STOL*.
12. MABY BOADO AMADOR , V.K., *MORPHING WING DESIGN FOR UAVs:A PROPOSED CONCEPT*
13. *https://en.wikipedia.org/wiki/Slipstream*.
14. *https://en.wikipedia.org/wiki/Circulation_control_wing*.
15. *https://en.wikipedia.org/wiki/Blown_flap*.
16. Narayan Parida , S.S.R.R., K. C. Rath.
17. *https://ar.wikipedia.org/wiki/sukhoi_su-35*.
18. *https://en.wikipedia.org/wiki/Saturn_AL-31#117S* .
19. *Su-35 multifunctional super-maneuverable fighter www.SUKHOI.org*.
20. Egbert_Torenbeek, *Advanced_Aircraft_Design__Conceptual_Design,_Technology_and_Optimization_of_Subsonic_Civil_Airplanes*. 2013.
21. james F . Schmidt, R.D.m., jerry R . Wood *supersonic through flow fan design*.
22. *http://www.neos-guide.org/content/optimization-introduction*
23. Daniel_P._Raymer, *Enhancing_Aircraft_Conceptual_Design_Using_Multidisciplinary_Optimization*.

24. *https://en.wikipedia.org/wiki/Multidisciplinary_design_optimization*.
25. *http://www.neos-guide.org/optimization-tree*.
26. *MULTIDISCIPLINARY AIRCRAFT CONCEPTUAL DESIGN OPTIMIZATION CONSIDERING FIDELITY UNCERTAINTIES*.
27. James F. Schmidt, D.M., Jerry R. Wood, Ronald J. Steinke, *supersonic through-flow fan design*: Cleveland Ohio,Lewis Research centre. p. ntrs.nasa.gov.
28. (Aerospace_Series)_AndraÌ• s_SoÌ• bester, A.I.J.F., *Aircraft_Aerodynamic_Design__Geometry_and_Optimization*. 2014.
29. Robert Cnelson, Flight stability and automatic control.
30. Anderson, Introduction to flight
31. T.H.G. Megson, Aircraft structure for engineering students, Third edition
32. Bandu N. Pamadi, Performance, stability dynamic, and control of airplanes
33. Bernard Etkin, Lloyod Duff Reid, Dynamics of flight stability and control, Third edition.
34. E. J. Hearn, Mechanics of materials 2, Third edition.
35. Steven C. Chapra, Applied numerical methods with MATLAB for engineers and scientists.

Appendixes

Appendix (A): modified lifting line theory code

```
%% lifting line theory code... this code estimate the lift distribution
L1.
% half wing
clear all
clc
b = 15.3-(2*0.12);  %without tip features
N = 14
M = N/2
alfa_0 =-0.046;
roh = 1.25;
temp=288
S = 62;
alfa=2*3.14/180
v_1=0.4*20.04*((temp)^0.5) %fan suck vel =free stream vel for fixed
aircraft
v_L1=v_1
alpha=(2*3.14/180)+ 0.02
%for alfa=1:4 % degrees
D(1:M)= alfa - alfa_0 + 0.02
%end
%% chord and theta as funtion in k
for k=1:M
    y_dash(k)= -(b/2)*(1-(2*k-1)/N)
    theta_0(k) = acos(-2*y_dash(k)/b)
end
for k=1:M
if  y_dash(k)>=-2.59 & y_dash(k)<=0
    chord(k)= 0.6*y_dash(k)+6.8
    %chord(N+1-k)=chord(k)
end
if y_dash(k)>=-7.22 &  y_dash(k)<=-4.01
       chord(k)= 0.58*y_dash(k)+6.36
       %chord(N+1-k)=chord(k)
```

```
end
if y_dash(k)>=-4.01 & y_dash(k)<=-2.61
       chord(k)= 0.1*y_dash(k)+3.63
       %chord(N+1-k)=chord(k)
end
if (y_dash(k)>=-7.52) & (y_dash(k)<=-7.22)
        chord(k)= 2.16  %meter
        %chord(N+1-k)=chord(k)
end
end
%% equations system generation
for k=1:M
    for n=1:M
    C(k,n)=(((2*b)/(3.142*chord(k)))+((2*n-1)/sin(theta_0(k))))*sin
((2*n-1)*theta_0(k))
    end
end
%% solving procedure
A = C\D'
%%lift distribution for L1
for k=1:M
    for n=1:M
        ss(k,n)=sin((2*n-1)*theta_0(k))*A(n)
    end
    sss(k)=sum (ss(k,:))
end
for k=1:M
    %for n=1:2:N
        l(k)=1.06*roh*v_1*cos(29*3.14/180)*(2*b*v_1*sss(k)) % per unit
span
        l_1(k)=l(k)*cos(alpha)
        plot (l_1,'b','linewidth',2)
        xlabel('k-half wing stations')
        ylabel('lift')
        title('modified lifting line theory results L_1')
        grid on
        hold on
    %end
```

```
end
CL_1=pi*((b^2)/S)*A(1)
CD_1=0.02+0.112*(CL_1^2)
L_1=0.5*roh*S*(v_1^2)*CL_1
D_1=0.5*roh*S*(v_1^2)*CD_1
```

Appendix (B): vortex panel code

```
clc ; clear all
roh = 1.225;
temp=288
s=62
v_6=0.05*20.04*((temp)^0.5) %mls
v_1=0.04*20.04*((temp)^0.5)
p_6=100000

x = [
5.27941092
4.9632345
4.5955875
4.2279405
3.67647
2.941176
2.205882
1.838235
1.470588
1.102941
0.5514705
0.367647
0.1470588
0.1102941
0.0367647
0.01102941
0.002205882
0 ]
x=x/5.27941092

y = [0
0.022573585
0.048308875
0.074044165
0.11744815
0.167837392
```

```
0.185787198
0.185979663
0.171003448
0.147917375
0.103596984
0.081092121
0.051410031
0.046179171
0.030780166
0.018383435
0.007352983
0]

n = length(x);
X = x
Y = y
xe = X'
ye = Y'

plot(xe,ye,'linewidth',3)
axis equal
grid on

for i = 1 : n - 1
    xs(i) = (xe(i + 1)- xe(i))/4 + xe(i)
    ys(i) = (ye(i + 1)- ye(i))/4 + ye(i)
    xr(i) = (xe(i + 1)- xe(i))/2 + xe(i)
    yr(i) = (ye(i + 1)- ye(i))/2 + ye(i)
    ds(i) = sqrt((xe(i + 1) - xe(i))^2 + (ye(i + 1) - ye(i))^2)
end

N = n-1 ;
for i = 1 : N
    for j = 1 : N
        r(i,j) = sqrt((xs(i) - xr(j))^2 +(ys(i) - yr(j))^2);
        A(i,j) = (ds(j)/(2*pi))*log(r(i,j));
    end
```

```
end

B = ones(N,1) ;
C = [A B] ;
D = zeros(1,N+1) ;
D(1,1) = 1;
D(1,N) = 1;
E = [ C ; D ];
V = (v_6-v_1);
a = 5;
u = V * cosd(a);
v = V * sind(a);
XS = [ xs 0 ]';
YS = [ ys 0 ]';
G =  E\ (u*YS-v*XS);
g = G(1:N);
cp = 1 - (g/V).^2;

figure
plot(xr(1:N),cp(1:N),'b -','linewidth',2)
xlabel('chord')
ylabel('pressure coeffcient')
title('pressure distribution over the vortex sheet placed over the
upper surface')
hold on
grid on
```

Appendix (C): stability analysis code

```
%% longitudenal stability check code
clear all
clc
d_CG=0.1
CG=2.05
M_1=0.4
CL=0.36
N_P_F= 33
%% wing body
c_ma_wb=((0.53+0.26*d_CG)-0.401)*(3.52*((1-(M_1)^2)^-0.5))
if c_ma_wb>0
    display('destablizig _ wing body')
else
    display('stable_wing body contribution')
end
%% tail
eff_t=1-2.602*((0.02+0.028*CL^2)^0.2)
c_ma_t=(0.444/sqrt(1-(eff_t*M_1)^2))*eff_t*(0.291-0.051*d_CG)
if c_ma_t>0
    display('destablizig_tail')
else
    display('stable_tail contribution')
end
%% prop fans contribution
for i=1:N_P_F
    l_p(i)=(l_b(i)/2)+CG+d_CG% the prop fan centre coincides with mid.
of l
    c_ma_N(i)=0.003*l_p(i)
    if c_ma_N(i)>0
        display('destablizig_ P.F')
    else
        display('stable_P.F contribution')
    end
end
```

Appendix (D): structural analysis code

```
%% structural analysis
clear all
clc
L=  % total lift = L1+L2
D=  % total drag
%thickness of spar webs and ... = constant
t=0.03 %meter - assumption
%yeilds stress
seg_yei=
taw_yei=

%% air loads
for alpha =1:3
    S_x(alpha)=L(alpha)*sin((alpha+1)*3.14/180)+D(alpha)*
cos(29*3.14/180)*cos((alpha+1)*3.14/180)
    S_y(alpha)=D*sin(29*3.14/180)
    S_z(alpha)=L(alpha)*cos((alpha+1)*3.14/180)-D(alpha)*
cos(29*3.14/180)*sin((alpha+1)*3.14/180)
end
%% (xr,yr,zr)
for alpha=1:3
a_bar(alpha)=0.61*sum (l(k)*(y(dy)
x_r(alpha)=0.25*5.50+0.57*a_bar(alpha)
y_r=0.82*a_bar(alpha)
end
%% geometrical
% spars (x)
y=linspace(0,5.24)
ny=length(y)
dy=1:ny
x=zeros(ny,dy)
n=1:34
for n=1
    for dy=1:ny
        if y(dy)>=0 & y(dy)<=3.08
           x(dy,n)=0.61*y(dy)+1.58
```

```
        elseif y(dy)>3.08 & y(dy)<=3.85
               x(dy,n)=0.82*y(dy)+0.94
        else
            x(dy,n)=0.54*y(dy)+2.02
        end
    end
end

for n=9
    for dy=1:ny
        x(dy,n)=0.54*y(dy)+2.73
    end
end
for n=17
    for dy=1:ny
        if y(dy)>=0 & y(dy)<=2.31
           x(dy,n)=0.26*y(dy)+4.24
        else
            x(dy,n)=0.48*y(dy)+3.73
        end
    end
end
for dy=1:ny
    plot(x(dy,n),dy,'*')
    hold on
end
% ribs numbering (i)(reffering to them by the y coordinate at the
second
% spar point
y_ddash=linspace(0.35,6.30,300) %between rib No.2 even rib No.20
nyy=length(y_ddash)
for ddy=1:nyy
    if dy==1
        i=2
    elseif dy==300
        i=20
    elseif y(dy)==0.27
        i=3
```

```
    elseif y(dy)>0.27 & y(dy)<=3
        for i=4:9
            y(dy)=0.27+0.39*(i-3)
        end
    elseif y(dy)>3 & y(dy)<=4.62
        for i=10:15
            y(dy)=3+0.33*(i-9)
        end
    elseif y(dy)>4.62 & y(dy)<=5.83
        for i=16:19
            y(dy)=3+0.31*(i-15)
        end
    end
end

%% stringers (x)
%n indicate the boom number
for dy=1:ny
    for i=2:9
        for n=2:8
            x(dy,n)=(-0.01*((n-1)^2)+(n-1)*(0.27*y(dy)-0.59)-3.8-
1.5*y(dy))/(-0.06*(n-1)-2.41)
            x(dy,34-n+1)=x(dy,n)
        end
        for n=10:16
            x(dy,n)=(0.01*((n-9)^2)+(n-9)*(0.1*y(dy)-0.26)-5.24-
1.13*y(dy))/(0.06*(n-9)-1.99)
            x(dy,34-n+1)=x(dy,n)
        end
    end
    for i=11:12
        for n=2:6
            x(dy,n)=((n-3)*(-0.01*y(dy)+0.13)-0.12-
0.24*y(dy))/(0.01*(n-3)-0.25)
            x(dy,34-n+1)=x(dy,n)
        end
        for n=10:14
            x(dy,n)=0.59*y(dy)+0.16*(n-9)+2.64
```

```
            x(dy,34-n+1)=x(dy,n)
        end
    end
    for i=13:20
        for n=2:5
            x(dy,n)=(0.01*(n-3)*(n-4)+(n-3)*(-0.13*y(dy)+1.02)+(n-4)*(-
0.18*y(dy)+0.64)-3.13-0.93*y(dy))/(0.07*(n-3)-1.65)
            x(dy,34-n+1)=x(dy,n)
        end
        for n=10:13
            x(dy,n)=(-0.01*((n-3)^2)+(n-9)*(-0.05*y(dy)-0.47)-5.83-
1.01*y(dy))/(-0.07*(n-9)-2)
            x(dy,34-n+1)=x(dy,n)
        end
    end
end
% chord distribution: difined for each boom idivedually
for dy=1:ny
    if y(dy)>=0 && y(dy)<=0.31
       C(dy,:)= -0.6*y(dy)+5.43
    else
       C(dy,:)= -0.41*y(dy)-0.23*x(dy,:)+5.38
    end
end

%booms (z)
%upper surface N_1
for dy=1
    for n=1:17
    if x(dy,n)>=1.58 & x(dy,n)<=1.84
       z(dy,n)=-0.03*(x(dy,n)^2)+0.14*x(dy,n)+0.03
    elseif x(dy,n)>1.84 & x(dy,n)<=3.68
       z(dy,n)=-0.03*(x(dy,n)^2)+0.13*x(dy,n)+0.045
    else
       z(dy,n)=-0.07*x(dy,n)+0.370
    end
    end
end
```

```
%lower surface N_1
for dy=1
    for n=18:34
    if x(dy,n)>=1.58 && x(dy,n)<=2.21
       z(dy,n)=0.01*(x(dy,n)^2)-0.05*x(dy,n)-0.06
    else
       z(dy,n)=0.01*(x(dy,n)^2)-0.03*x(dy,n)-0.11
    end
    end
end
%other sections
for dy=2:ny
    for n=1:17  % upper surface
        z(dy,n)=(C(dy,n)/C(1,n))*z(1,n)
    end
    for n=18:34 % lower surface
        z(dy,n)=(C(dy,n)/C(1,n))*z(1,n)
    end
end

%booms areas in mm^2
%flanges
for dy=1:ny
    B(dy,1)=-908.22*x(dy,1)+436.36*y(dy)+245.090
    B(dy,9)=-024.28*x(dy,2)+044.01*y(dy)+1266.29
    B(dy,17)=348.00*x(dy,3)-192.00*y(dy)+274.040
    B(dy,34-n+1)=B(dy,n)
end
% stringers
for dy=1:ny
    for n=1:17
        for i=2:9
        if n<9
            B(dy,n)=((-300*y(dy)+93)/(2.41+0.06*(n-1)))+900
            B(dy,34-n+1)=B(dy,n)
        elseif n>9
            B(dy,n)=((-300*y(dy)-93)/(-1.99+0.06*(n-9)))+900
            B(dy,34-n+1)=B(dy,n)
```

```
        end
        end
        for i=11:20
            if n<9
            B(dy,n)=((300*y(dy)-1572)/(-1.90+0.08*(n-3)))+300
            B(dy,34-n+1)=B(dy,n)
        elseif n>9
            B(dy,n)=((300*y(dy)-1572)/(-2.29-0.07*(n-9)))+300
            B(dy,34-n+1)=B(dy,n)
        end
    end
end

%% I_xx
for dy=1:ny
    z_bar(dy)=sum (B(dy,:)*z(dy,:)/sum (B(dy,:)))
end
    Ixx(dy)=sum(B(dy,:)*(z_bar(dy)-z(dy,:))^2)
%% I_zz
for dy=1:ny
    x_bar(dy)=sum (B(dy,:)*x(dy,:)/sum (B(dy,:)))
end
    Izz(dy)=sum(B(dy,:)*(x_bar(dy)-x(dy,:))^2)
%% I_xz
    Ixz(dy)=sum(B(dy,:)*(x_bar(dy)-x(dy,:))*(z_bar(dy)-z(dy,:)))

% cells areas
for dy=2:ny
    A_1=(C(dy)/C(1))*0.36
    A_2=(C(dy)/C(1))*0.35
    A_3=(C(dy)/C(1))*0.34
    A_4=(C(dy)/C(1))*0.07
end

for dy=2:ny
    for n=1:16
```

```
        ds(dy,n,n+1)=abs(sqrt(((z(dy,n+1)-z(dy,n))^2)+((x(dy,n+1)-
x(dy,n))^2)))
        ds(dy,1,9)=  abs(sqrt(((z(dy,n+1)-z(dy,n))^2)+((x(dy,n+1)-
x(dy,n))^2)))
        ds(dy,9,17)= abs(sqrt(((z(dy,n+1)-z(dy,n))^2)+((x(dy,n+1)-
x(dy,n))^2)))


    end
    for n=18:33
        ds(dy,n,n+1)=abs(sqrt(((z(dy,n+1)-z(dy,n))^2)+((x(dy,n+1)-
x(dy,n))^2)))
        ds(dy,18,26)=abs(sqrt(((z(dy,n+1)-z(dy,n))^2)+((x(dy,n+1)-
x(dy,n))^2)))
        ds(dy,26,34)=abs(sqrt(((z(dy,n+1)-z(dy,n))^2)+((x(dy,n+1)-
x(dy,n))^2)))
    end
    for n=[1 9 17]
        ds(dy,n,34-n+1)=abs(z(dy,n)-z(dy,n+1))
    end
    ds_c(dy,17,18)=C(dy)-x(dy,17)
    ds_c(dy,1,34)=x(dy,1)
end



% bending moment and direct stresses in booms due to the bending
moments
for alpha=1:3
for dy=2:ny
    M_ac(alpha)=
    M_x(alpha,dy)= (L(alpha)* cos(alpha)-D(alpha)*
sin(alpha))*(y_r(alpha)-y(dy))+M_ac(alpha)* sin(35*3.14/180)
    for n=1:34
        seg(alpha,dy,n)=(M_x(alpha,dy)/Ixx(dy))*z(dy,n)
    end
end
end
% shear shress distribution
```

```
for alpha=1:3
for dy=2:ny
    for n=1:34
        if n==1:17
            p_x_n(alpha,dy,n)=seg(alpha,dy,n)*B(dy,n)*0.03
            d_y(dy)=y(dy)-0.5
            delta_p_z(alpha,dy,n)=0.5*(p_z_n(alpha,dy,n)-
p_z_n(alpha,d_y(dy),n))
            p_z_n(alpha,dy,n)= p_x_n(alpha,dy,n)+delta_p_z(alpha,dy,n)
        else
            p_x_n(alpha,dy,n)=0
            p_z_n(alpha,dy,n)= p_x_n(alpha,dy,n)
        end
        S_x_w(alpha,dy,n)=S_x(alpha,dy,n)-sum (p_x_n(alpha,dy,:))
        S_z_w(alpha,dy,n)=S_z(alpha,dy,n)-sum (p_z_n(alpha,dy,:))
    end
end
end
% basic shear flow
for alpha=1:3
for dy=2:ny
    for n=1:34
        if n==1:16
            q_b(alpha,dy,n,n+1)=0 % basic shear in cuts = 0
        elseif n==18:33
            q_b(alpha,dy,n+1,n)=-((S_x_w(alpha)*Ixx(dy)-
S_z_w(alpha)*Ixz(dy))/(Ixx(dy)*Izz(dy)-(Ixz(dy)^2))*(B(dy,n)*x(dy,n)))-
((S_z_w(alpha)*Izz(dy)-S_x_w(alpha)*Ixz(dy))/(Ixx(dy)*Izz(y)-
(Ixz(y)^2))*B(dy,n)*z(dy,n))
        end
        for n=[1 9 17]
            q_b(alpha,dy,n,34-n+1)=-((S_x_w(alpha)*Ixx(dy)-
S_z_w(alpha)*Ixz(dy))/(Ixx(dy)*Izz(dy)-(Ixz(dy)^2))*(B(dy,n)*x(dy,n)))-
((S_z_w(alpha)*Izz(dy)-S_x_w(alpha)*Ixz(dy))/(Ixx(dy)*Izz(y)-
(Ixz(y)^2))*B(dy,n)*z(dy,n))
        end
    end
end
```

```
end
% shear flow in cuts
for alpha=1:3
for dy=2:ny
    for i=1:4 % initial guess
        q_s_o(alpha,dy,i)=0
    end
end
end

% the coeffcient matrix
for alpha=1:3
for dy=2:ny
    for i=1:4 % i-cell number=rows No.
        for j=1:4 % j-stress contribution by cell j=collnmns No.
            A(alpha,dy,i,j)=[
(ds_c(dy,1,34)*(1/t)*(1/A_1(dy))+ds(dy,1,34)*(1/t)*((1/A_1(dy))+(1/A_2(
dy)))
(ds(dy,1,34)*(1/t)*((1/A_1(dy))+(1/A_2(dy))+(ds(dy,1,34)+ds(dy,1,9)+ds(
dy,26,34)+ds(dy,9,26))*(1/t)*(1/A_2(dy))
(ds(dy,9,26)*(1/t)*(1/A_2(dy)))
0;
                                -(ds(dy,1,34)*(1/t)*(1/A_2(dy)))
(ds(dy,9,26)*((1/A_2)+(1/A_3))*(1/t)+(ds(dy,1,34)+ds(dy,1,9)+ds(dy,26,3
4)+ds(dy,9,26))*(1/t)*(1/A_2(dy)))            -
(ds(dy,9,26)*((1/A_2)+(1/A_3))*(1/t)+(ds(dy,9,17)+ds(dy,18,26)+ds(dy,17
,18))*(1/t)*(1/A_2(dy)))                (ds(dy,17,18)*(1/t)*(1/A_3(dy)))
;
                                    0
-(ds(dy,9,26)*(1/t)*(1/A_3(dy)))
(ds(dy,17,18)*((1/A_3)+(1/A_4))*(1/t)+(ds(dy,9,26)+ds(dy,9,17)+ds(dy,18
,26))*(1/t)*(1/A_2(dy)))                (ds(dy,17,18)*((1/A_3)-
(1/A_4))*(1/t)-ds_c(dy,17,18)*(1/t)*(1/A_4(dy)))
                                  (ds_c(dy,1,34)+ds(dy,1,34))*(1/t)*(1/A_1)
-(ds(dy,1,34))*(1/t)*(1/A_1)
(ds(dy,17,18)*(1/t)*(1/A_4))
-(ds(17,18)+ds_c(dy,17,18)*(1/t)*(1/A_4))]
```

```
E(alpha,dy,i)=[((ds_c(dy,1,34)*q_b(alpha,dy,1,34)+ds(dy,1,34)*q_b(alpha
,dy,1,34))*(1/A_1(dy))-
(ds(dy,1,34)*q_b(alpha,dy,1,34)+ds(dy,1,9)*q_b(alpha,dy,1,9)+ds(dy,9,26
)*q_b(alpha,dy,9,26)+ds(dy,26,34)*q_b(alpha,dy,26,34))*(1/A_2(dy)))/t;

((ds(dy,1,34)*q_b(alpha,dy,1,34)+ds(dy,1,9)*q_b(alpha,dy,1,9)+ds(dy,9,2
6)*q_b(alpha,dy,9,26)+ds(dy,26,34)*q_b(alpha,dy,26,34))*(1/A_2(dy))-
(ds(dy,9,17)*q_b(alpha,dy,9,17)+ds(dy,9,26)*q_b(alpha,dy,9,26)+ds(dy,17
,18)*q_b(alpha,dy,17,18)+ds(dy,18,26)*q_b(alpha,dy,18,26))*(1/A_3(dy)))
/t;

((ds(dy,9,17)*q_b(alpha,dy,9,17)+ds(dy,9,26)*q_b(alpha,dy,9,26)+ds(dy,1
7,18)*q_b(alpha,dy,17,18)+ds(dy,18,26)*q_b(alpha,dy,18,26))*(1/A_3(dy))
-
(ds_c(dy,17,18)*q_b(alpha,dy,17,18)+ds(dy,17,18)*q_b(alpha,dy,17,18)*(1
/A_4(dy))))/t;

((ds_c(dy,1,34)*q_b(alpha,dy,1,34)+ds(dy,1,34)*q_b(alpha,dy,1,34))*(1/A
_1(dy))-
(ds_c(dy,17,18)*q_b(alpha,dy,17,18)+ds(dy,17,18)*q_b(alpha,dy,17,18))*(
1/A_4(dy)))/t]
        end
    end
end
end

% iteration procedure
error =1
for alpha=1:3
for dy=2:ny
    for i=1:4
         for j=1:4
            if i==j
                EE(alpha,dy,i)=E(alpha,dy,i)/A(alpha,dy,i,i)
                AA(alpha,dy,i,j)=0
            else
                AA(alpha,dy,i,j)=A(alpha,dy,i,j)/A(alpha,dy,i,i)
```

```
            end
         end
    end
end
while error>0.1
for dy=2:ny
    for i=1:4
        for j=n
            AAA(alpha,dy,i)=AA(alpha,dy,i,:)*q_s_o(alpha,dy,i)
            q_s_o(alpha,dy,i)=-EE(alpha,dy,i)-AAA(alpha,dy,i)
        end
    end
end
    error=abs(q_s_o_old(alpha,dy,i)-q_s_o(alpha,dy,i))
    q_s_o_old(alpha,dy,:)=q_s_o(alpha,dy,:)
    plot (i,error,'*')
    hold on
end
end
for alpha=1:3
for dy=2:ny
    q_c(alpha,dy,1,34)=q_s_o(alpha,dy,1)
    q_c(alpha,dy,17,17)=q_s_o(alpha,dy,4)
    q(alpha,dy,1,17 )=q_b(alpha,dy,n,34-N+1)+q_s_o(alpha,dy,2)-
+q_s_o(alpha,dy,1)
    q(alpha,dy,9,26) =q_b(alpha,dy,n,34-N+1)+q_s_o(alpha,dy,3)-
+q_s_o(alpha,dy,2)
    q(alpha,dy,17,18)=q_b(alpha,dy,n,34-N+1)+q_s_o(alpha,dy,4)-
+q_s_o(alpha,dy,3)
    for n=1:34
        if n==1:8
            q(alpha,dy,n,n+1)=q_s_o(alpha,dy,2)
            taw(alpha,dy,n,n+1)=q(alpha,dy,n,n+1)/t
        elseif n==9:16
            q(alpha,dy,n,n+1)=q_s_o(alpha,dy,3)
            taw(alpha,dy,n,n+1)=q(alpha,dy,n,n+1)/t
        elseif n==17:25
            q(alpha,dy,n,n+1)=q_b(alpha,dy,n,n+1)+q_s_o(alpha,dy,3)
```

```
            taw(alpha,dy,n,n+1)=q(alpha,dy,n,n+1)/t
        elseif n==26:33
            q(alpha,dy,n,n+1)=q_b(alpha,dy,n,n+1)+q_s_o(alpha,dy,4)
            taw(alpha,dy,n,n+1)=q(alpha,dy,n,n+1)/t
        end
    end
end
end
%% torsion analysis
for alpha=1:3
    T(alpha)=L((alpha)*cos(alpha)-D(alpha)*sin(alpha))*(x_r-
x(dy,n)+M_ac*cos(35*3.14/180))
end
```

Appendix (E): prop-fans axial momentum code

```
%% axial momentum (prop.fans)
E=0.4
T=288
mu=0.04*(10^-6)*T^0.67
lam=-(2/3)*mu
pi_fan=1.06
roh=1.225
T=288
v_1=20.04*sqrt(T)*0.4
p_1=100000
%% rotor
for i=1:N_P_F
    for j=1:3
    r(i,1)=D_f_hub(i)/2
    r(i,2)=(D_f_hub(i)/2)+(l_b(i)/2)
    r(i,3)=(D_f_hub(i)/2)+l_b(i)
    c(i,1)=c_hub(i)
    c(i,2)=c_mid(i)
    c(i,2)=c_tip(i)
    betaa_2(i,j)=((-2.17)/l_b(i)^2)*((r(i,j))^2+(r(i,1)-r(i,j))*(0.5*
l_b(i)+D_f_hub(i))-(r(i,1))^2)+32.06
    v_2(i,j)=((-0.001*E)/(sqrt(T)*(l_b(i)^2)))*(r(i,j)^2+(r(i,1)-
r(i,j))*(0.5* l_b(i)+D_f_hub(i))-(r(i,1))^2)+2.36*E
    u_2(i,j)=((0.001*E)/(sqrt(T)*(l_b(i)^2)))*(r(i,j)^2+(r(i,1)-
r(i,j))*(0.5* l_b(i)+D_f_hub(i))-(r(i,1))^2)+2*E
    u_3(i,j)=((0.012*E)/(sqrt(T)*(l_b(i)^2)))*(r(i,j)^2+(r(i,1)-
r(i,j))*(0.5* l_b(i)+D_f_hub(i))-(r(i,1))^2)+2.76*E
    d_u_2(i,j)=((0.001*E)/(sqrt(T)*(l_b(i)^2)))*(2*r(i,j)^2-(0.5*
l_b(i)+D_f_hub(i)))
    d_u_3(i,j)=((0.012*E)/(sqrt(T)*(l_b(i)^2)))*(2*r(i,j)^2-(0.5*
l_b(i)+D_f_hub(i)))
    d_u_3_out(i,j)=((0.007*E)/(sqrt(T)*(l_b(i)^2)))*(2*r(i,j)^2-(0.5*
l_b(i)+D_f_hub(i)))
    eps(i,j)=(-10.69/l_b(i)^2)*((r(i,j))^2+(r(i,1)-r(i,j))*(0.5*
l_b(i)+D_f_hub(i))-(r(i,1))^2)-4.88
    end
```

```
end
%R_x
for i=1:N_P_F
    for j=1:3
        cl_0(i)=(0.404/l_b(i)^2)*((r(i,j)^2)+((r(i,j)-r(i,j))*(0.5*
l_b(i)+D_f_hub(i))-((r(i,j))^2)+1.056))
        R_xx(i,j)=-
0.5*roh*((v_2(i,j))^2)*(c(i,j)*(cl_0(i)*((1/cosd(betaa_2(i,j)))-
0.441*cosd(betaa_2(i,j)))-0.011*cosd(betaa_2(i,j))))
        R_x(i)=sum (R_xx(i,:))/3  % average
    end
end
%press_force
for i=1:N_P_F
    for j=1:3
        pp(i,j)=0.14*r(i,j)* (1/2*(v_1^2)+ p_1- 0.5*(u_2(i,j)^2) )*(1-
1/pi_fan)
        p(i)=sum (pp(i,:))/3
    end
end


%shear_force_1
for i=1:N_P_F
    for j=1:3
    Re_x(i,j)=roh*u_2(i,j)*c(i,j)/mu
    c_f(i,j)=0.664/Re_x(i,j)

ssh_1(i,j)=0.14*r(j,j)*(lam*(d_u_3_out(i,j)*sind(eps(i,j))+(0.5*roh*(u_
3(i,j)^2)*c(i,j)/mu)+(1/d_u_3(i,j)))-((u_3(i,j)-
u_2(i,j))/b_r(i))*(lam+2*mu))
    sh_1(i)=sum (ssh_1(i,:))/3
    end
end
%shear_force_1
for i=1:N_P_F
    for j=1:2
```

```
ssh_2(i,j)=0.14*r(i,j)*b_r(i)*mu*0.5*((d_u_2(i,j)+d_u_2(i,j))+(d_u_3(i,
j+1)+d_u_3(i,j+1)))
        sh_2(i)=sum (ssh_2(i,:))/3
    end
    sh(i)=sh_1(i)+sh_2(i)
end

%P_E
for i=1:N_P_F
    for j=1:3
        P_EE(i,j)=9.81*pi*roh*(((D_f(i)^2)-(D_f_hub(i)^2))/4)*b_r(i)
        P_E(i)=sum (P_EE(i,:))/3
    end
end
%% axial momentum
for i=1:1:N_P_F
    M_xx(i)=-p(i)+sh(i)+P_E(i)+R_x(i)
end
M_x= sum(M_xx(:))
```

Appendix (F): design optimization and the prop-fans rescale code

```
%% sliding part optimization
clear all
clc
t_1=1
t_2=1
y_dddash=linspace(3.58,4.62,3);
ny = length(y_dddash);
for dy = 1:ny
        Q(dy)=1.04+0.23*(4.62-y_dddash(dy))+(-t_1-t_2)/100;
        B(dy)=10.78-1.82*y_dddash(dy)+((-t_1-t_2)/100)-Q(dy);
        g_1=1.62%y_ddashatQ%
        g_2(dy)=0.97*(5.47-y_dddash(dy))  %y_ddashatQ%
    if Q<=B
        S_exp_1(dy)=5.25
        S_exp_2(dy)=1.25+0.85*Q(dy)*(7.11-g_1-g_2(dy))+0.11*((7.11-g_1-
g_2(dy))^2)
        S_exp_3(dy)=0.43*Q(dy)*g_2(dy)
        S_exp(dy)=S_exp_1(dy)+S_exp_2(dy)+S_exp_3(dy)
    end
end
S_exp_max=2*max(max(max((S_exp))))

%% fan dimensions optimization
%const.
W=1.30
K=0.21
t_1=0.01
t_2=0.01
QQ=Q(3)
dl=0.08
y_ddash(1)=0.35
N(1)=0.85*(1.04+0.23*(4.62-y_ddash(1)))-t_1-t_2
c(1)=0.65*N(1)
l(1)=0.20*N(1)
```

```
b_r(1)=dl*l(1)
t(1)=0.05*b_r(1)
t_cf(1)=2*b_r(1)
t_cr(1)=2*b_r(1)
B_f(1)=(1+W)*b_r(1)+t(1)+t_cf(1)+t_cr(1)
D_f(1)=b_r(1)/K
T(1)=D_f(1)
M=100 % i = the prop-fan number**** 100 is high enough un-real value to
run the code
% chord distribution/disk width and clearances/prop-fans number

for i=2:M-1
        y_ddash(i)=y_ddash(i-1)+3*T(i-1)
        if  y_ddash(i)<7.11
        N(i)=0.85*(1.04+0.23*(4.62-y_ddash(i)))-t_1-t_2
        c(i)=0.65*N(i)
        l(i)=0.20*N(i)
        b_r(i)=dl*l(i)
        t(i)=0.05*b_r(i)
        t_cf(i)=2*b_r(i)
        t_cr(i)=2*b_r(i)
        B_f(i)=(1+W)*b_r(i)+t(i)+t_cf(i)+t_cr(i)
        D_f(i)=b_r(i)/K
        T(i)=D_f(i) % step between the prop-fans
        else
        N_P_F=i
        end
end
t_max_2412 = 0.12
for i=1:N_P_F
        t(i)=0.12*c(i)
        if t(i)<D_f(i)
           i
        else
        end
end
%%
P=0.35
```

```
betta_tip=38.003
for i=1:N_P_F
    D_f_hub(i)=P*D_f(i)
    l_b(i)=D_f(i)-D_f_hub(i)
    c_tip(i)=b_r(i)/sind (betta_tip)
    c_hub(i)=0.79*c_tip(i)
    c_mid(i)=0.98*c_tip(i)
end
```

Appendix (G): design optimization and the prop-fans rescale code

```
%% consumed power code
E=0.4
for i=1:N_P_F
    R_a(i)=(100000-00000/1.061)*(l_b(i)^2)*0.14+14*(0.91*E)
    P_i(i)=14*R_a(i)*2*b_r(i)
end
P=sum (P_i(:))
```